

Cellular Automata Models for the Two Dimensional Scalar Wave Equation

by

Nikhil Adnani

A thesis
presented to the University of Manitoba
in fulfilment of the
thesis requirement for the degree of
Master of Science
in
Electrical Engineering

Winnipeg, Manitoba, Canada 1996

©Nikhil Adnani 1996



National Library
of Canada

Acquisitions and
Bibliographic Services Branch

395 Wellington Street
Ottawa, Ontario
K1A 0N4

Bibliothèque nationale
du Canada

Direction des acquisitions et
des services bibliographiques

395, rue Wellington
Ottawa (Ontario)
K1A 0N4

Your file *Votre référence*

Our file *Notre référence*

The author has granted an irrevocable non-exclusive licence allowing the National Library of Canada to reproduce, loan, distribute or sell copies of his/her thesis by any means and in any form or format, making this thesis available to interested persons.

L'auteur a accordé une licence irrévocable et non exclusive permettant à la Bibliothèque nationale du Canada de reproduire, prêter, distribuer ou vendre des copies de sa thèse de quelque manière et sous quelque forme que ce soit pour mettre des exemplaires de cette thèse à la disposition des personnes intéressées.

The author retains ownership of the copyright in his/her thesis. Neither the thesis nor substantial extracts from it may be printed or otherwise reproduced without his/her permission.

L'auteur conserve la propriété du droit d'auteur qui protège sa thèse. Ni la thèse ni des extraits substantiels de celle-ci ne doivent être imprimés ou autrement reproduits sans son autorisation.

ISBN 0-612-12947-0

Canada

Name _____

Dissertation Abstracts International and *Masters Abstracts International* are arranged by broad, general subject categories. Please select the one subject which most nearly describes the content of your dissertation or thesis. Enter the corresponding four-digit code in the spaces provided.

Electrical and Electronics

SUBJECT TERM

0544

UMI

SUBJECT CODE

Subject Categories

THE HUMANITIES AND SOCIAL SCIENCES

COMMUNICATIONS AND THE ARTS

Architecture 0729
 Art History 0377
 Cinema 0900
 Dance 0378
 Fine Arts 0357
 Information Science 0723
 Journalism 0391
 Library Science 0399
 Mass Communications 0708
 Music 0413
 Speech Communication 0459
 Theater 0465

EDUCATION

General 0515
 Administration 0514
 Adult and Continuing 0516
 Agricultural 0517
 Art 0273
 Bilingual and Multicultural 0282
 Business 0688
 Community College 0275
 Curriculum and Instruction 0727
 Early Childhood 0518
 Elementary 0524
 Finance 0277
 Guidance and Counseling 0519
 Health 0680
 Higher 0745
 History of 0520
 Home Economics 0278
 Industrial 0521
 Language and Literature 0279
 Mathematics 0280
 Music 0522
 Philosophy of 0998
 Physical 0523

Psychology 0525
 Reading 0535
 Religious 0527
 Sciences 0714
 Secondary 0533
 Social Sciences 0534
 Sociology of 0340
 Special 0529
 Teacher Training 0530
 Technology 0710
 Tests and Measurements 0288
 Vocational 0747

LANGUAGE, LITERATURE AND LINGUISTICS

Language
 General 0679
 Ancient 0289
 Linguistics 0290
 Modern 0291

Literature
 General 0401
 Classical 0294
 Comparative 0295
 Medieval 0297
 Modern 0298
 African 0316
 American 0591
 Asian 0305
 Canadian (English) 0352
 Canadian (French) 0355
 English 0593
 Germanic 0311
 Latin American 0312
 Middle Eastern 0315
 Romance 0313
 Slavic and East European 0314

PHILOSOPHY, RELIGION AND THEOLOGY

Philosophy 0422
 Religion
 General 0318
 Biblical Studies 0321
 Clergy 0319
 History of 0320
 Philosophy of 0322
 Theology 0469

SOCIAL SCIENCES

American Studies 0323
 Anthropology
 Archaeology 0324
 Cultural 0326
 Physical 0327
 Business Administration
 General 0310
 Accounting 0272
 Banking 0770
 Management 0454
 Marketing 0338
 Canadian Studies 0385
 Economics
 General 0501
 Agricultural 0503
 Commerce-Business 0505
 Finance 0508
 History 0509
 Labor 0510
 Theory 0511
 Folklore 0358
 Geography 0366
 Gerontology 0351
 History
 General 0578

Ancient 0579
 Medieval 0581
 Modern 0582
 Black 0328
 African 0331
 Asia, Australia and Oceania 0332
 Canadian 0334
 European 0335
 Latin American 0336
 Middle Eastern 0333
 United States 0337
 History of Science 0585
 Law 0398
 Political Science
 General 0615
 International Law and Relations 0616
 Public Administration 0617
 Recreation 0814
 Social Work 0452
 Sociology
 General 0626
 Criminology and Penology 0627
 Demography 0938
 Ethnic and Racial Studies 0631
 Individual and Family Studies 0628
 Industrial and Labor Relations 0629
 Public and Social Welfare 0630
 Social Structure and Development 0700
 Theory and Methods 0344
 Transportation 0709
 Urban and Regional Planning 0999
 Women's Studies 0453

THE SCIENCES AND ENGINEERING

BIOLOGICAL SCIENCES

Agriculture
 General 0473
 Agronomy 0285
 Animal Culture and Nutrition 0475
 Animal Pathology 0476
 Food Science and Technology 0359
 Forestry and Wildlife 0478
 Plant Culture 0479
 Plant Pathology 0480
 Plant Physiology 0817
 Range Management 0777
 Wood Technology 0746

Biology
 General 0306
 Anatomy 0287
 Biostatistics 0308
 Botany 0309
 Cell 0379
 Ecology 0329
 Entomology 0353
 Genetics 0369
 Limnology 0793
 Microbiology 0410
 Molecular 0307
 Neuroscience 0317
 Oceanography 0416
 Physiology 0433
 Radiation 0821
 Veterinary Science 0778
 Zoology 0472

Biophysics
 General 0786
 Medical 0760

Geodesy 0370
 Geology 0372
 Geophysics 0373
 Hydrology 0388
 Mineralogy 0411
 Paleobotany 0345
 Paleocology 0426
 Paleontology 0418
 Paleozoology 0985
 Palynology 0427
 Physical Geography 0368
 Physical Oceanography 0415

HEALTH AND ENVIRONMENTAL SCIENCES

Environmental Sciences 0768
 Health Sciences
 General 0566
 Audiology 0300
 Chemotherapy 0992
 Dentistry 0567
 Education 0350
 Hospital Management 0769
 Human Development 0758
 Immunology 0982
 Medicine and Surgery 0564
 Mental Health 0347
 Nursing 0569
 Nutrition 0570
 Obstetrics and Gynecology 0380
 Occupational Health and Therapy 0354
 Ophthalmology 0381
 Pathology 0571
 Pharmacology 0419
 Pharmacy 0572
 Physical Therapy 0382
 Public Health 0573
 Radiology 0574
 Recreation 0575

Speech Pathology 0460
 Toxicology 0383
 Home Economics 0386

PHYSICAL SCIENCES

Pure Sciences
 Chemistry
 General 0485
 Agricultural 0749
 Analytical 0486
 Biochemistry 0487
 Inorganic 0488
 Nuclear 0738
 Organic 0490
 Pharmaceutical 0491
 Physical 0494
 Polymer 0495
 Radiation 0754
 Mathematics 0405

Physics
 General 0605
 Acoustics 0986
 Astronomy and Astrophysics 0606
 Atmospheric Science 0608
 Atomic 0748
 Electronics and Electricity 0607
 Elementary Particles and High Energy 0798
 Fluid and Plasma 0759
 Molecular 0609
 Nuclear 0610
 Optics 0752
 Radiation 0756
 Solid State 0611
 Statistics 0463

Applied Sciences
 Applied Mechanics 0346
 Computer Science 0984

Engineering
 General 0537
 Aerospace 0538
 Agricultural 0539
 Automotive 0540
 Biomedical 0541
 Chemical 0542
 Civil 0543
 Electronics and Electrical 0544
 Heat and Thermodynamics 0348
 Hydraulic 0545
 Industrial 0546
 Marine 0547
 Materials Science 0794
 Mechanical 0548
 Metallurgy 0743
 Mining 0551
 Nuclear 0552
 Packaging 0549
 Petroleum 0765
 Sanitary and Municipal 0554
 System Science 0790
 Geotechnology 0428
 Operations Research 0796
 Plastics Technology 0795
 Textile Technology 0994

PSYCHOLOGY

General 0621
 Behavioral 0384
 Clinical 0622
 Developmental 0620
 Experimental 0623
 Industrial 0624
 Personality 0625
 Physiological 0989
 Psychobiology 0349
 Psychometrics 0632
 Social 0451

EARTH SCIENCES

Biogeochemistry 0425
 Geochemistry 0996

THE UNIVERSITY OF MANITOBA

FACULTY OF GRADUATE STUDIES

COPYRIGHT PERMISSION

CELLULAR AUTOMATA MODELS FOR THE TWO DIMENSIONAL

SCALAR WAVE EQUATION

BY

NIKHIL ADNANI

A Thesis/Practicum submitted to the Faculty of Graduate Studies of the University of Manitoba in partial fulfillment of the requirements for the degree of

MASTER OF SCIENCE

Nikhil Adnani

© 1996

Permission has been granted to the LIBRARY OF THE UNIVERSITY OF MANITOBA to lend or sell copies of this thesis/practicum, to the NATIONAL LIBRARY OF CANADA to microfilm this thesis/practicum and to lend or sell copies of the film, and to UNIVERSITY MICROFILMS INC. to publish an abstract of this thesis/practicum..

This reproduction or copy of this thesis has been made available by authority of the copyright owner solely for the purpose of private study and research, and may only be reproduced and copied as permitted by copyright laws or with express written authorization from the copyright owner.

Abstract

In this thesis, Cellular Automata methods are applied to model the scalar wave equation in two dimensions. We consider cellular automata which conserve mass and momentum at the particle level and thus fall under the more specific category known as Lattice Gas Automata. Various HPP and FHP lattice gas models are discussed and applied in the modelling of inhomogeneous media. The Fermi-Dirac distribution for particles in a lattice gas which obeys semi-detailed balance, enables an accurate prediction of the equilibrium conditions. This is used as a starting point for most simulations. The Chapman-Enskog analysis provides us with a tool for analysing the HPP and FHP lattice gases. Using this method we could derive the macroscopic differential equation that results from the microscopic particle dynamics. The transport coefficients in the Navier-Stokes equation (which results from the HPP and FHP models) could be then obtained. Experimental results from simulations run on a special-purpose cellular automata machine (CAM-8) are compared with theory. A comparison between the two and results obtained using conventional numerical techniques then enables an assessment of the feasibility of the lattice gas approach.

Acknowledgements

I am very grateful to Dr. Greg Bridges for his faith in my abilities, encouragement, generosity, support and most importantly, for being a good friend. Working for him has been a pleasure and a very important part of my academic career thus far.

I should like to thank Dr. Neil Simons for his guidance in numerical matters which were beyond my understanding; for those very intense discussions in *The Groove Chamber* and for taking an active interest in my thesis. Without his guidance this project would have met with little success.

I am thankful to Dr. Bruce Boghosian for giving us so much of his time and patiently answering our questions regarding Lattice Gases. Thanks to Dr. Norman Margolus and the Information Mechanics Group for inviting us to MIT and explaining several aspects of CAM-8.

Many thanks to the staff of the Directorate of Antennas and Integrated Electronics at the Communications Research Centre (Ottawa), especially Rene Douville and Michel Cuhaci.

Financial support from the Natural Sciences and Engineering Research Council of Canada and InfoMagnetics Corporation is acknowledged.

I am grateful to Ming Zhang for reviewing and correcting the math in this document and for the many stimulating discussions which have helped toward a better understanding of the subject. Special thanks to Dino Cule for all the encouragement.

Words cannot express my gratitude to Mr. Satvinder Singh, who has guided me through difficult times and always supported my academic endeavours. I am forever indebted to him. And finally, a very special acknowledgement to my mother, Ravana Adnani, who has always encouraged my creative ability. I could never have achieved anything without her love and support.

Contents

Abstract	1
Acknowledgements	2
List of Principal Symbols	11
1 Introduction	1
1.1 Cellular Automata	1
1.2 Lattice Gases	3
1.2.1 The HPP Model	4
1.2.2 The FHP Model	6
1.3 CAM-8	7
1.4 The Stochastic Element	10
1.5 Macroscopic Quantities	11
1.6 Summary	13
2 Lattice Gas Automata	14
2.1 Introduction	14

2.2	Microscopic Dynamics	15
2.3	The Ensemble Average	19
2.4	Semi-Detailed Balance	20
2.5	Conserved Quantities	21
2.6	The Equilibrium Particle Distribution	24
2.7	Equilibria in the $4m \leftrightarrow 1r$ Lattice Gas	27
2.8	Experimental Results	28
2.8.1	Rest Particles of Mass $4m$	28
2.8.2	Rest Particles of Mass $2m$	31
2.9	Violation of Semi-Detailed Balance	35
2.10	Violation of Detailed Balance	37
2.11	The Particle Pool	39
2.12	Implementing a Stochastic Model	40
2.13	Summary	48
3	The Chapman-Enskog Analysis	50
3.1	Introduction	50
3.2	The Fermi Metric	53
3.3	Zero-Order Conservation Equations	56
3.4	The Linearized Boltzmann Equation	57
3.5	First-Order Solution	59
3.6	First-Order Conservation Equations	60
3.7	Ordering the Conserved Quantities	62

4	Lattice Gas Fluids	65
4.1	Analysis of the $4m \leftrightarrow 1r$ ($s = 1$) Lattice Gas	65
4.2	Summary of Results	84
5	LGA Experiments for Homogeneous Systems	86
5.1	Measurements for Propagation Speed	86
5.1.1	The HPP Model	87
5.1.2	The $4m \leftrightarrow 1r$ Model	89
5.1.3	The $2m \leftrightarrow 1r$ Model	89
5.1.4	The FHP $6m \leftrightarrow 1r$ Model	92
5.2	Lattice Gas Mixtures	96
5.3	Viscosity	99
6	LGA Experiments for Heterogeneous Systems	101
6.1	Boundaries Between Different Media	101
6.2	Numerical Experiments	103
6.2.1	Wave Propagation Across an Interface Using the $4m \leftrightarrow 1r$ ($s = 1$) Lattice Gas	104
6.2.2	Wave Propagation Across an Interface Using the $4m \leftrightarrow 1r$ ($s =$ 2) Lattice Gas	112
6.2.3	Wave Propagation Across an Interface Using the $4m \leftrightarrow 1r$ Lat- tice Gas Mixture	116
6.2.4	Modelling a Dielectric Strip Using the $4m \leftrightarrow 1r$ Model.	117
6.2.5	The Two-Layered Dielectric Cylinder	120

7	Conclusions	123
7.1	CA Versus Conventional Numerical Techniques	123
7.2	Simulation Time	124
7.3	Advantages of the CA Approach	125
7.4	Modelling Inhomogenieties	125
7.5	Special-Purpose Architectures	125
7.6	Future Work	127
A	Acoustic Waves in Fluids	128
A.1	Conservation of Mass	128
A.2	Conservation of Momentum	129
A.3	Acoustic Field Equations	130
B	Propagation Speed Measurements	132
	References	135

List of Figures

1.1	Two dimensional lattice of cells.	2
1.2	Example of voting rule.	2
1.3	Some examples of HPP lattice gas automata collision rules.	5
1.4	One step in the evolution of a lattice-gas dynamics.	6
1.5	Example of possible FHP lattice gas collision rules.	8
1.6	Update and Transfer stages in the CAM.	9
1.7	Counting particles within a square sampling window.	12
2.1	A non-interacting particle lattice gas.	16
2.2	Transition matrix for the $4m \leftrightarrow 1r$ lattice gas.	22
2.3	Equilibria for 1 rest particle of mass $4m$	29
2.4	Equilibria for 2 rest particles of mass $4m$ each	30
2.5	Collision details for the $2m \leftrightarrow 1r$ model	31
2.6	Collision details for the $3m \leftrightarrow 1r + 1m$ model	32
2.7	Equilibria for 1 rest particle of mass $2m$	33
2.8	Collision details for the $2m \leftrightarrow 1r$ stack	34

2.9	Equilibria for 2 rest particles of mass $2m$ each	35
2.10	Collision details for a model that violates SDB	36
2.11	Equilibria in the case when SDB is violated	38
2.12	Collision details for a model in which DB is violated	38
2.13	Equilibria in the case when DB is violated	39
2.14	Collision details for the modified $2m \leftrightarrow 1r$ stack	41
2.15	Collision details for the modified $4m \leftrightarrow 1r$ stack	42
2.16	Stack-length = 2 in the $2m \leftrightarrow 1r$ model	43
2.17	Stack-length = 2 in the $4m \leftrightarrow 1r$ model	44
2.18	Equilibria for the $2m \leftrightarrow 1r$ ($s=2$) model	45
2.19	Equilibria for the $4m \leftrightarrow 1r$ ($s=2$) model	45
2.20	The $2m \leftrightarrow 1r$ ($s=3$) model	46
2.21	Decomposing the stack model	47
2.22	Kicking the random bit in the $2m \leftrightarrow 1r$ model	48
5.1	The two dimensional lattice.	87
5.2	Time domain waveforms	90
5.3	Propagation speeds for the $4m \leftrightarrow 1r$ model	91
5.4	Propagation speeds for the $2m \leftrightarrow 1r$ model	93
5.5	The hexagonal lattice.	94
5.6	The FHP $6m \leftrightarrow 1r$ model.	95
5.7	Propagation speeds for the $4m \leftrightarrow 1r$ lattice gas mixture as a function of the density of sites in the lattice which can hold rest particles . . .	98

5.8	Viscosity as a function of moving particle density.	100
6.1	The two dimensional lattice with two regions.	102
6.2	Equilibria between Region I ($s=0$) and Region II ($s=1$).	103
6.3	Equilibria between Region I ($s=1$) and Region II ($s=2$).	104
6.4	The two dimensional lattice with two regions.	105
6.5	Reflecting lattice boundaries.	105
6.6	The two region interface: HPP and $4m \leftrightarrow 1r$ ($s=1$), $f_m = 0.40$	107
6.7	Ensemble averaging for the two region interface: HPP and $4m \leftrightarrow 1r$ ($s=1$), $f_m = 0.40$	109
6.8	The two region interface: HPP and $4m \leftrightarrow 1r$ ($s=1$), $f_m = 0.50$	111
6.9	Time domain waveform (in the dielectric region) for $4m \leftrightarrow 1r$ ($s=1$), $f_m = 0.50$	112
6.10	Time domain waveform for the two region test; $4m \leftrightarrow 1r$ ($s=2$), $f_m =$ 0.35	114
6.11	Frequency response for the reflected wave in Region I; $4m \leftrightarrow 1r$ ($s=2$), $f_m = 0.35$	115
6.12	Frequency response for the reflected wave in Region I; $4m \leftrightarrow 1r$ ($s=2$), $f_m = 0.50$	115
6.13	Frequency response for the two region experiment; $4m \leftrightarrow 1r$ ($s=1$) and HPP (no rest) rest mixture.	117
6.14	Frequency response for the two region experiment; $4m \leftrightarrow 1r$ ($s=2$) and HPP (no rest) rest mixture.	118
6.15	The two dimensional lattice with dielectric strip; $\epsilon_{strip} = 3.2957$	119

6.16	Time domain waveform for dielectric strip.	119
6.17	Frequency response for dielectric strip.	120
6.18	Collision rules for the creation of rest particles.	121
6.19	Two dimensional lattice with dielectric cylinder.	122
6.20	Two dimensional lattice with dielectric cylinder: results.	122
7.1	ϵ_r as a function of k	126
A.1	Control volume	129
B.1	Two dimensional lattice.	133
B.2	Time domain waveforms.	133

List of Principal Symbols

Symbol	Description
*	Used in place of an index to indicate possible functional dependence on all values of an index
α_γ	Parameters of the Fermi-Dirac equilibrium
$\Gamma_{\mu\nu}^\eta$	Fermi connection
$\Gamma(k)_{\mu\nu}^\eta$	Generalized Fermi connection
δ_ν^μ	Kronecker delta
$\delta(k)_\nu^\mu$	Generalized Kronecker delta
ϵ	Perturbation expansion parameter
ϵ_r	Relative permittivity of a region
λ^μ	Eigenvalue of J_j^i
$a(s \rightarrow s')$	Microscopic transition matrix element
$A(s \rightarrow s')$	Ensemble-averaged transition matrix element
$A^\mu(Q^*)$	Advection coefficients in hydrodynamic equation
$b_i(\mathbf{x}, t)$	i th bit at site \mathbf{x} at time-step t
$\mathbf{b}(\mathbf{x}, t)$	Vector of all bits in cell \mathbf{x} at time-step t
c_s	Propagation speed
\mathbf{c}^j	Lattice vector along which a particle can move
c_i	Microscopic collision operator
C_i	Ensemble averaged collision operator
C_v^i	v th order, ensemble averaged collision operator
D	Spatial dimension of lattice
$\mathcal{D}_\xi^\mu(Q^*)$	Diffusion coefficients in hydrodynamic equation
\mathbf{e}^i	Dimensionless lattice vectors
f_m	Density per cell of moving particles
f_r	Density per cell of rest particles

$g_{\mu\xi}$	Fermi metric
$\mathbf{g}(k)_{\mu\xi}$	Generalized Fermi metric
H	Set of hydrodynamic modes, $1, \dots, n_c$
J_j^i	Jacobian matrix of collision operator at equilibrium
k	Maximum number of rest particles at a site
K	Set of kinetic modes, $n_c + 1, \dots, N_l$
ℓ	Characteristic lattice spacing
n_c	Number of conserved quantities
$N^i(\mathbf{x}, t)$	Ensemble average of $b_i(\mathbf{x}, t)$
N_v^i	v th order, ensemble averaged distribution function
N_l	Total number of bits at a site in a lattice
n	Total number of bits at a site in a lattice
$P(s)$	Probability that that a state s exists at any site
$q^\mu(\mathbf{x}, t)$	Value of the μ th conserved quantity at site \mathbf{x} and at time-step t
q_i^μ	Coefficient of dependence of μ th conserved quantity on bit i , for $\mu = 1, \dots, n_c$; also left eigenvector of J_j^i for $\mu = 1, \dots, N_l$.
q_μ^j	Right eigenvector of J_j^i for $\mu = 1, \dots, N_l$.
$Q^\mu(\mathbf{x}, t)$	Ensemble average of $q^\mu(\mathbf{x}, t)$
s	A state of a site
s_j	The j th bit of a site in state s
$\mathbf{S}^\mu(Q^*)$	Source term in hydrodynamic equation
Δt	Time-step
t	Discrete time

Chapter 1

Introduction

1.1 Cellular Automata

A Cellular Automaton is a discrete dynamical system which consists of a lattice of identical cells. The state of any cell in this lattice is determined by a *rule* which is local in both space and time. Each cell has a small number of states and hence the number of bits required for its representation is small as well.

To better illustrate this definition let us consider the lattice of cells in Figure 1.1.

Every cell within a large lattice of cells is connected to its four nearest neighbours (North, South, East and West). The state of any cell within this lattice at a given time is either 0 or 1. The following rule then governs the evolution of this lattice:

A cell's state changes to the state of the majority of its neighbours. In case of a tie (an equal number of 1's and 0's in neighbouring cells) the cell's state remains unchanged.

This rule, known as a *Voting* or *Majority* rule [1] is implemented in all cells simultaneously, and at every time step. It illustrates the aspect of *parallelism* which is a

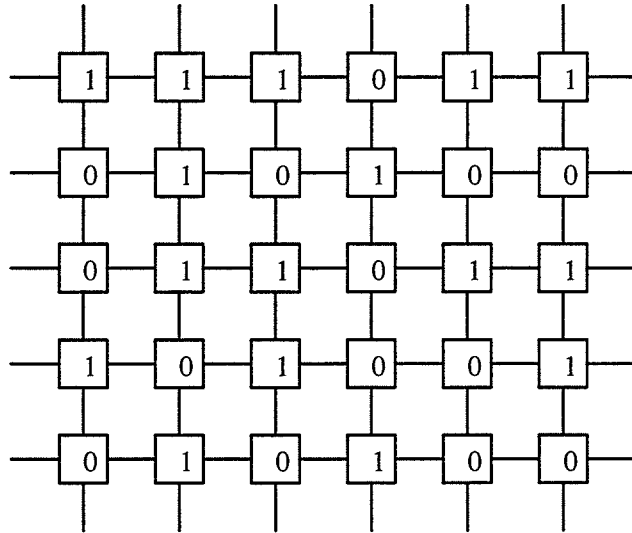


Figure 1.1: Two dimensional lattice of cells.

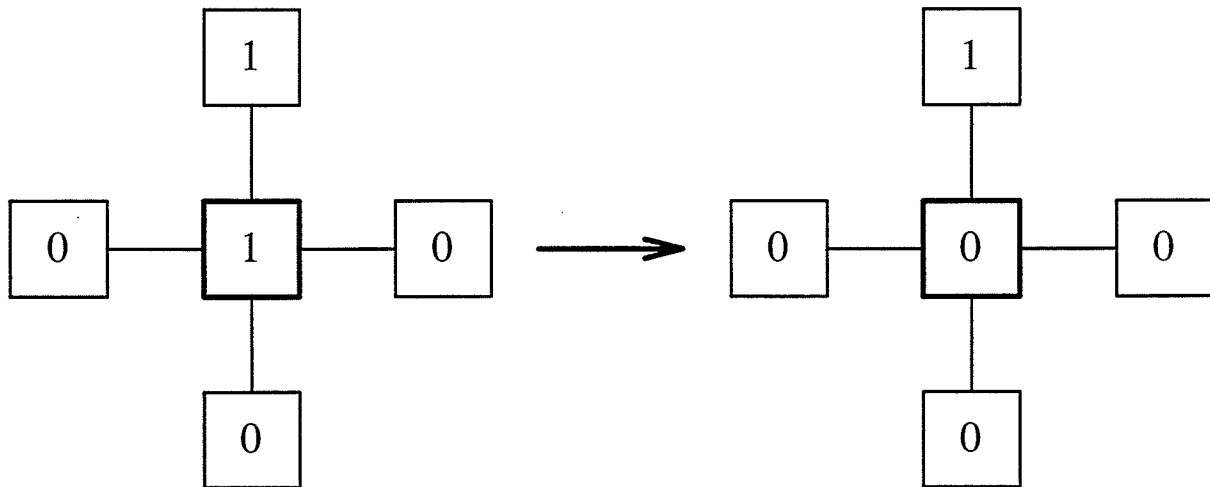


Figure 1.2: Example of voting rule.

characteristic of every CA simulation. In other words, we could run this simulation concurrently (and more *naturally* [2]) on a number of processors, each of which represents a cell. The locality both in space and time of the CA's laws, small number of states (2) for every cell are also illustrated and part of every CA simulation. Furthermore the CA's laws are *uniform*. That is, the same rule applies to every cell within the lattice. In Figure 1.2, the state of the cell in the centre changes from 1 to 0. The states of the neighbouring cells are updated simultaneously (not shown).

The CA simulation then involves

- a process of communication between neighbouring processors whereby each processor informs its neighbours of its state and
- a process of internal bit manipulation during which each processor determines its new state based on this information.

Cellular Automata was the brainchild of John von Neumann and Stanislaw Ulam who used it to formulate biological models of living organisms [3]. In the early 1980s, Wolfram [4] used one-dimensional cellular automata to demonstrate the complexity that emerges from simple microscopic rules. Ever since its introduction however, it has been used in a number of different applications some of which include modelling diffusion [5], semiconductor device modelling [6], generating random numbers [7] and modelling Ising systems [8].

1.2 Lattice Gases

The term Lattice Gas refers to a discrete system of interacting particles. Its inclusion under the broad umbrella of Cellular Automata is referred to as Lattice Gas Automata. Lattice Gas Automata are implemented as a set of rules, just like any

Cellular Automaton. The bits in a CA represent particles in the lattice gas. The rules govern the manner in which particles interact with one another. In fluid models when particles collide at a node on the lattice, the interaction conserves mass and momentum. However, rules in which momentum is not necessarily conserved are also used in physical modelling. One such rule which is used to model Burger's Equation is discussed in [9].

In the rest of the chapter we shall discuss the HPP and FHP lattice gases in which both mass and momentum are conserved. These models form the basis for most of the experiments contained in this thesis.

1.2.1 The HPP Model

In the HPP lattice gas automaton (HPP stands for Hardy, Pazzis, Pomeau - the creators of this model), particles are restricted to moving in the North, South, East and West directions and occupy discrete positions (sites) on an orthogonal grid [10]. Each site on this grid can hold up to a maximum of four particles with no more than one moving particle in each direction. A total of four bits are used to represent these particles at each site.

Particles move in straight lines, unless a head-on, binary collision occurs after which they travel at right-angles to the original direction of motion. All other particle configurations remain unchanged and they simply pass through one another. The interactions between particles conserve mass and momentum. The collision rules are shown in Figure 1.3. The HPP rule is characterized by rotational symmetry. This means that the rule remains unchanged when input particle configurations are rotated by 90° . For the four bit model, we have a total of sixteen collision rules.

One step in the evolution of the LGA consists of two stages as shown in Figure 1.4 which are usually referred to as *Collision* and *Advection*. In the Collision stage parti-

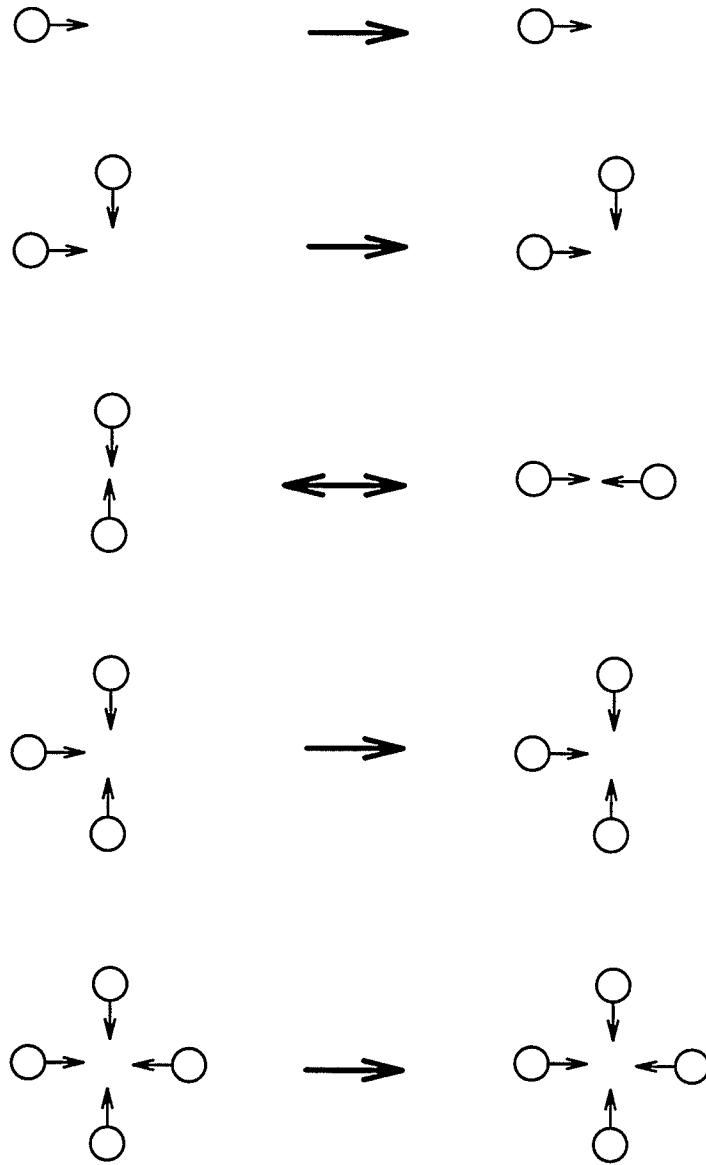


Figure 1.3: Some examples of HPP lattice gas automata collision rules.

cles at a site are rearranged according to the lattice gas rule. In the Advection stage particles move to neighbouring sites.

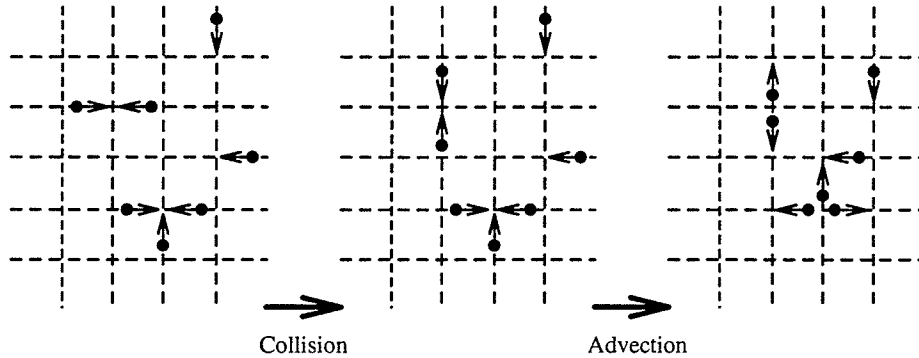


Figure 1.4: One step in the evolution of a lattice-gas dynamics.

As an example, consider a cell which might have only an East moving particle present in it. The collision phase leaves the contents of the cell unchanged. During the advection step, the particle is transferred to the next cell on its right. Hence the particle has moved one step in the East direction.

1.2.2 The FHP Model

The idea of a mass and momentum conserving lattice gas on a triangular grid with hexagonal symmetry was presented by FHP (Frisch, Hasslacher and Pomeau) in [11]. In this model, as shown in Figure 1.5, a site holds a maximum of six particles. Collisions occur when there are exactly two or three particles at a site, arranged as shown in the example. When two particles collide head-on at a site, there are two possible outcomes. Each outcome occurs with equal probability of 0.50. Modifications to this model could be made by allowing for the creation of *rest particles* at sites in the lattice [12]. In Figure 1.5, a double arrow without a number indicates that both forward and reverse events occur with probabilities of 1.0. Similarly, a single arrow without a number indicates that the event following the direction of the arrow occurs

with a probability of 1.0. We shall adhere to this notation for the remainder of this document.

In the HPP model there is an additional conserved quantity (momentum along each horizontal and vertical line in the lattice is conserved). In the FHP model however, there is no additional conserved quantity other than mass and momentum. Also, as will be explained later, the viscosity in the HPP lga is anisotropic. This is not the case in the FHP model.

1.3 CAM-8

Conventional, general-purpose, serial machines are very inefficient as far as CA simulations are concerned. The Information Mechanics Group at the MIT Laboratory for Computer Science has been involved in the development of special-purpose architectures for the efficient evaluation of cellular automata. The 8 module Cellular Automata Machine, CAM-8, is their newest [13]. For CA rules with 16 bits per site, simulations run at about 200 million site updates per second on spaces of up to 32 million sites.

The Cellular Automata Machine is actually a Lattice Gas Machine. Each step in the operation of the machine consists of two stages [13]. A data-update stage during which each cell's contents are sent to the look-up table from which a new value is sent back to the cell. A data-transfer stage during which each cell communicates with its neighbours. The data-update and data-transfer stages correspond to the collision and advection phases of a lattice gas step, respectively.

As an example let us consider the HPP implemented on CAM-8. We use a 4-bit binary representation for each cell in the lattice. The presence of a "1" in bits 0, 1, 2, 3 represents a particle moving in North, South, East or West directions, respectively.

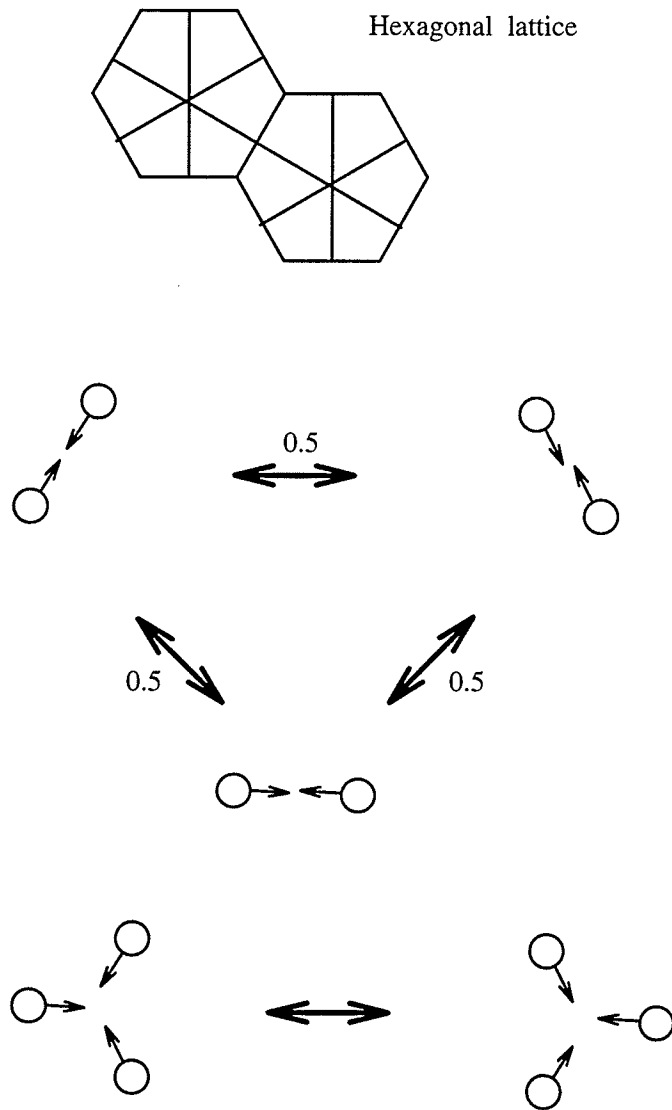


Figure 1.5: Example of possible FHP lattice gas collision rules.

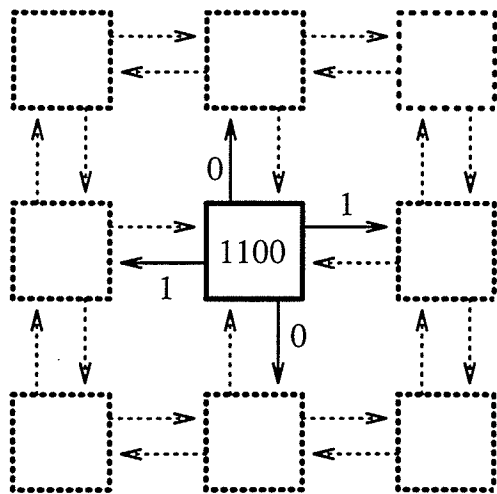
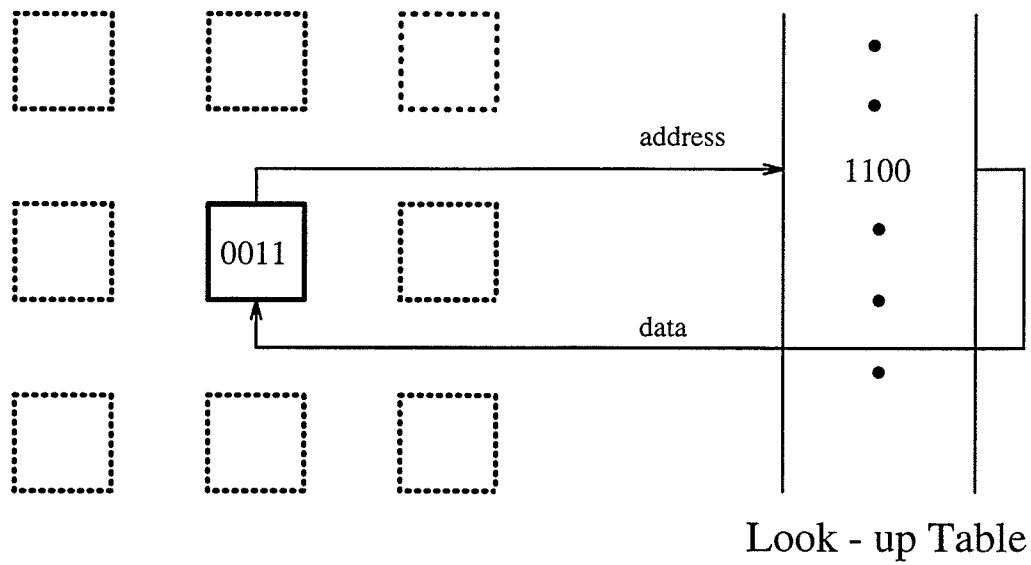


Figure 1.6: Update and Transfer stages in the CAM.

If a cell's state at time t is 0011, then we have two particles, one moving North and one South as shown in Figure 1.6. During the *data-update* step, the state of the cell is referred to a look-up table and the result returned to the cell to become its new state. In this case, 0011 would return a 1100, i.e., two particles, one moving East and the other West. During the *data-transfer* step, the four bits are *kicked* to the four neighbouring cells. Bit 2, for example, is moved over to the next cell on the right since it represents an East moving particle. Bit 0 is moved to the cell to the North and so on. This two-step process applies to every cell within the array of sites. Kicking a bit, r steps, involves the transfer of that bit to the same bit in another cell, r cells away. In the HPP lga for example, the West bit of each cell, during the data-transfer stage, is kicked by -1 in the x direction. Thus, CAM-8 is well suited to the simulation of lattice gas algorithms owing to the nature of its architecture. In actual practice, CAM-8 does not physically move data during the advection or data-transfer stage but uses a pointer-based relative data movement technique [14].

1.4 The Stochastic Element

Very often a Cellular Automaton uses a *random variable* [15] to select one of two or more possible outcomes. In the FHP lattice gas (Figure 1.5) for example, a head-on binary collision has two equally probable outcomes. In order to model a problem of this kind on CAM-8, we use a *probability bit*. One of the bit planes is filled with a certain percentage of 1's. The percentage depends on the probability we want to simulate. At each update stage then, within every cell, the rule checks to see if this bit is set. This is in case we have two possible outputs for any input cell configuration. In general, n bits are needed to implement a stochastic CA with a maximum of 2^n equally possible outcomes. In CAM-8 the random bits may be kicked around (random distances) from one cell to another, thus further randomizing the

lattice (without destroying any bits).

1.5 Macroscopic Quantities

Macroscopic quantities within a lattice gas such as density and flow can be determined using a process of statistical averaging. A sampling window, as shown in Figure 1.7, is created and particles are counted within this region at every iteration or step. The HPP lattice gas automaton could be used to model the wave equation. For small perturbations to an equilibrium background, a density perturbation behaves according to the linear wave equation. Please see Appendix A for details on how the Wave Equation is derived. The perturbation ρ_p thus propagates as

$$\nabla^2 \rho_p = \frac{1}{c_s^2} \frac{\partial^2 \rho_p}{\partial t^2}. \quad (1.1)$$

The microscopic density at a particular cell j will be defined as the density of particles in the cell,

$$\rho_{cell}(x_j, y_j) = \sum_{i=1}^4 N_i(x_j, y_j), \quad (1.2)$$

where (x_j, y_j) indicates the location and $N_i(x_j, y_j)$ indicates presence of particles moving in direction i in cell j . The latter is equivalent to counting the particles inside the cell j .

The macroscopic density ρ at a particular spatial location (x, y) can be determined by averaging the values of ρ_{cell} as

$$\rho(x, y) = \frac{1}{N_T} \sum_R \left(\sum_{i=1}^4 N_i(x_R, y_R) \right), \quad (1.3)$$

where R describes a neighbourhood of cells centred around (x, y) , (x_R, y_R) is the location of a particular cell within R , and N_T is the total number of states within R . For the TM or the TE cases in electromagnetics, the density perturbation ρ_p represents E_z and H_z , respectively.

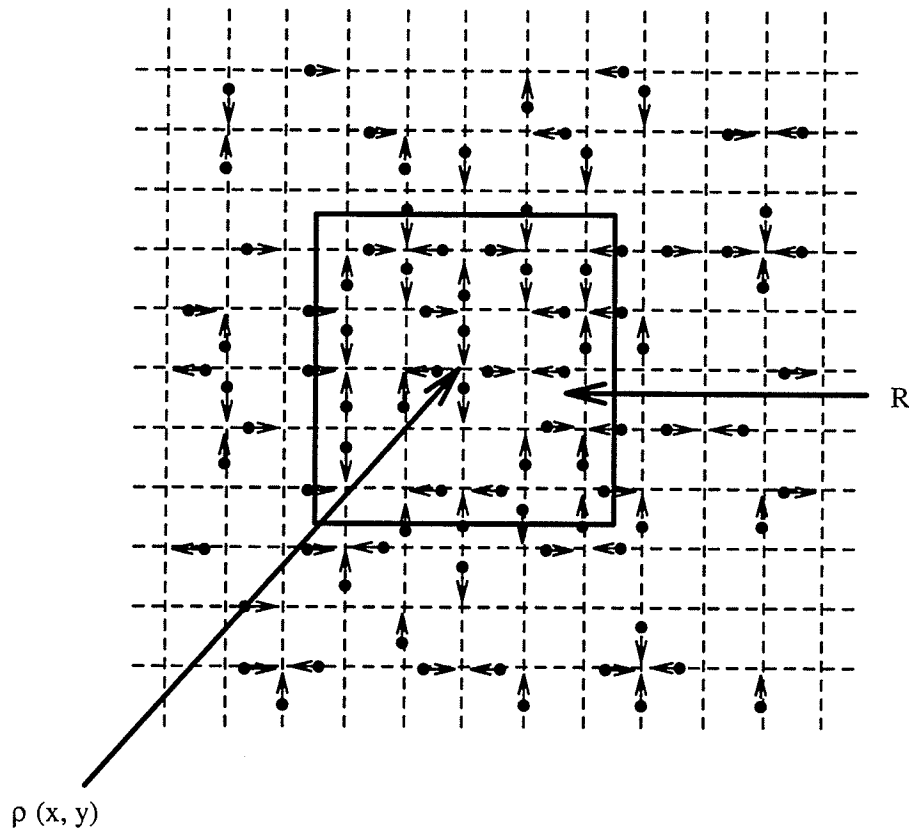


Figure 1.7: Counting particles within a square sampling window.

The individual bits of the lattice gas could be thought of as *kinetic* variables while the density defined in Equation (1.3) is the *hydrodynamic* variable. One interesting aspect of a CA simulation is that even though the microscopic dynamics are simple, the macroscopic properties that emerge are sometimes very complex.

1.6 Summary

Chapter 2 introduces the Lattice Gas Automata and presents a mathematical description of the rules which govern the evolution of such a system. The ideas of detailed and semi-detailed balance and their effects on equilibria in a lattice are determined both theoretically and experimentally. In addition, this chapter discusses various rest particle models and introduces rules which can be used to model inhomogeneous media.

In Chapter 3, the Chapman-Enskog method for lattice gases is presented in a general framework. This is a summarized version of the analysis which was presented by Boghosian and Taylor for the first time in [16].

In Chapter 4, we then apply this very elegant method to a lattice gas with rest particles to determine parameters such as propagation speed and viscosity. The extension to similar models could then be deduced with relative ease.

In Chapter 5, results from different computational experiments carried out on CAM-8 are presented. A comparison with results from the theoretical analysis is made as well.

Experiments are carried out to determine whether different regions can exist in equilibrium with one another in Chapter 6. Experiments to investigate electromagnetic plane wave interaction with dielectric media in two dimensions are carried out as well and results presented.

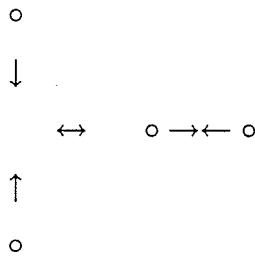
The thesis then concludes with some recommendations for further work and a summary of the differences between the cellular automata approach and conventional numerical techniques.

Chapter 2

Lattice Gas Automata

2.1 Introduction

The HPP lattice gas dynamics are confined to a Cartesian grid in two dimensions. Each site has up to a maximum of four particles, one moving in each of North, South, East and West directions. Head-on collisions cause particles to move away from the lattice node at right-angles to their original direction of motion as shown below.



With the inclusion of a rest particle [17], a site can hold five particles (four moving particles and one stationary particle). The presence or absence of a particle at a site is denoted by a 1 or 0. We shall consider here the case of one rest particle and later generalize it to k rest particles.

The bits of the dependent variable at each site are denoted by $b_i(\mathbf{x}, t)$ where $i = 1, \dots, N_l$, \mathbf{x} denotes a lattice site, and t denotes time. In our rest particle model ($N_l = 5$), we have

$$\begin{aligned} \mathbf{c}^j &= \ell \hat{\mathbf{x}} \cos \frac{\pi}{2}(j-1) + \ell \hat{\mathbf{y}} \sin \frac{\pi}{2}(j-1), & j = 1, 2, 3, 4 \\ &= \mathbf{0}, & j = 5. \end{aligned} \quad (2.1)$$

\mathbf{c}^j represents the velocity states in which particles at a site might exist. ℓ is the characteristic lattice spacing and

$$\ell \mathbf{e}^i \equiv \mathbf{c}^i. \quad (2.2)$$

2.2 Microscopic Dynamics

In what follows we let $b_i(\mathbf{x}, t)$ represent the presence or absence of a particle (its value being 1 or 0, respectively) in the i th velocity state at a particular site \mathbf{x} at time t . In order to write a mathematical description [18] of the microscopic dynamics of this lattice gas, we must derive an equation for $b_i(\mathbf{x}, t + \Delta t)$ in terms of $b_i(\mathbf{x}, t)$. Δt denotes the time step. In the case where the particles simply pass through one another without interacting, the microscopic dynamics could be described by

$$b_i(\mathbf{x} + \mathbf{c}^i, t + \Delta t) = b_i(\mathbf{x}, t). \quad (2.3)$$

Here one bit from a cell is passed to an adjacent cell at the next time step as shown in Figure 2.1. In this figure, a particle moving to the East and one to the West

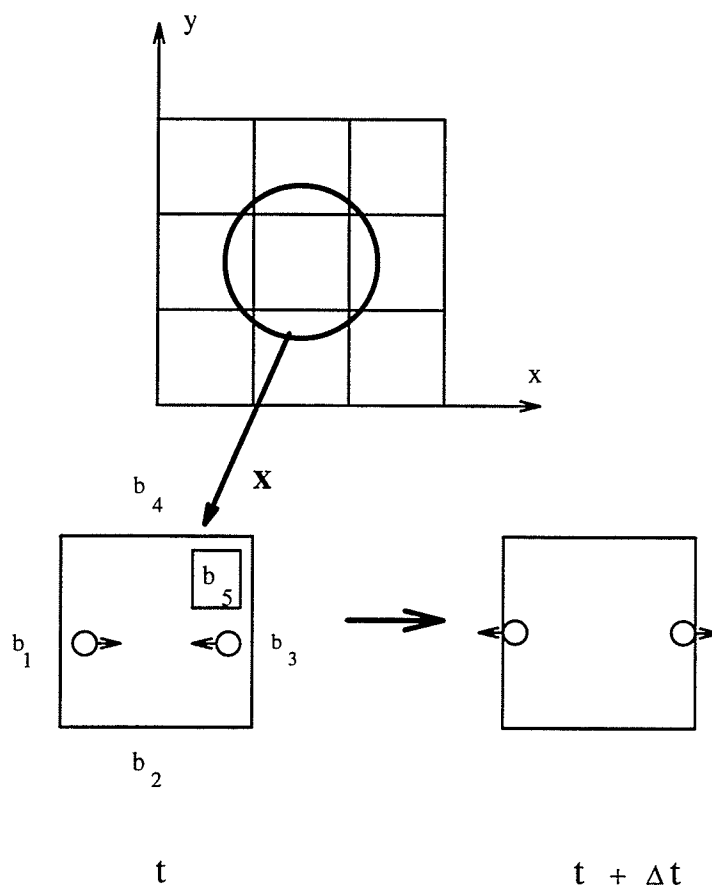
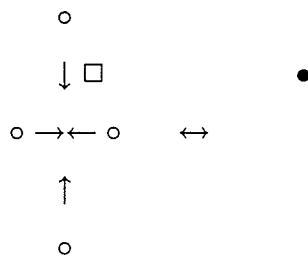


Figure 2.1: A non-interacting particle lattice gas.

are moved over to the next cell on the right and left, respectively. Using Equation (2.3), with $i = 5$, $\mathbf{c}^5 = \mathbf{0}$, and hence the particle does not advect. If we were now to consider collisions between particles at each step, the dynamics could be described by

$$b_i(\mathbf{x} + \mathbf{c}^i, t + \Delta t) = b_i(\mathbf{x}, t) + c_i(\mathbf{b}(\mathbf{x}, t)). \quad (2.4)$$

where, $c_i(\mathbf{b}(\mathbf{x}, t))$ is the *microscopic collision operator* and $\mathbf{b}(\mathbf{x}, t)$ is the vector of all bits in cell \mathbf{x} at time t . Several possible collision rules could be described using the above notation but we shall consider the $4m \leftrightarrow 1r$ model. In this model, shown below, four moving particles give rise to a rest particle of mass $4m$ if none existed prior to their coming together. In addition, the reverse event might occur, i.e., the creation of four moving particles if a rest state was occupied and there were no moving particles present.



Furthermore, the only other collision event that occurs is a binary head-on collision. In this case the colliding particles move away from the site at right angles to their original direction of approach just as in the HPP. This happens with or without the presence of a rest particle at the site.

The following set of equations then describe the dynamics of this model, where we use the subscripts E, N, W, S, R for numbers $j = 1, 2, 3, 4, 5$ (Equation (2.1)), respectively.

$$b_E(x+\ell, y, t+\Delta t) = b_E + c_E = b_E + \overline{b_E} \overline{b_N} \overline{b_W} \overline{b_S} - b_E \overline{b_N} \overline{b_W} \overline{b_S} - b_E b_N b_W b_S \overline{b_R} + \overline{b_E} \overline{b_N} \overline{b_W} \overline{b_S} b_R. \quad (2.5)$$

$$b_N(x, y+\ell, t+\Delta t) = b_N + c_N = b_N + b_E \overline{b_N} \overline{b_W} \overline{b_S} - \overline{b_E} \overline{b_N} \overline{b_W} \overline{b_S} - b_E b_N b_W b_S \overline{b_R} + \overline{b_E} \overline{b_N} \overline{b_W} \overline{b_S} b_R. \quad (2.6)$$

$$b_W(x-\ell, y, t+\Delta t) = b_W + c_W = b_W + \overline{b_E} \overline{b_N} \overline{b_W} \overline{b_S} - b_E \overline{b_N} \overline{b_W} \overline{b_S} - b_E b_N b_W b_S \overline{b_R} + \overline{b_E} \overline{b_N} \overline{b_W} \overline{b_S} b_R. \quad (2.7)$$

$$b_S(x, y-\ell, t+\Delta t) = b_S + c_S = b_S + b_E \overline{b_N} \overline{b_W} \overline{b_S} - \overline{b_E} \overline{b_N} \overline{b_W} \overline{b_S} - b_E b_N b_W b_S \overline{b_R} + \overline{b_E} \overline{b_N} \overline{b_W} \overline{b_S} b_R. \quad (2.8)$$

$$b_R(x, y, t + \Delta t) = b_R + c_R = b_R + b_E b_N b_W b_S \overline{b_R} - \overline{b_E} \overline{b_N} \overline{b_W} \overline{b_S} b_R. \quad (2.9)$$

The collision details of an n -bit model could also be completely specified by a 2^n by 2^n Boolean transition matrix, a , whose element $a(s \rightarrow s')$ is unity if and only if the particles in state s always collide to yield particles in state s' . Since there is only one incoming state for each outgoing state,

$$\sum_{s'} a(s \rightarrow s') = 1. \quad (2.10)$$

2.3 The Ensemble Average

In what follows, the ensemble average of the quantity $b_i(\mathbf{x}, t)$ is denoted by $N^i(\mathbf{x}, t)$. That is,

$$N^i(\mathbf{x}, t) = \langle b_i(\mathbf{x}, t) \rangle. \quad (2.11)$$

It is important to note that the ensemble average value of bit i at position \mathbf{x} and time t is a real quantity while $b_i(\mathbf{x}, t)$ is a binary value.

When we consider the collision operator in Equations (2.5)-(2.9), we encounter the average of a product. According to the Boltzmann Molecular Chaos Assumption (BMCA) [18], the streaming phase of the simulation decorrelates the bits at every site. In other words we assume that colliding particles have never encountered one another before. This approximation is reasonably accurate in three or more dimensions but in two dimensions one must consider renormalization [16]. If we neglect correlations then,

$$\langle b_i b_j \rangle = \langle b_i \rangle \langle b_j \rangle. \quad (2.12)$$

Also from Equation (2.4),

$$\begin{aligned} \langle b_i(\mathbf{x} + \mathbf{c}_i, t + \Delta t) \rangle &= \langle b_i(\mathbf{x}, t) + c_i(\mathbf{b}(\mathbf{x}, t)) \rangle \\ &= \langle b_i(\mathbf{x}, t) \rangle + \langle c_i(\mathbf{b}(\mathbf{x}, t)) \rangle \\ &= \langle b_i(\mathbf{x}, t) \rangle + c_i(\langle \mathbf{b}(\mathbf{x}, t) \rangle) \\ &= N^i(\mathbf{x}, t) + C_i(\mathbf{N}(\mathbf{x}, t)). \end{aligned}$$

And therefore,

$$N^i(\mathbf{x} + \mathbf{c}^i, t + \Delta t) = N^i(\mathbf{x}, t) + C_i(\mathbf{N}). \quad (2.13)$$

This is known as the *Lattice Boltzmann Equation*. Also, the ensemble average of $a(s \rightarrow s')$ is given by

$$A(s \rightarrow s') = \langle a(s \rightarrow s') \rangle. \quad (2.14)$$

2.4 Semi-Detailed Balance

The semi-detailed balance criterion is used to derive the equilibrium particle concentrations in a lattice gas simulation. Simply stated, it checks to see if the sum of probabilities of each input configuration that leads to a particular output configuration of particles, is one. As stated in [16], a lattice gas is said to obey detailed balance if its transition matrix satisfies

$$A(s \rightarrow s') = A(s' \rightarrow s). \quad (2.15)$$

This means that the forward and reverse events are equally probable. It is said to obey semi-detailed balance if its transition matrix satisfies

$$\sum_s A(s \rightarrow s') = 1. \quad (2.16)$$

It is important to note the difference between the above and

$$\sum_{s'} A(s \rightarrow s') = 1, \quad (2.17)$$

which is a statement of conservation of probability. The manner in which the above conditions affect a lattice gas simulation will be shown in sections 2.9 and 2.10. The boolean transition matrix for the $4m \leftrightarrow 1r$ model is shown in Figure 2.2. In this case both detailed as well as semi-detailed balance are adhered to. All possible input particle configurations (s) are not shown in the matrix; only those involving collisions. The remaining rules could be obtained by referring to the HPP rule in which particles simply pass through one another unless a binary head-on collision occurs. In the $4m \leftrightarrow 1r$ model, the binary head-on collision occurs in the presence or absence of a rest particle. This is denoted by an “x” in Figure 2.2. We shall continue to use this notation to describe collision rules which do not depend on the presence or absence of rest particles. It should be noted that collision rules are rotationally symmetric (under 90° rotations).

2.5 Conserved Quantities

A characteristic feature of lattice gases is the presence of some form of conservation [19]. When modelling the diffusion equation, for instance, the total number of particles in the lattice remains the same. In this situation, we have only one conserved quantity, namely, particle mass. Mass is conserved in each collision, i.e., at the microscopic level. As a result, mass is conserved macroscopically. In the case of lattice gas fluids in 2 dimensions, we have 3 conserved quantities, viz., the total number of particles, the x-momentum and the y-momentum. The x and y momenta are conserved at both the microscopic as well as macroscopic level.

From Equations (2.5)-(2.9) and (2.13), it follows that,

$$C_E + C_N + C_W + C_S + 4C_R = 0. \quad (2.18)$$


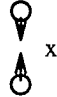



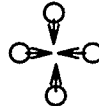




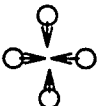

		s'					
$a(s \rightarrow s')$			 x	 x			
s		1	0	0	0	0	0
	 x	0	1	0	0	0	0
	 x	0	0	1	0	0	0
		0	0	0	1	0	0
		0	0	0	0	1	0
		0	0	0	0	0	1

Figure 2.2: Transition matrix for the $4m \leftrightarrow 1r$ lattice gas.

	$\mu = 1$	$\mu = 2$	$\mu = 3$
$i = E$	1	\hat{x}	0
$i = N$	1	0	\hat{y}
$i = W$	1	$-\hat{x}$	0
$i = S$	1	0	$-\hat{y}$
$i = R$	4	0	0

Table 2.1: Table for q_i^μ

$$C_E - C_W = 0. \quad (2.19)$$

$$C_N - C_S = 0. \quad (2.20)$$

Where the first equation indicates the conservation of mass while the latter two represent the conservation of momentum in the x and y directions, respectively. If we denote the value of the μ th conserved quantity at site \mathbf{x} and at time t by $q^\mu(\mathbf{x}, t)$ where,

$$q^\mu(\mathbf{x}, t) = \sum_{i=1}^{N_i} q_i^\mu b_i(\mathbf{x}, t), \quad \mu = 1, \dots, n_c. \quad (2.21)$$

$n_c = 3$ in the $4m \leftrightarrow 1r$ lattice gas. This gives us 3 equations and 5 unknowns. The coefficients q_i^μ satisfy

$$0 = \sum_{i=1}^{N_i} q_i^\mu c_i(\mathbf{b}), \quad \mu = 1, \dots, n_c. \quad (2.22)$$

For example, from Equations (2.18)-(2.20) the values for q_i^μ are presented in Table 2.1.

Then considering ensemble-averaged values of the conserved quantities,

$$Q^\mu(\mathbf{x}, t) \equiv \langle q^\mu(\mathbf{x}, t) \rangle = \sum_{i=1}^{N_l} q_i^\mu N^i(\mathbf{x}, t), \quad \mu = 1, \dots, n_c. \quad (2.23)$$

2.6 The Equilibrium Particle Distribution

In this section we derive the individual particle concentrations for each direction (North, South, East, West and Rest) in terms of the coefficients, q_i^μ , under equilibrium conditions. N_0^j is the zero or lowest order equilibrium for the j th particle in the lattice. The collision operator for each particle direction could be written in a more general manner. If s_j denotes the j th bit of state s (its value is either 0 or 1), and $P(s)$, the probability that that a state s exists at any site then,

$$P(s) = \prod_{j=1}^{N_l} (N_0^j)^{s_j} (1 - N_0^j)^{1-s_j}. \quad (2.24)$$

As an example, $P(01001) \equiv P(\overline{R}S\overline{W}NE)$ is the probability that we have only one South and one East bit present at the site under consideration. Using the notation just stated, this could be written as

$$P(01001) = N_0^1(1 - N_0^2)(1 - N_0^3)N_0^4(1 - N_0^5).$$

The ensemble averaged collision operator, C_i could be written as

$$C_i = \sum_{s, s'} A(s \rightarrow s')(s'_i - s_i)P(s). \quad (2.25)$$

To better illustrate this mathematical definition let us consider the HPP lattice gas in which a binary head-on collision between a West-East pair gives a North-South pair

of particles. In this situation $A(0101 \rightarrow 1010) = 1$, $s'_E = 0$ and $s_E = 1$. The latter two represent the states of the East bit after and before the collision, respectively. Also the reverse is true, i.e., $A(1010 \rightarrow 0101) = 1$, $s'_E = 1$ and $s_E = 0$. In all cases in which collisions do not occur, $(s'_i - s_i) = 0$. C_E could then be written as

$$C_E = N_0^S \overline{N_0^W} N_0^N \overline{N_0^E} - \overline{N_0^S} N_0^W \overline{N_0^N} N_0^E.$$

The collision operator C_E then, is simply a collection of terms which state conditions (particle configurations) which lead to the creation and removal of an East bit from a site.

Now substituting Equation (2.24) in (2.25),

$$\begin{aligned} C_i &= \sum_{s,s'} A(s \rightarrow s') (s'_i - s_i) \prod_{j=1}^n (N_0^j)^{s_j} (1 - N_0^j)^{1-s_j} \\ &= \left(\prod_j (1 - N_0^j) \right) \sum_{s,s'} A(s \rightarrow s') (s'_i - s_i) \prod_j \left(\frac{N_0^j}{1 - N_0^j} \right)^{s_j}. \end{aligned} \quad (2.26)$$

We assume that

$$\frac{N_0^j}{1 - N_0^j} = \exp\left(\sum_{\gamma=1}^{n_c} \alpha_\gamma q_j^\gamma\right). \quad (2.27)$$

This gives us 5 equations with 3 parameters in the $4m \leftrightarrow 1r$ model. Then C_i could be rewritten as

$$C_i = \left(\prod_j (1 - N_0^j) \right) \sum_{s,s'} A(s \rightarrow s') (s'_i - s_i) \prod_j \exp\left(\sum_\gamma \alpha_\gamma q_j^\gamma\right)^{s_j}$$

$$\begin{aligned}
&= \left(\prod_j (1 - N_0^j) \right) \sum_{s,s'} A(s \rightarrow s') (s'_i - s_i) \exp\left(\sum_j \sum_\gamma \alpha_\gamma q_j^\gamma s_j\right) \\
&= \left(\prod_j (1 - N_0^j) \right) \sum_{s,s'} A(s \rightarrow s') (s'_i - s_i) \exp\left(\sum_\gamma \alpha_\gamma Q^\gamma(s)\right). \quad (2.28)
\end{aligned}$$

$Q^\gamma(s) = \sum_j q_j^\gamma s_j = Q^\gamma(s')$, and represents the γ th conserved quantity.

Thus,

$$\begin{aligned}
C_i &= \left(\prod_j (1 - N_0^j) \right) \left\{ \sum_{s,s'} A(s \rightarrow s') s'_i \exp\left(\sum_\gamma \alpha_\gamma Q^\gamma(s)\right) \right. \\
&\quad \left. - \sum_{s,s'} A(s \rightarrow s') s_i \exp\left(\sum_\gamma \alpha_\gamma Q^\gamma(s)\right) \right\} \\
&= \left(\prod_j (1 - N_0^j) \right) \left\{ \sum_{s'} s'_i \exp\left(\sum_\gamma \alpha_\gamma Q^\gamma(s)\right) - \sum_s s_i \exp\left(\sum_\gamma \alpha_\gamma Q^\gamma(s)\right) \right\} \\
&= 0. \quad (2.29)
\end{aligned}$$

Here we have made use of the semi-detailed balance and conservation of probability criteria. Hence, stable and spatially uniform Boltzmann equilibria exist for any lattice gas obeying semi-detailed balance. These equilibria are described by the Fermi-Dirac distribution,

$$N_0^j = \frac{1}{1 + \exp\left(-\sum_{\gamma=1}^{n_c} \alpha_\gamma q_j^\gamma\right)}, \quad j = 1, \dots, 5. \quad (2.30)$$

The α_γ are n_c arbitrary multipliers. An example of this distribution is illustrated in the next section.

2.7 Equilibria in the $4m \leftrightarrow 1r$ Lattice Gas

In this section, we shall use Equation (2.30) to calculate the equilibrium particle distributions for North, South, East, West and Rest particles in the $4m \leftrightarrow 1r$ lattice gas. Equilibrium particle concentrations are used as the starting point in setting up most lattice gas experiments. Let us assume that bit i at a site represents the presence of a particle of unit mass and momentum $\mathbf{c}^i/\Delta t$. The ensemble-averaged mass and momentum densities could be written as

$$\rho = \sum_{i=1}^{N_l} N^i \equiv Q^\rho \quad (2.31)$$

and

$$\mathbf{u} = \sum_{i=1}^{N_l} \frac{\mathbf{c}^i}{\Delta t} N^i \equiv Q^\mathbf{u}, \quad (2.32)$$

respectively. To simplify the analysis, we use $|\mathbf{c}^i| = \Delta t = 1$. Hence in the case of our lattice gas, we have $q_i^\rho = 1$ for $i = 1, 2, 3, 4$ and $q_i^\rho = 4$ for $i = 5$. Also, $q_i^\mathbf{u} = \mathbf{e}^i$ for $i = 1, 2, 3, 4$ and $q_i^\mathbf{u} = \mathbf{0}$ for $i = 5$. For an incompressible fluid, the conserved densities are ordered [20] in the expansion parameter, ϵ as follows.

$$\rho = \rho_0 + \epsilon^2 \rho_2. \quad (2.33)$$

$$\mathbf{u} = \epsilon \mathbf{u}_1. \quad (2.34)$$

Thus, the zero-order Fermi-Dirac equilibrium is found by considering only q^ρ in Equation (2.30). Hence we get

$$N_0^i = \frac{1}{1 + e^{-\alpha}} \equiv f_m, \quad i = 1, 2, 3, 4. \quad (2.35)$$

$$N_0^i = \frac{1}{1 + e^{-4\alpha}} \equiv f_r, \quad i = 5. \quad (2.36)$$

From the above two equations we get

$$f_r = \frac{f_m^4}{f_m^4 + (1 - f_m)^4}. \quad (2.37)$$

Hence, the density of the rest bit (mass = 4m) is related by a non-linear law to the average density of the moving particles (mass = m). We could then use this to initialize moving and rest particles in the lattice in such a way that their concentrations do not change with time, during an experiment. For example, if we initialize each of North, South, East and West directions with a density x , then the Rest position at each site must be initialized with a density y , where,

$$y = \frac{x^4}{x^4 + (1 - x)^4}.$$

2.8 Experimental Results

In this section we verify the theoretical results derived in previous sections for equilibria in lattice gas experiments. These experiments are run on CAM-8, which is a special-purpose cellular automata machine.

2.8.1 Rest Particles of Mass 4m

The $4m \leftrightarrow 1r$ experiment was set up on CAM-8. The simulation space was a rectangular lattice (size 2048 x 512). The lattice was initialized with only moving particles.

Each direction was initialized with an equal probability, that is, there was no net flow. Equilibrium was reached after a few steps. The particle densities were calculated by summing the number of moving and rest particles within a sampling window and then dividing by the size of the window (size 99 by 99).

$$\text{Density of rest particles} = (4f_r) = \frac{4 * \sum_{\text{window}} \text{rp}'s}{9801}.$$

$$\text{Density of moving particles} = (f_m) = \frac{\sum_{\text{window}} \text{mp}'s}{4 * 9801}.$$

This was done at every time step for 10000 iterations. Results of the simulation are shown in Figure 2.3. The solid line represents the relationship between moving and rest particles using Equation (2.37).

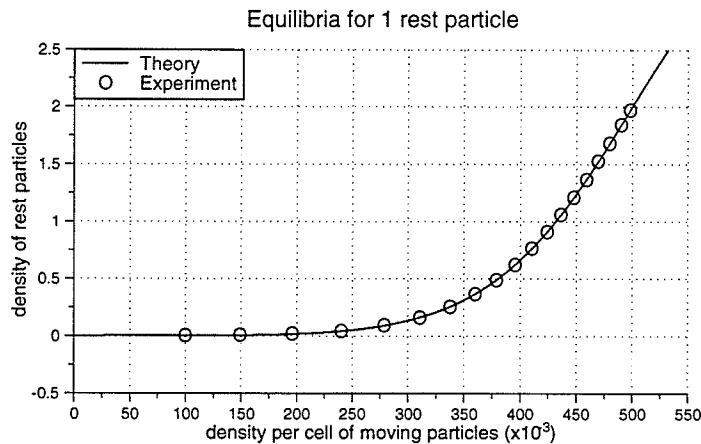
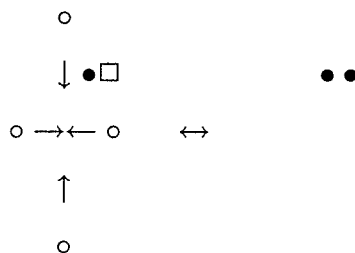


Figure 2.3: Equilibria for 1 rest particle of mass $4m$

This experiment was then modified by allowing for the existence of two rest particles at a site, as shown on the next page.



Results obtained are shown in Figure 2.4. Hence in the one rest particle case we have good agreement between experimental and theoretical values. The experimental results from the stack model, however, don't match as closely with values obtained using Equation (2.37). The reason for this error will be explained later in section 2.11.

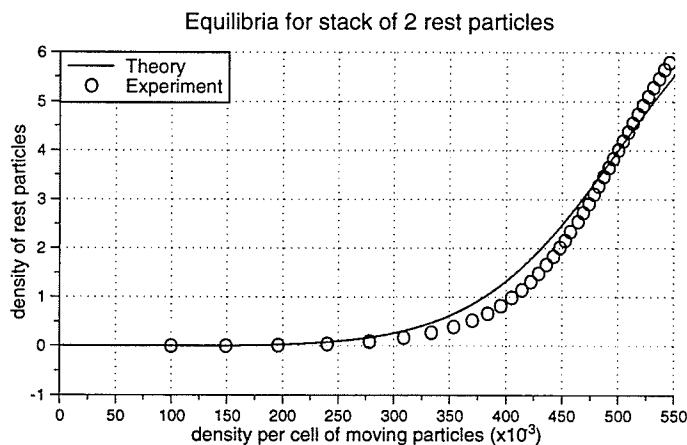


Figure 2.4: Equilibria for 2 rest particles of mass $4m$ each

2.8.2 Rest Particles of Mass $2m$

Yet another variation to the HPP lattice gas automaton, which was discussed in section 1.2.1, would be the creation of a rest particle, with twice the mass of a moving particle. This occurs with a probability of 0.5 when two particles collide head-on. This is an example of a stochastic lattice gas which was discussed earlier in Chapter 1, section 1.4. In order to implement this rule a random bit-plane is filled with 50% 1's and 50% 0's. Then a 1 occurs at any site with a probability of 0.5. This is used to decide which of the two probabilistic events is to occur. Collision details are shown in Figure 2.5. In another model, a rest particle of mass $2m$ is created using 3-particle collisions as shown in Figure 2.6.

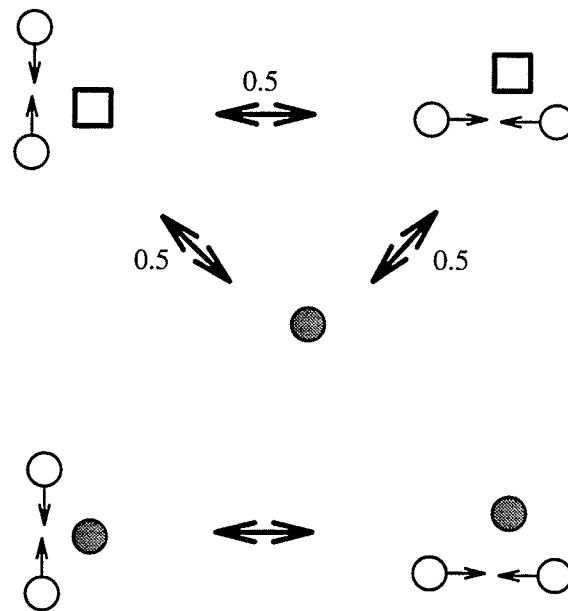


Figure 2.5: Collision details for the $2m \leftrightarrow 1r$ model

The $2m \leftrightarrow 1r$ lattice gas could be developed in the same manner as the $4m \leftrightarrow 1r$, with changes in the collision rules resulting in changes in the collision operator.

Figure 2.6: Collision details for the $3m \leftrightarrow 1r + 1m$ model

$$\begin{aligned}
 c_E &= 0.5\overline{b_E b_N b_W b_S b_R} + \overline{b_E b_N b_W b_S b_R} + 0.5\overline{b_E b_N b_W b_S b_R} - \overline{b_E b_N b_W b_S b_R} - \overline{b_E b_N b_W b_S b_R} \\
 &= c_W.
 \end{aligned}$$

$$\begin{aligned}
 c_N &= 0.5\overline{b_E b_N b_W b_S b_R} + \overline{b_E b_N b_W b_S b_R} + 0.5\overline{b_E b_N b_W b_S b_R} - \overline{b_E b_N b_W b_S b_R} - \overline{b_E b_N b_W b_S b_R} \\
 &= c_S.
 \end{aligned}$$

$$c_R = 0.5\overline{b_E b_N b_W b_S b_R} + 0.5\overline{b_E b_N b_W b_S b_R} - \overline{b_E b_N b_W b_S b_R}.$$

From the above equations and Equation (2.13), the three conservation equations could be written as

$$C_E + C_N + C_W + C_S + 2C_R = 0. \quad (2.38)$$

$$C_E - C_W = 0. \quad (2.39)$$

$$C_N - C_S = 0. \quad (2.40)$$

The concentrations of moving and rest particles are related as

$$f_r = \frac{f_m^2}{f_m^2 + (1 - f_m)^2}. \quad (2.41)$$

f_r and f_m are the densities of the rest and moving particles respectively.

Once again, equilibria were measured for each of the above experiments using a simulation space with the same dimensions as in the $4m \leftrightarrow 1r$ lattice gas experiment. The experimental values compare well with the curve obtained using Equation (2.41) and are shown in Figure 2.7. In addition, an experiment in which both 2-body as well as 3-body collisions led to the creation of rest particles was conducted. This was done in an attempt to create rules that are maximally random with respect to events that can occur within the lattice [21]. Furthermore, none of the rules violate either detailed or semi-detailed balance. Figure 2.7 indicates that equilibria do not change by any significant amount and they compare well with theory.

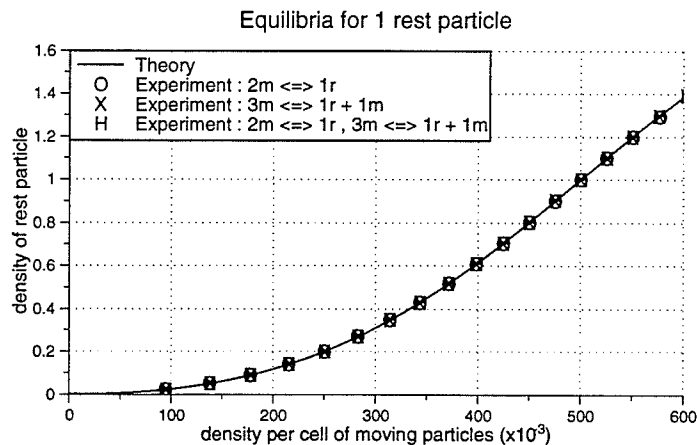


Figure 2.7: Equilibria for 1 rest particle of mass $2m$

The idea of the stack as shown in Figure 2.8, is applied to this model as well. Once

again, the experimental values don't agree as well with theory (Equation (2.41)) as shown in Figure 2.9. It is interesting to note, however, that the experimental equilibria for each of the above experiments agree well with each other (even though they do not match to the theoretically determined equilibria). The reason for the experimental error will be explained later in section 2.11.

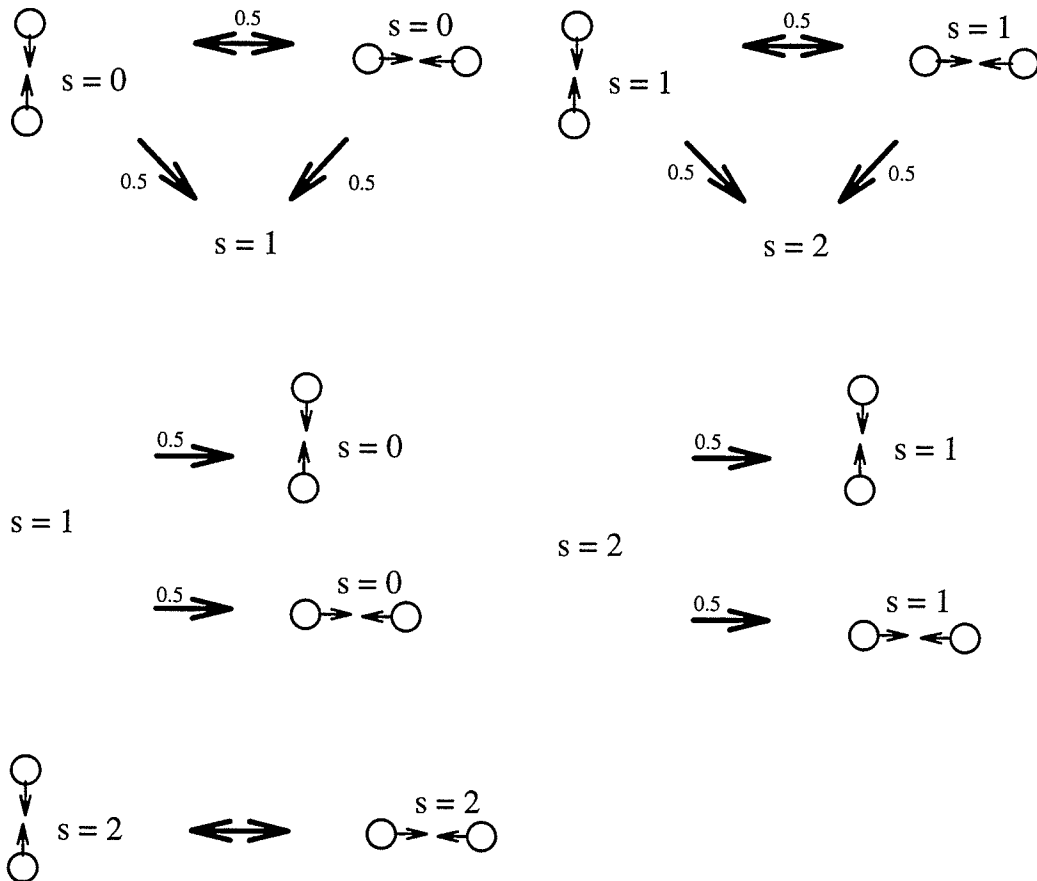


Figure 2.8: Collision details for the $2m \leftrightarrow 1r$ stack

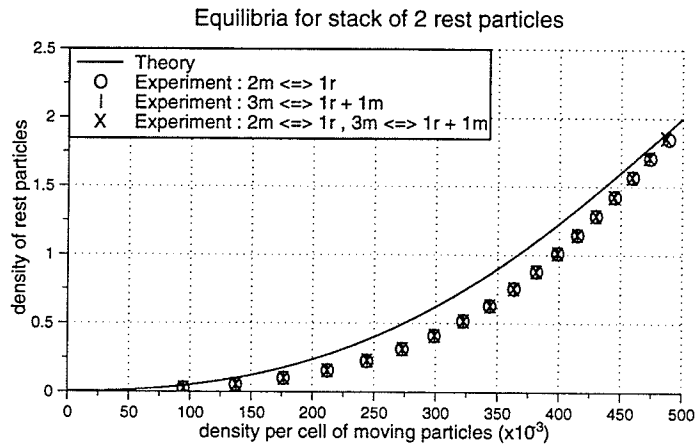


Figure 2.9: Equilibria for 2 rest particles of mass $2m$ each

2.9 Violation of Semi-Detailed Balance

Consider a model which allows for the creation of a rest-particle (mass $2m$, where m is the mass of the moving particle). Two different types of collisions, 4-body and 2-body, are allowed to occur as shown in Figure 2.10.

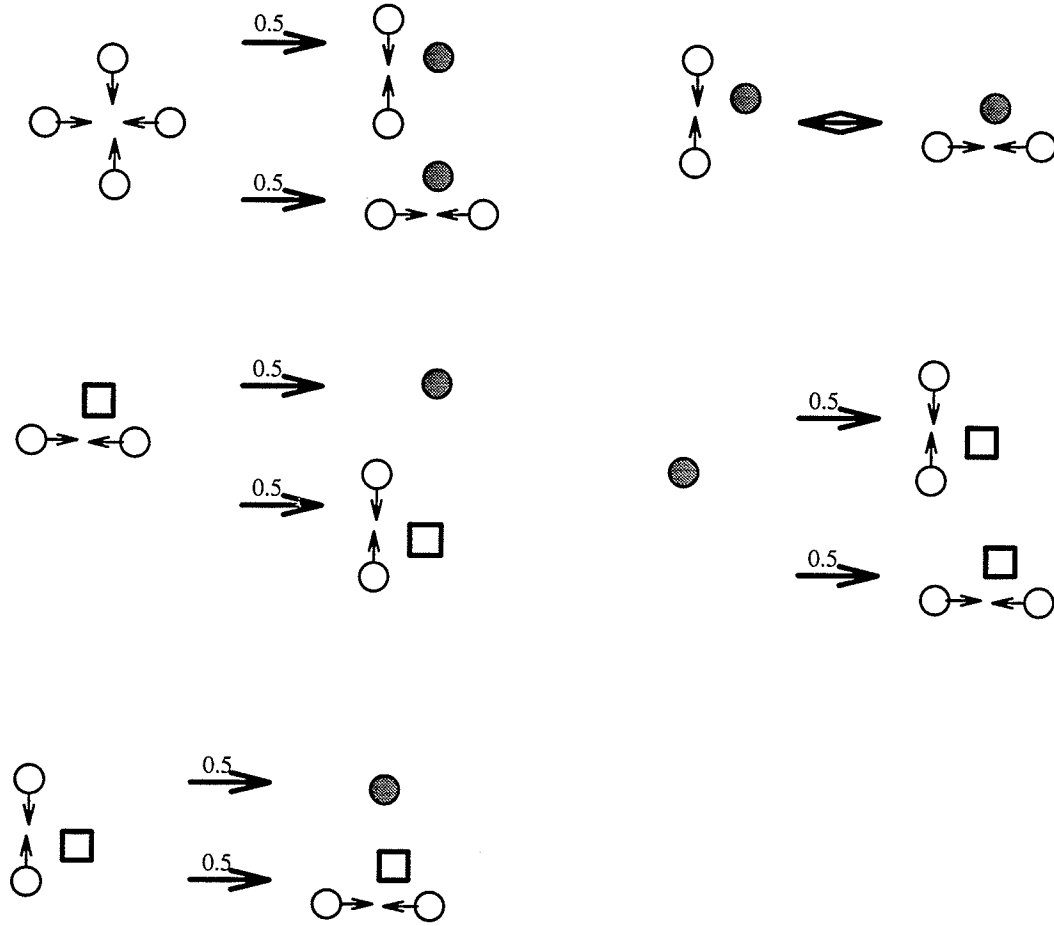


Figure 2.10: Collision details for a model that violates SDB

If the final state s' after collision is

$$s' = \begin{array}{c} \circ \\ \downarrow \\ \bullet \\ \uparrow \\ \circ \end{array}$$

Adding all the initial states s that lead to s' we have,

$$\sum_s A(s \rightarrow s') = 1.5. \quad (2.42)$$

Thus semi-detailed balance is violated.

The solid line in Figure 2.11 shows the theoretical relationship between rest and moving particles using Equation (2.41). Experimental results from a simulation conducted on CAM-8 are plotted as well and the error is quite obvious. This experiment thus proves that the semi-detailed balance condition is necessary for the existence of the Fermi-Dirac particle distribution in a lattice.

2.10 Violation of Detailed Balance

In this section we conduct an experiment which violates the condition of detailed balance. In other words, the forward and reverse collision events occur with different probabilities. Figure 2.12 shows the possible outcomes of two-body collision in a model that violates detailed balance.

a and b are probabilities with which the events occur. If $b = 1 - a$, semi-detailed balance is obeyed. However, since the forward and reverse events are not equally likely ($a \neq b$), detailed balance is violated. The theoretical relationship between moving and

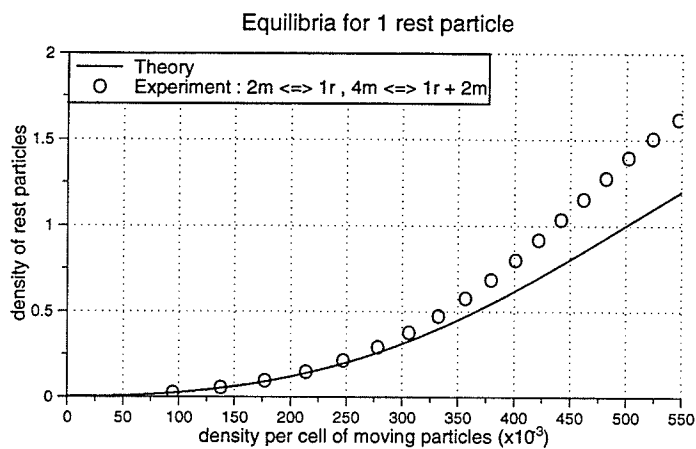


Figure 2.11: Equilibria in the case when SDB is violated

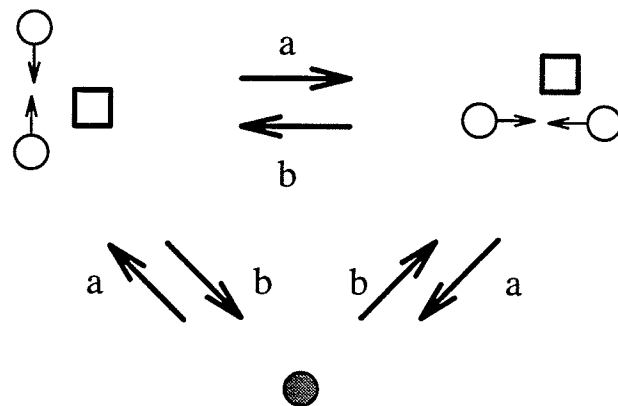


Figure 2.12: Collision details for a model in which DB is violated

rest particle densities is obtained from Equation (2.41). An experiment was conducted on CAM-8 with the same lattice size as in the previous experiments. Furthermore, $a = 0.2$. Results are shown in Figure 2.13. In deriving a theoretical expression for the Fermi-Dirac equilibria, the only necessary conditions were the conservation of probability (Equation (2.17)) and the semi-detailed balance criterion (Equation (2.16)). Violation of detailed balance does not have any effect on the equilibria, as expected.

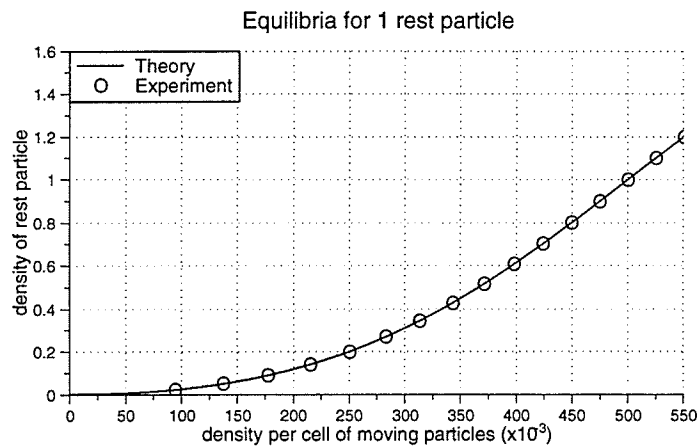


Figure 2.13: Equilibria in the case when DB is violated

2.11 The Particle Pool

In the previous models where multiple rest particles at a site were modelled, a newly created rest particle always occupied the first vacant rest bit, and then the second, and so on. A model in which a rest particle is created and allowed to occupy *any* of the possible rest positions may be described by the collisions shown in Figure 2.14

(for rest particles of mass $2m$) and in Figure 2.15 (for rest particles of mass $4m$). This can be visualized as a pool of particles rather than a stack.

In order to simplify the programming of such a model into the CAM, we could implement a stack (of length 2) as shown in Figure 2.16 and Figure 2.17 for the $2m$ and $4m$ cases, respectively. The equilibrium particle concentrations from the simulations are plotted in Figure 2.18 and Figure 2.19 where the solid line describes the relationship between moving and rest particles in the $2m$ (Equation (2.41)) and $4m$ (Equation (2.37)) cases, respectively. The $2m \leftrightarrow 1r$ case with a stack length of 3 is shown in Figure 2.20(a). Results from this simulation are plotted in the graph in Figure 2.20(b). The solid line once again results from Equation (2.41).

Let us now to consider the stack model in the $4m \leftrightarrow 1r$ lattice gas and decompose it into the particle pool. Figure 2.21 shows the rule for the $s=2$ case. There are 2 possible situations with 4 moving particles and $s=1$. Each of these gives $s=2$ with a probability of 1, thus violating semi-detailed balance. A similar argument could be applied in the $2m \leftrightarrow 1r$ lattice gas. Hence the errors in our earlier experiments. In constructing a lattice gas rule for multiple rest particles at a site, it would then be wise to use the particle pool model as our starting point. The probabilities with which different collision events occur would then be constrained by the conservation of probability and the condition of semi-detailed balance.

2.12 Implementing a Stochastic Model

In experiments where the collision phase involves a probabilistic outcome, we utilize a random bit (discussed in section 1.4). This bit is initialized in the lattice with a certain probability. During the course of the experiment it is kicked around (in the advection phase) to make the occurrence of the probabilistic event more random. The

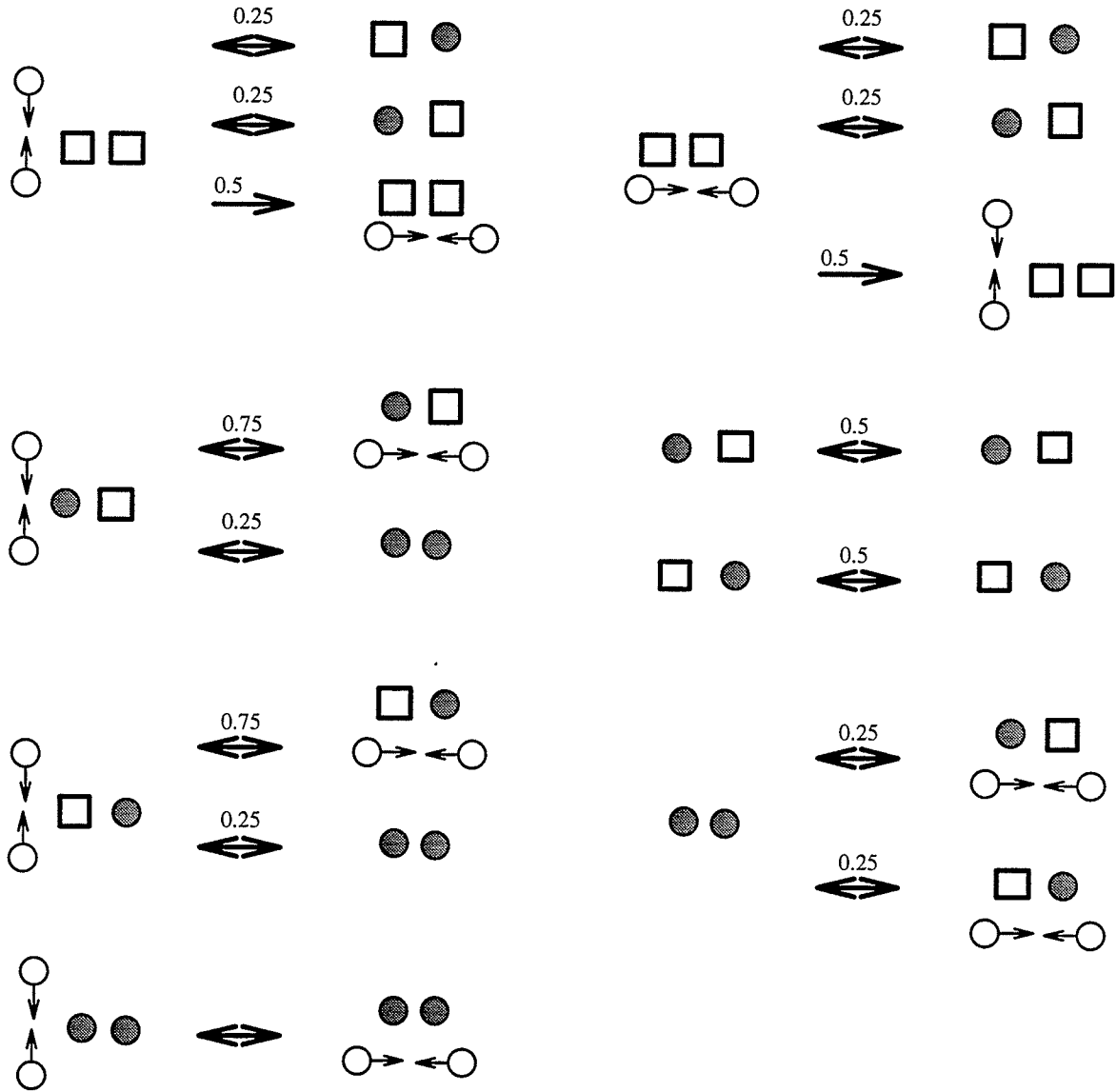


Figure 2.14: Collision details for the modified $2m \leftrightarrow 1r$ stack

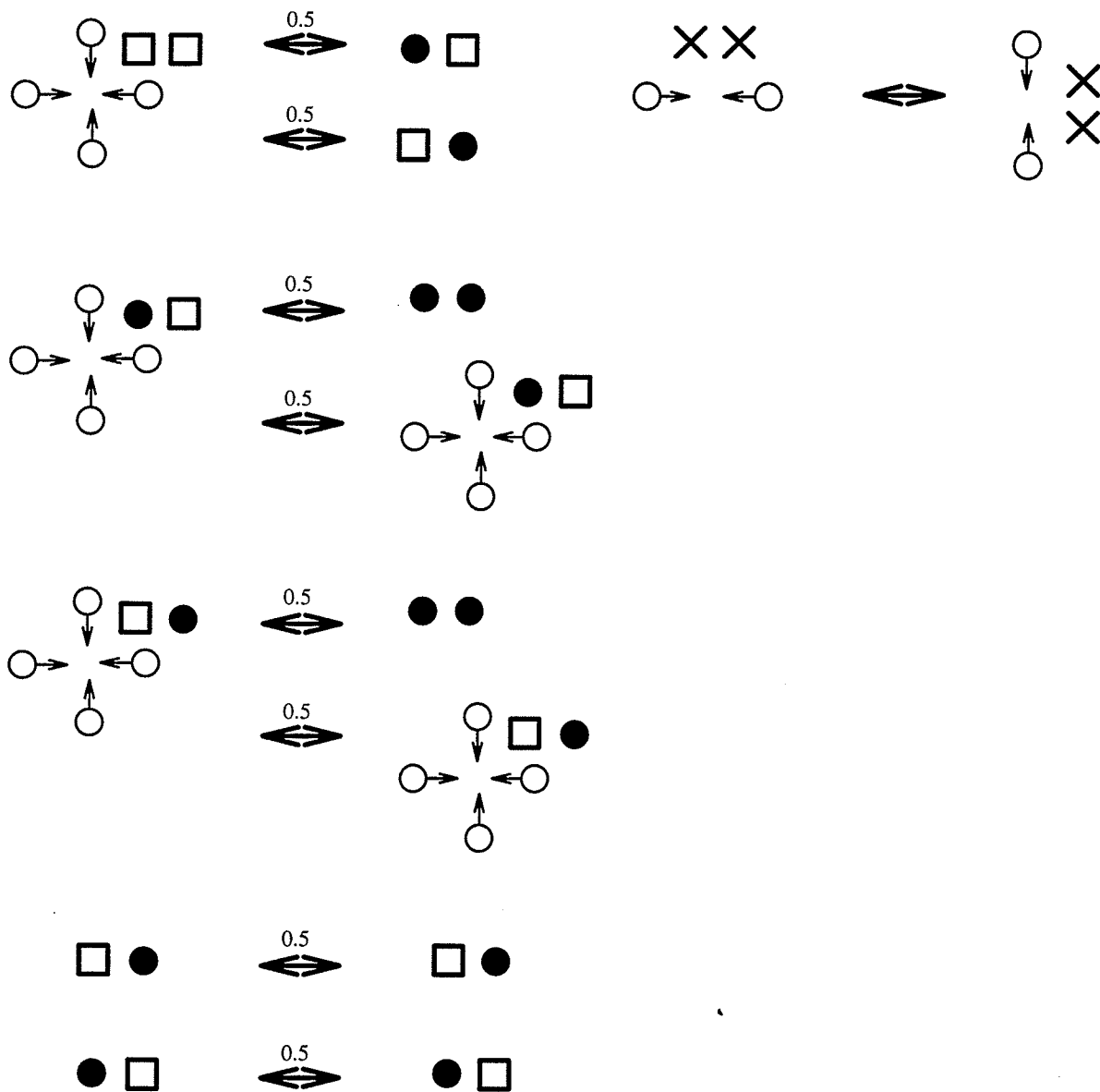


Figure 2.15: Collision details for the modified $4m \leftrightarrow 1r$ stack

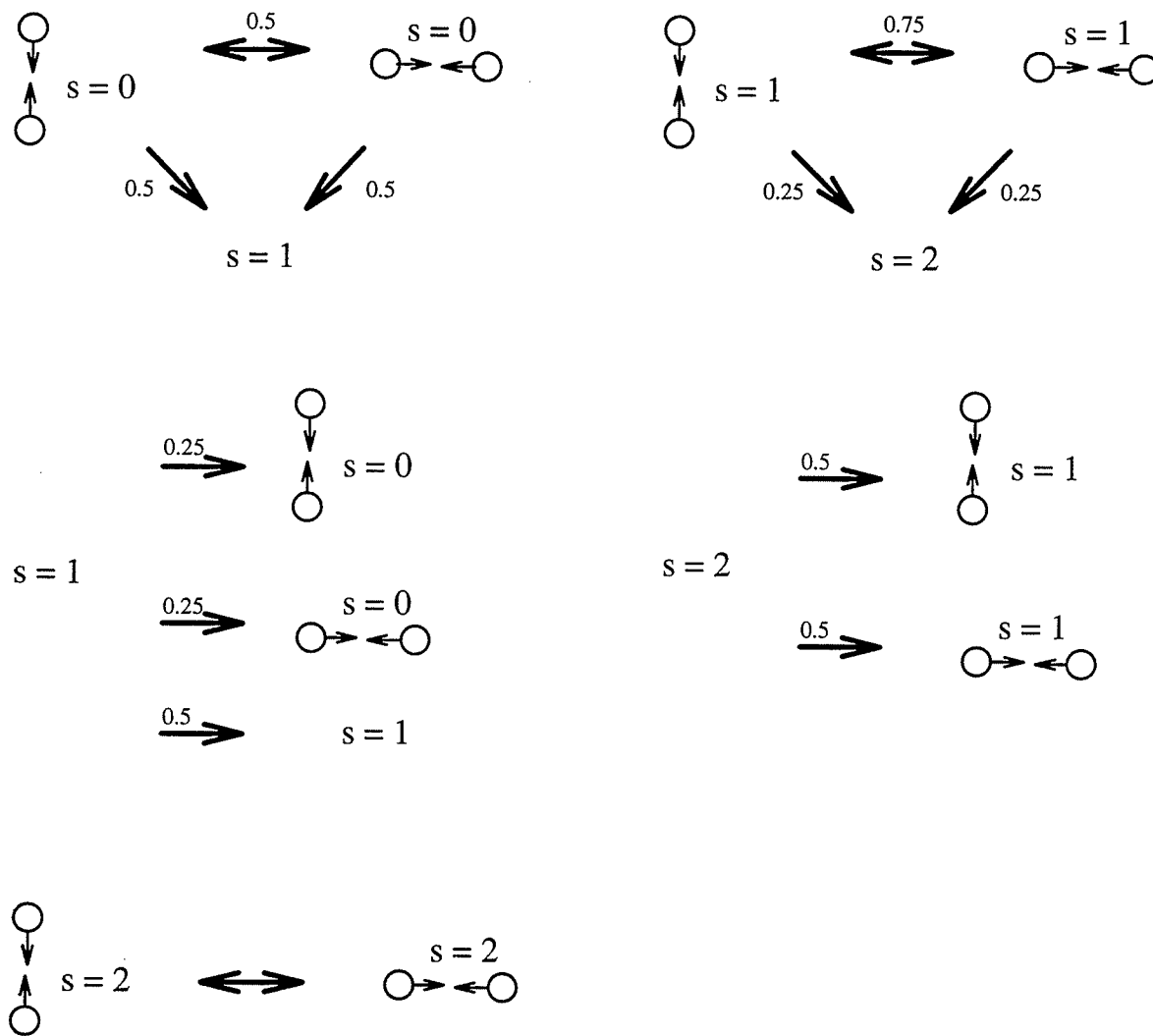


Figure 2.16: Stack-length = 2 in the $2m \leftrightarrow 1r$ model

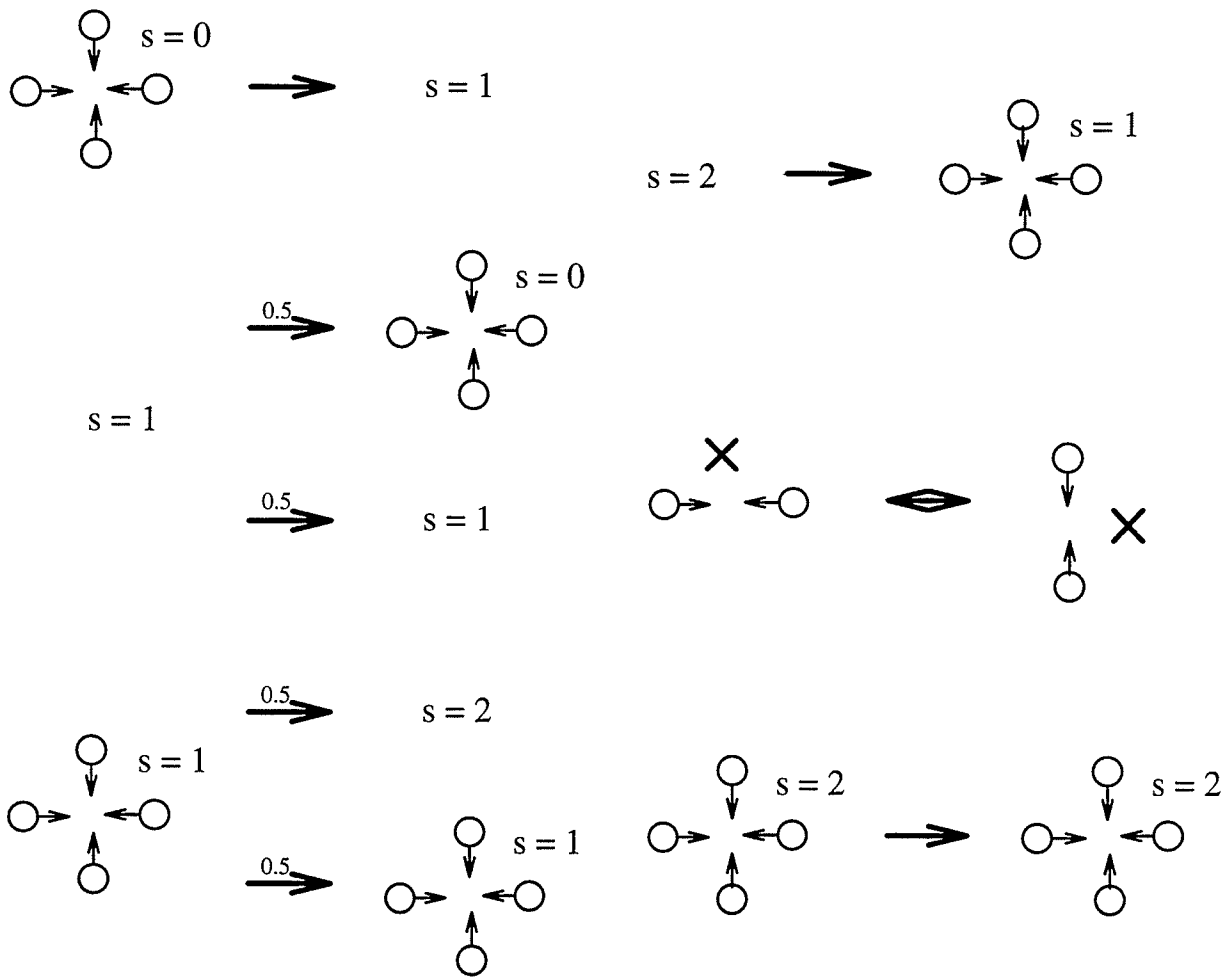


Figure 2.17: Stack-length = 2 in the $4m \leftrightarrow 1r$ model

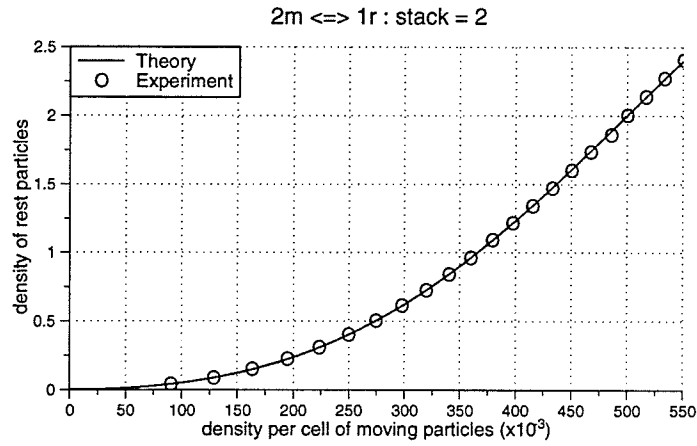


Figure 2.18: Equilibria for the $2m \leftrightarrow 1r$ ($s=2$) model

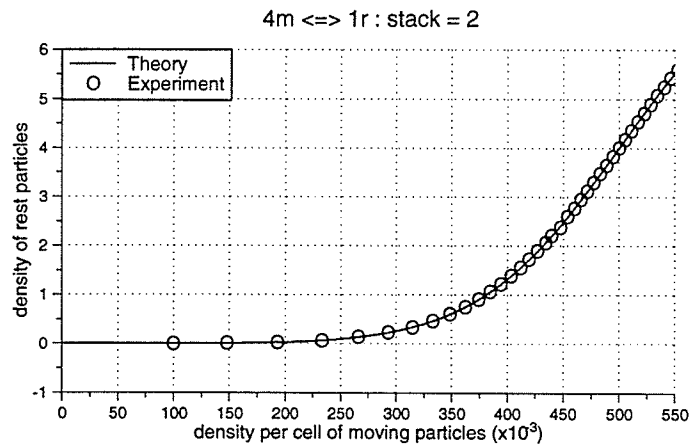


Figure 2.19: Equilibria for the $4m \leftrightarrow 1r$ ($s=2$) model

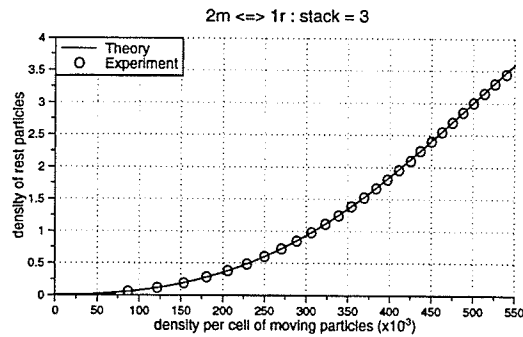
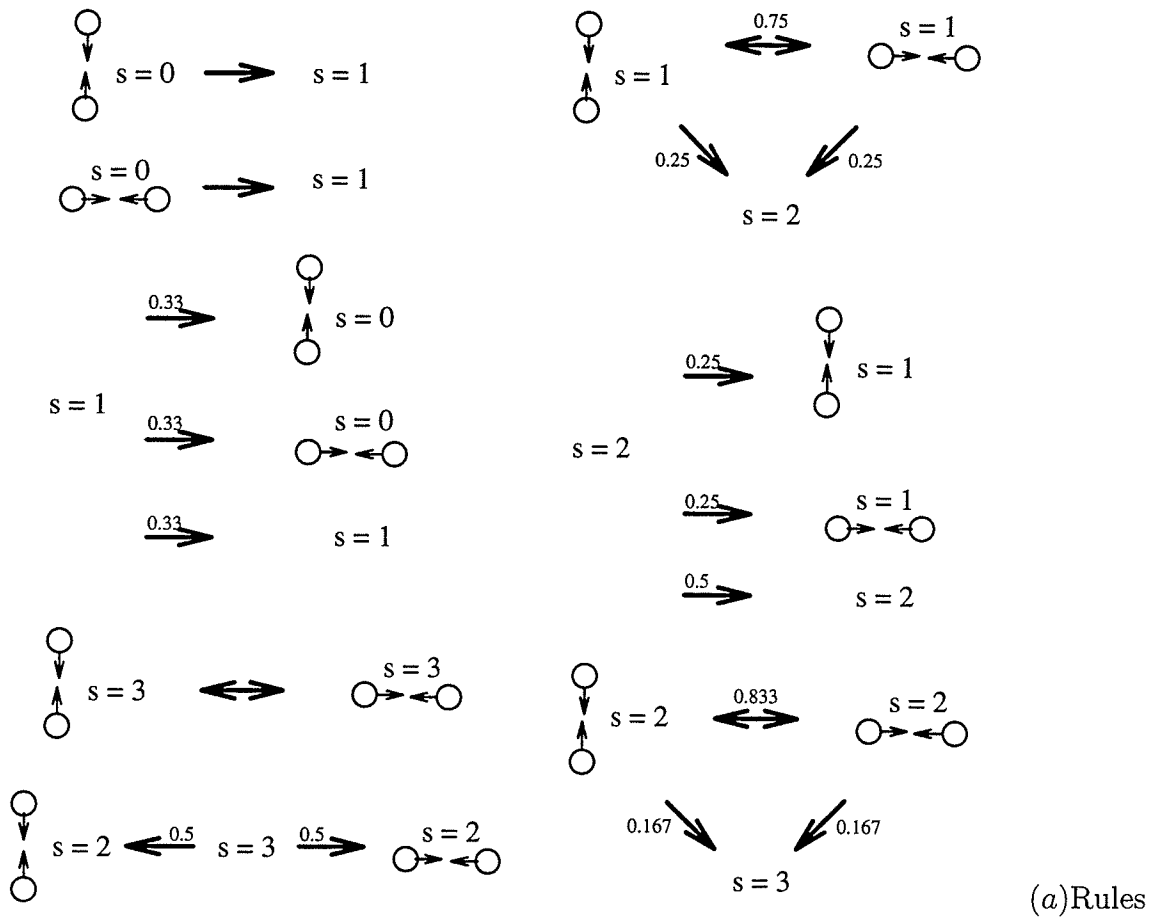


Figure 2.20: The $2m \leftrightarrow 1r$ ($s=3$) model

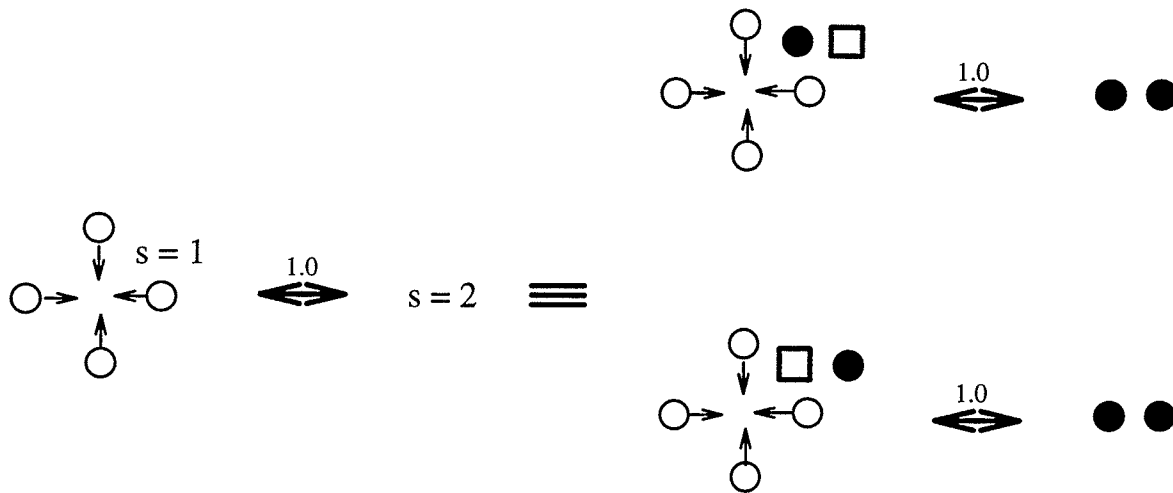
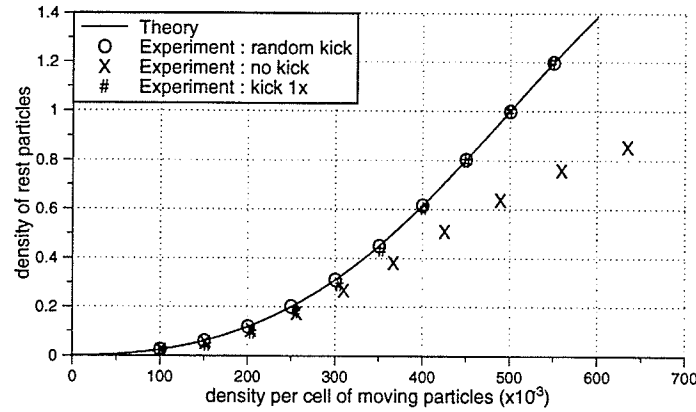


Figure 2.21: Decomposing the stack model

results in Figure 2.22 show the equilibrium in three different cases for the $2m \leftrightarrow 1r$ model:

- The kick is random.
- The bit is not kicked.
- The bit is kicked 1 lattice unit in the x direction.

The solid line describes the relationship between moving and rest particles stated in Equation (2.41). Hence, in the experiments in which the random bit is kicked, the experimental results agree well with the theoretical equilibrium (determined using Equation (2.41)). The experiment in which the random bit is not kicked does not compare well with theory. In this model, the decision as to which type of collision is to occur at any site in the lattice is made during the lattice initialization process. The value of the probability bit does not change with time. Thus the probability that a stochastic event occurs at a site is not probabilistic in any way.

Figure 2.22: Kicking the random bit in the $2m \leftrightarrow 1r$ model

2.13 Summary

In conclusion, the Fermi-Dirac equilibria describes an equilibrium between moving and rest particles in the following manner:

$$f_r(z) = \frac{f_m^z}{f_m^z + (1 - f_m)^z}, \quad (2.43)$$

where the masses of moving and rest particles are related in the following manner:

$$\frac{m_{rest}}{m_{moving}} = z.$$

In the HPP model, if both mass and momentum are conserved in each collision, $z = 2$ or $z = 4$.

For the remainder of this thesis we shall refer to the $4m \leftrightarrow 1r$ rule in which a site can hold a maximum of 1 rest particle as $4m \leftrightarrow 1r$ ($s=1$). In a similar manner, we

have $2m \leftrightarrow 1r$ ($s=2$) for the $2m \leftrightarrow 1r$ rule in which a site can hold upto a maximum of 2 rest particles. In this thesis, we only deal with multiple rest particles at a site, each of which have identical mass. Alternative FHP cases where sites can have multiple rest particles of different mass, have been considered in [17].

Chapter 3

The Chapman-Enskog Analysis

3.1 Introduction

The following is a summarized version of an analysis presented by Boghosian and Taylor in [16]. The Chapman-Enskog procedure is used to obtain a perturbative solution to the lattice Boltzmann equation for near-equilibrium distributions [18]. We have adhered to the same notation used by Boghosian and Taylor and made use of this theory in Chapter 4 to derive lattice gas fluid equations for the $4m \leftrightarrow 1r$ case.

Recall that

$$Q^\mu = \sum_{i=1}^{N_l} q_i^\mu N^i(\mathbf{x}, t), \quad \mu = 1, \dots, n_c \quad (3.1)$$

is the ensemble average of the n_c conserved quantities in the lattice gas. Furthermore, N_0^i refers to the Boltzmann equilibria for the i th particle in the lattice. This quantity was derived for moving as well as rest particles ($4m \leftrightarrow 1r$ and $2m \leftrightarrow 1r$ models) in the previous chapter. As well, the lattice Boltzmann equation was discussed earlier and is

$$N^i(\mathbf{x} + \mathbf{c}^i, t + \Delta t) = N^i(\mathbf{x}, t) + C_i(N^*(\mathbf{x}, t)) \quad (3.2)$$

The form $f(x^*)$ is used to denote a function of x for all possible values of the index replaced by the asterisk.

In this analysis, the *diffusion ordering* [16] is used. In a diffusive process, particles follow a random walk and the average distance a particle travels on a discrete grid is proportional to the square root of the number of steps [22]. Hence we let $\mathbf{c} \rightarrow \epsilon \mathbf{c}$ and $\Delta t \rightarrow \epsilon^2 \Delta t$ in the dynamical equations, where ϵ is an expansion parameter. Hence, we are taking $\Delta t \sim \ell^2 \equiv O(\epsilon^2)$.

It is important to note that the N^i are real numbers and could be approximated as smooth functions. Hence we could Taylor expand the same. The lattice Boltzmann equation is then Taylor expanded up to terms of order ϵ^2 .

$$N^i(\mathbf{x}, t + \Delta t) = N^i(\mathbf{x}, t) + \epsilon^2 \Delta t \frac{\partial N^i}{\partial t}.$$

$$\begin{aligned} N^i(x + \Delta x, y + \Delta y, t) &= N^i(x, t) + \epsilon \Delta x \frac{\partial N^i}{\partial x} + \epsilon \Delta y \frac{\partial N^i}{\partial y} \\ &+ \frac{\epsilon^2}{2} \Delta x^2 \frac{\partial^2 N^i}{\partial x^2} + \frac{\epsilon^2}{2} \Delta y^2 \frac{\partial^2 N^i}{\partial y^2} \\ &+ \frac{\epsilon^2}{2} \Delta x \Delta y \frac{\partial^2 N^i}{\partial x \partial y} + \frac{\epsilon^2}{2} \Delta y \Delta x \frac{\partial^2 N^i}{\partial y \partial x}. \end{aligned}$$

Expanding the collision operator we get

$$C_i(N^*(\mathbf{x}, t)) = C_0^i(N^*) + \epsilon C_1^i(N^*) + \epsilon^2 C_2^i(N^*).$$

Equation (3.2) could then be rewritten as

$$\epsilon^2 \Delta t \frac{\partial N^i}{\partial t} + \epsilon \mathbf{c}^i \cdot \nabla N^i + \frac{\epsilon^2}{2} \mathbf{c}^i \cdot \underline{\underline{A}} \cdot \mathbf{c}^i = C_0^i(N^*) + \epsilon C_1^i(N^*) + \epsilon^2 C_2^i(N^*), \quad (3.3)$$

where $\underline{\underline{A}}$ is a tensor $[A]_{pq} = \frac{\partial^2 N^i}{\partial x_p \partial x_q}$ and $i = 1 \dots N_l$.

By contracting the above N_l equations using q_i^μ and summing over the index i , we get the n_c equations

$$\epsilon \frac{\partial Q^\mu}{\partial t} + \nabla \cdot \left[\left(q_i^\mu \frac{\mathbf{c}^i}{\Delta t} N^i \right) + \epsilon \nabla \cdot \left(q_i^\mu \frac{\mathbf{c}^i \mathbf{c}^i}{2 \Delta t} N^i \right) \right] = \frac{\epsilon}{\Delta t} q_i^\mu C_2^i(N^*), \mu = 1 \dots n_c. \quad (3.4)$$

We assume that C_0 and C_1 obey the conservation equations exactly but C_2 does not necessarily do so. This is done in order that we might consider lattice gases whose conservation laws are only approximate. Thus only $C_2^i(N^*)$ remains in Equation (3.4).

Next, N^i is expanded in a perturbation series in powers of ϵ about an equilibrium state,

$$N^i = N_0^i + \epsilon N_1^i + \epsilon^2 N_2^i + \dots \quad (3.5)$$

N_0^i is a local thermodynamic equilibrium described by the Fermi-Dirac distribution which we have derived in Chapter 2. It is the lowest order term in the Boltzmann equation representing a spatially uniform distribution in the lattice. Note the $n_c = 3$ unknown parameters, α_γ .

$$N_0^j = \frac{1}{1 + \exp(-\sum_{\gamma=1}^{n_c} \alpha_\gamma q_j^\gamma)}. \quad (3.6)$$

3.2 The Fermi Metric

We now proceed to find the derivatives of the equilibrium state with respect to each conserved quantity which is later used to determine the transport coefficients in the hydrodynamic equations for the lattice gas. In order to compute the first two derivatives of N_0^i with respect to the Q^μ , we first differentiate Equation (3.6) with respect to α_ν ,

$$\frac{\partial N_0^i}{\partial \alpha_\nu} = N_0^i (1 - N_0^i) q_i^\nu. \quad (3.7)$$

Next, differentiating Equation (3.1) with respect to Q^ν , we obtain, using the chain rule,

$$\frac{\partial Q^\mu}{\partial Q^\nu} = \sum_{\xi=1}^{n_c} q_j^\mu \frac{\partial N_0^j}{\partial \alpha_\xi} \frac{\partial \alpha_\xi}{\partial Q^\nu} = \delta_\nu^\mu. \quad (3.8)$$

We now define a symmetric rank-two tensor,

$$g^{\mu\xi} \equiv N_0^j (1 - N_0^j) q_j^\mu q_j^\xi. \quad (3.9)$$

Then using Equations (3.7), (3.8) and (3.9),

$$\sum_{\xi=1}^{n_c} g^{\mu\xi} \frac{\partial \alpha_\xi}{\partial Q^\nu} = \delta_\nu^\mu. \quad (3.10)$$

The inverse of $g^{\mu\xi}$ is denoted by $g_{\xi\nu}$ so that

$$\sum_{\xi=1}^{n_c} g^{\mu\xi} g_{\xi\nu} = \delta_\nu^\mu. \quad (3.11)$$

Since $g_{\xi\nu}$ is a symmetric second-rank tensor, it could be identified as a metric on the space of hydrodynamic variables, Q^ν . We shall refer to it as the *Fermi metric*. Then, in terms of this metric,

$$\frac{\partial \alpha_\xi}{\partial Q^\nu} = g_{\xi\nu}. \quad (3.12)$$

Thus, the first derivative of N_0^i with respect to Q_μ is found to be

$$\frac{\partial N_0^i}{\partial Q^\mu} = \sum_{\nu=1}^{n_c} N_0^i (1 - N_0^i) q_i^\nu g_{\nu\mu}. \quad (3.13)$$

The second derivative is computed using the chain rule in the following manner:

$$\begin{aligned} \frac{\partial}{\partial Q^\nu} \left[\frac{\partial N_0^i}{\partial Q^\mu} \right] &= \frac{\partial}{\partial Q^\nu} \left[\frac{\partial N_0^i}{\partial \alpha_\xi} \frac{\partial \alpha_\xi}{\partial Q^\mu} \right] \\ &= \underbrace{N_0^i (1 - N_0^i) q_i^\xi \frac{\partial g_{\xi\mu}}{\partial Q^\nu}}_I + \underbrace{g_{\xi\mu} \frac{\partial}{\partial Q^\nu} [N_0^i (1 - N_0^i) q_i^\xi]}_{II}. \end{aligned}$$

$$\begin{aligned} II &= g_{\xi\mu} \frac{\partial}{\partial Q^\nu} [N_0^i (1 - N_0^i) q_i^\xi] \\ &= g_{\xi\mu} q_i^\xi \left[\frac{\partial N_0^i}{\partial \alpha_\eta} - \frac{\partial (N_0^i)^2}{\partial \alpha_\eta} \right] \frac{\partial \alpha_\eta}{\partial Q^\nu} \\ &= q_i^\xi q_i^\eta g_{\xi\mu} g_{\eta\nu} (1 - 2N_0^i) N_0^i (1 - N_0^i). \end{aligned}$$

$$\begin{aligned} I &= N_0^i (1 - N_0^i) q_i^\xi \frac{\partial g_{\xi\mu}}{\partial Q^\nu} \\ &= N_0^i (1 - N_0^i) q_i^\xi g_{\xi\eta} g^{\xi\eta} \frac{\partial g_{\xi\mu}}{\partial Q^\nu} \end{aligned}$$

$$\begin{aligned}
&= N_0^i(1 - N_0^i)q_i^\xi g_{\xi\eta}(-g^{\xi\mu} \frac{\partial g^{\xi\eta}}{\partial Q^\nu}) \\
&= N_0^i(1 - N_0^i)q_i^\xi g_{\xi\eta}(-g^{\xi\mu} \frac{\partial(N_0^j(1 - N_0^j)q_j^\xi q_j^\eta)}{\partial Q^\nu}) \\
&= 2N_0^i(1 - N_0^i)q_i^\xi g_{\eta\xi} \Gamma_{\mu\nu}^\eta.
\end{aligned}$$

$$\Gamma_{\mu\nu}^\eta = -\frac{1}{2}g_{\xi\mu}g_{\nu\zeta}N_0^j(1 - N_0^j)(1 - 2N_0^j)q_j^\eta q_j^\xi q_j^\zeta. \quad (3.14)$$

Equation (3.14) is defined as the *Fermi connection* which we use in the result for the second derivative.

$$\frac{\partial^2 N_0^i}{\partial Q^\mu \partial Q^\nu} = N_0^i(1 - N_0^i)(1 - 2N_0^i)q_i^\xi q_i^\eta g_{\xi\mu}g_{\eta\nu} + 2N_0^i(1 - N_0^i)q_i^\xi g_{\xi\eta} \Gamma_{\mu\nu}^\eta. \quad (3.15)$$

It is important to note that in the momentum conservation equations for the lattice gases under consideration the coefficients q^μ are vector quantities. The completely symmetric outer product of k of vectors e^i is denoted by $\otimes^k e^i$. The *generalized Fermi metric* is then defined to be

$$\mathbf{g}(k) \equiv N_0^j(1 - N_0^j)q_j^\mu q_j^\xi \left(\otimes^k e^j \right), \quad (3.16)$$

and the *generalized Fermi connection*,

$$\Gamma(k)_{\mu\nu}^\eta \equiv -\frac{1}{2}g_{\xi\mu}g_{\nu\zeta}N_0^j(1 - N_0^j)(1 - 2N_0^j)q_j^\eta q_j^\xi q_j^\zeta \left(\otimes^k e^j \right). \quad (3.17)$$

The Fermi connection could also be written as

$$\Gamma_{\mu\nu}^\eta = \frac{1}{2}g^{\eta\xi} \left(\frac{\partial g_{\xi\mu}}{\partial Q^\nu} + \frac{\partial g_{\xi\nu}}{\partial Q^\mu} - \frac{\partial g_{\mu\nu}}{\partial Q^\xi} \right), \quad (3.18)$$

and the *generalized Fermi connection* is

$$\Gamma_{\mu\nu}^{\eta} = \frac{1}{2}g^{\eta\xi} \left(\frac{\partial \mathbf{g}(k)_{\xi\mu}}{\partial Q^{\nu}} + \frac{\partial \mathbf{g}(k)_{\xi\nu}}{\partial Q^{\mu}} - \frac{\partial \mathbf{g}(k)_{\mu\nu}}{\partial Q^{\xi}} \right). \quad (3.19)$$

From Equations (3.13) and (3.16) we get

$$\frac{\partial}{\partial Q^{\mu}} \left[q_i^{\eta} N_0^i \left(\bigotimes^k \mathbf{e}^j \right) \right] = \mathbf{g}(k)_{\mu}^{\eta} \quad (3.20)$$

and from Equations (3.15), (3.17) and (3.20),

$$\frac{\partial^2}{\partial Q^{\mu} \partial Q^{\nu}} \left[q_i^{\eta} N_0^i \left(\bigotimes^k \mathbf{e}^j \right) \right] = 2 \left[\mathbf{g}(k)_{\xi}^{\eta} \Gamma_{\mu\nu}^{\xi} - \Gamma(k)_{\mu\nu}^{\eta} \right]. \quad (3.21)$$

3.3 Zero-Order Conservation Equations

We could now use Equation (3.4) and accumulate terms in $O(1)$, $O(\epsilon)$, $O(\epsilon^2)$. In order to remain consistent with the notation in [16], we define $\mathbf{c}^i = c\mathbf{e}^i$. Equation (3.4) at $O(1)$ gives us

$$\nabla \cdot \left(q_i^{\mu} \frac{\mathbf{c}^i}{\Delta t} N_0^i \right) = 0, \quad \mu = 1, \dots, n_c. \quad (3.22)$$

This could be rewritten as,

$$\begin{aligned} 0 &= q_i^{\mu} \frac{\mathbf{c}^i}{\Delta t} \sum_{\nu=1}^{n_c} \frac{\partial N_0^i}{\partial Q^{\nu}} \cdot \nabla Q^{\nu} \\ &= \sum_{\nu=1}^{n_c} \frac{\mathbf{c}^i}{\Delta t} N_0^i (1 - N_0^i) q_i^{\mu} q_i^{\xi} g_{\xi\nu} \cdot \nabla Q^{\nu} \\ &= \frac{c}{\Delta t} \sum_{\nu=1}^{n_c} \mathbf{g}(1)_{\nu}^{\mu} \cdot \nabla Q^{\nu} = 0, \quad \mu = 1, \dots, n_c. \end{aligned}$$

3.4 The Linearized Boltzmann Equation

At $O(\epsilon)$, by substituting Equation (3.5) in Equation (3.3),

$$\nabla \cdot \left(\frac{\mathbf{c}^i}{\Delta t} N_0^i \right) = \frac{1}{\Delta t} \left[J_j^i N_1^j + C_1^i(N_0^*) \right]. \quad (3.23)$$

The Jacobian matrix of the lowest order collision operator at equilibrium is defined as

$$J_j^i \equiv \left. \frac{\partial C_0^i}{\partial N^j} \right|_{N=N_0}. \quad (3.24)$$

Also, the q_i^μ 's comprise the components of n_c null left eigenvectors of J_j^i , since

$$q_i^\mu J_j^i \equiv \left. \frac{\partial}{\partial N^j} (q_i^\mu C_0^i) \right|_{N=N_0}. \quad (3.25)$$

We denote the eigenvalues of J by λ^μ .

$$J_j^i q_\beta^j = \lambda^\mu q_\beta^i. \quad (3.26)$$

$$q_i^\eta J_j^i = \lambda^\eta q_j^\eta. \quad (3.27)$$

The modes enumerated $1, \dots, n_c$, correspond to null eigenvalues of J and are called *hydrodynamic modes* (denoted by H), while those modes enumerated $n_c + 1, \dots, n$ are *kinetic modes* (denoted by K). The kinetic modes enable us to determine the diffusion coefficients while the hydrodynamic modes give us the advection coefficients.

Postmultiplying Equation (3.27) by q_β^j and premultiplying Equation (3.26) by q_i^η , and subtracting, we get

$$0 = (\lambda^\beta - \lambda^\eta) q_i^\eta q_\beta^i. \quad (3.28)$$

Right and left eigenvectors corresponding to different eigenvalues are thus orthogonal. Thus, they may be chosen so that

$$\delta_\nu^\mu = q_i^\mu q_\nu^i. \quad (3.29)$$

By including $\otimes^k \mathbf{e}^i$ in the above equation, we could then define a *generalized Kronecker delta*,

$$\delta(k)_\nu^\mu \equiv q_j^\mu \left(\otimes^k \mathbf{e}^j \right) q_\nu^j. \quad (3.30)$$

Also, since

$$C_0^i(N_0^*(\mathbf{x}, t)) = 0 \quad (3.31)$$

and

$$\frac{\partial N_0^i}{\partial \alpha_\nu} = N_0^i (1 - N_0^i) q_\nu^i, \quad (3.32)$$

we have

$$0 = \frac{\partial}{\partial \alpha_\mu} C_0^i(N_0^*) = J_j^i \frac{\partial N_0^j}{\partial \alpha_\mu} = J_j^i [q_j^\mu N_0^j (1 - N_0^j)]. \quad (3.33)$$

From this we can say that the right hydrodynamic eigenvectors are

$$q_\mu^i = q_i^\mu N_0^i (1 - N_0^i). \quad (3.34)$$

3.5 First-Order Solution

Consider Equation (3.23) for the N_1^i . Premultiplying this equation by the null left eigenvectors, we require that

$$\nabla \cdot \left(q_i^\mu \frac{\mathbf{c}^i}{\Delta t} N_0^i \right) = \frac{1}{\Delta t} q_i^\mu \left[J_j^i N_1^j + C_1^i(N_0^*) \right] = 0. \quad (3.35)$$

for $\mu \in H$. It follows that $\nabla \cdot (\mathbf{c}^i N_0^i) - C_1^i(N_0^*)$ has no components in the null space of J , since we have assumed linear stability. Owing to the completeness and orthonormality of the eigenvectors, this expression can be written as

$$\nabla \cdot (\mathbf{c}^i N_0^i) - C_1^i(N_0^*) = \sum_{\nu \in K} \eta^\nu q_\nu^i, \quad (3.36)$$

where $\eta^\nu \equiv q_j^\nu [\nabla \cdot (\mathbf{c}^i N_0^i) - C_1^i(N_0^*)]$ for $\nu \in K$.

The above could also be derived from Equation (3.23) in the following manner:

$$\nabla \cdot \left(q_i^\mu \frac{\mathbf{c}^i}{\Delta t} N_0^i \right) - \frac{1}{\Delta t} q_i^\mu C_1^i(N_0^*) = \frac{1}{\Delta t} q_i^\mu J_j^i N_1^j = 0, \quad (3.37)$$

or

$$\nabla \cdot \left(q_i^\mu \mathbf{c}^i N_0^i \right) - q_i^\mu C_1^i(N_0^*) = \lambda^\mu q_j^\mu N_1^j = 0. \quad (3.38)$$

Premultiplying the above equation by q_ν^j , we obtain

$$\sum_{\nu \in K} \frac{1}{\lambda^\nu} q_\nu^j q_i^\nu \left[\nabla \cdot \mathbf{c}^i N_0^i - C_1^i(N_0^*) \right] = N_1^j. \quad (3.39)$$

The solution for N_1^i could be written as

$$N_1^i = \sum_{\nu \in H} \theta^\nu q_\nu^i + \sum_{\nu \in K} \frac{\eta^\nu}{\lambda^\nu} q_\nu^i, \quad (3.40)$$

where the θ^ν are arbitrary. We hence fix $\theta^\nu = 0$ and obtain a final result for N_1^i .

$$N_1^i = \sum_{\nu \in K} \frac{q_\nu^i q_j^\nu}{\lambda^\nu} \left[\nabla \cdot (\mathbf{c}^i N_0^i) - C_1^i(N_0^*) \right] \quad (3.41)$$

and

$$N^i = N_0^i + \epsilon \sum_{\nu \in K} \frac{q_\nu^i q_j^\nu}{\lambda^\nu} \left[\nabla \cdot (\mathbf{c}^i N_0^i) - C_1^i(N_0^*) \right] + O(\epsilon^2). \quad (3.42)$$

3.6 First-Order Conservation Equations

Rewriting Equation (3.4) retaining terms to $O(\epsilon)$, we have

$$\frac{\partial Q^\mu}{\partial t} + \nabla \cdot \left[\left(q_i^\mu \frac{\mathbf{c}^i}{\Delta t} N_1^i \right) + \nabla \cdot \left(q_i^\mu \frac{\mathbf{c}^i \mathbf{c}^i}{2\Delta t} N^i \right) \right] = \frac{1}{\Delta t} q_i^\mu C_2^i(N^*), \mu \in H. \quad (3.43)$$

Substituting in the above equation, the value for N_1^i , we get the following:

$$\frac{\partial Q^\mu}{\partial t} + \nabla \cdot \left[\left(q_i^\mu \frac{\mathbf{c}^i}{\Delta t} \sum_{\nu \in K} \frac{q_\nu^i q_j^\nu}{\lambda^\nu} \left[\nabla \cdot (\mathbf{c}^i N_0^i) - C_1^i(N_0^*) \right] \right) + \nabla \cdot \left(q_i^\mu \frac{\mathbf{c}^i \mathbf{c}^i}{2\Delta t} N^i \right) \right] = \frac{1}{\Delta t} q_i^\mu C_2^i(N^*). \quad (3.44)$$

Next, rearranging terms, we get

$$LHS = \frac{\partial Q^\mu}{\partial t} + \nabla \cdot \left(q_i^\mu \frac{\mathbf{c}^i}{\Delta t} \sum_{\nu \in K} \frac{q_\nu^i q_j^\nu}{-\lambda^\nu} C_1^j(N_0^*) \right) \quad (3.45)$$

and

$$RHS = \frac{1}{\Delta t} q_i^\mu C_2^i(N_0^*) - \nabla \cdot \left[q_i^\mu \frac{\mathbf{c}^i}{\Delta t} \sum_{\nu \in K} \frac{q_\nu^i q_j^\nu}{\lambda^\nu} (\nabla \cdot \mathbf{c}^j N_0^j) + \nabla \cdot q_i^\mu \frac{\mathbf{c}^i \mathbf{c}^i}{2\Delta t} N_0^i \right]. \quad (3.46)$$

Next, we use $\mathbf{e}^i \equiv \frac{\mathbf{c}^i}{c}$ to rewrite the left hand-side as

$$LHS = \frac{\partial Q^\mu}{\partial t} + \frac{c}{t} \nabla \cdot \left[\sum_{\nu \in K} \frac{1}{-\lambda^\nu} q_i^\mu q_\nu^i \mathbf{e}^i (q_j^\nu C_1^j(N_0^*)) \right]. \quad (3.47)$$

This could be written in a more compact form, as

$$LHS = \frac{\partial Q^\mu}{\partial t} + \nabla \cdot \mathcal{A}^\mu, \quad (3.48)$$

where, $\mathcal{A}^\mu(Q^*)$ is given by

$$\mathcal{A}^\mu(Q^*) = \frac{c}{\Delta t} \sum_{\nu \in K} \frac{\delta(1)_\nu^\mu q_j^\nu C_1^j(N_0^*)}{-\lambda^\nu}. \quad (3.49)$$

The right-hand side of the equation could be written as

$$\begin{aligned} RHS = & \frac{1}{\Delta t} q_i^\mu C_2^i(N_0^*) - \nabla \cdot \sum_{\xi \in H} \left(\left[\frac{1}{\Delta t} \sum_{\nu \in K} q_i^\mu q_\nu^i q_j^\nu \frac{1}{\lambda^\nu} \mathbf{c}^i \mathbf{c}^j \frac{\partial N_0^j}{\partial \alpha_\eta} \frac{\partial \alpha_\eta}{\partial Q^\xi} \right. \right. \\ & \left. \left. - q_i^\mu \frac{\mathbf{c}^i \mathbf{c}^i}{2\Delta t} \frac{\partial \alpha_\eta}{\partial Q^\xi} \frac{\partial N_0^i}{\partial \alpha_\eta} \right] \cdot \nabla Q^\xi \right). \end{aligned} \quad (3.50)$$

Using Equations (3.7), (3.12), (3.16), (3.20), (3.30) and (3.31), the above could be rewritten as

$$RHS = \frac{1}{\Delta t} q_i^\mu C_2^i(N_0^*) + \sum_{\xi \in H} \nabla \cdot \left[\frac{c^2}{\Delta t} \left(\sum_{\nu \in K} \frac{\delta(1)_\nu^\mu \otimes \mathbf{g}(1)_\xi^\nu}{-\lambda^\nu} - \frac{1}{2} \mathbf{g}(2)_\xi^\mu \right) \right]. \quad (3.51)$$

In a more compact form then,

$$RHS = \sum_{\xi \in H} \nabla \cdot (\mathcal{D}_{\xi}^{\mu} \cdot \nabla Q^{\xi}) + \mathbf{S}^{\mu}, \mu \in H, \quad (3.52)$$

where,

$$\mathcal{D}_{\xi}^{\mu}(Q^*) = \left[\frac{c^2}{\Delta t} \left(\sum_{\nu \in K} \frac{\delta(1)_{\nu}^{\mu} \otimes \mathbf{g}(1)_{\xi}^{\nu}}{-\lambda^{\nu}} - \frac{1}{2} \mathbf{g}(2)_{\xi}^{\mu} \right) \right] \quad (3.53)$$

and

$$\mathbf{S}^{\mu}(Q^*) = \frac{1}{\Delta t} q_i^{\mu} C_2^i(N_0^*). \quad (3.54)$$

Hence, we have

$$\frac{\partial Q^{\mu}}{\partial t} + \nabla \cdot \mathcal{A}^{\mu} = \sum_{\xi \in H} \nabla \cdot (\mathcal{D}_{\xi}^{\mu} \cdot \nabla Q^{\xi}) + \mathbf{S}^{\mu}, \mu \in H. \quad (3.55)$$

This is the hydrodynamic equation which results from the Chapman-Enskog analysis with the Diffusion and Source terms being given by Equations (3.53) and (3.54), respectively. The Advection coefficients are given by Equation (3.49).

3.7 Ordering the Conserved Quantities

In lattice gas fluids the conserved quantities are ordered in the expansion parameter, ϵ . In an incompressible fluid, the hydrodynamic density is assumed to vary by $O(\epsilon^2)$ from a constant background value, and the hydrodynamic velocity is assumed to be $O(\epsilon)$. Hence, we consider the general ordering,

$$Q^{\mu} = Q_0^{\mu} + \epsilon Q_1^{\mu} + \epsilon^2 Q_2^{\mu} + \dots \quad (3.56)$$

We could then expand the Fermi-Dirac equilibrium in the following manner:

$$\begin{aligned}
N^i(Q^*) &= N_0^i(Q_0^*) + \sum_{\mu \in H} \left. \frac{\partial N_0^i}{\partial Q^\mu} \right|_0 (\epsilon Q_1^\mu + \epsilon^2 Q_2^\mu) + \frac{1}{2} \sum_{\mu, \nu \in H} \left. \frac{\partial^2 N_0^i}{\partial Q^\mu \partial Q^\nu} \right|_0 (\epsilon^2 Q_1^\mu Q_1^\nu) + \dots \\
&= N_{00}^i + \epsilon \sum_{\xi \in H} N_{00}^i (1 - N_{00}^i) q_i^\xi g_{\xi\mu} Q_1^\mu \\
&\quad + \epsilon^2 \sum_{\xi \in H} N_{00}^i (1 - N_{00}^i) q_i^\xi g_{\xi\mu} Q_2^\mu + \epsilon^2 \sum_{\xi, \eta \in H} N_{00}^i (1 - N_{00}^i) q_i^\xi g_{\xi\eta} \Gamma_{\mu\nu}^\eta Q_1^\mu Q_1^\nu \\
&\quad + \frac{\epsilon^2}{2} \sum_{\xi, \eta \in H} N_{00}^i (1 - N_{00}^i) (1 - 2N_{00}^i) q_i^\xi q_i^\eta g_{\xi\mu} g_{\eta\nu} Q_1^\mu Q_1^\nu + \dots, \tag{3.57}
\end{aligned}$$

where the lowest-order Chapman-Enskog equilibrium is denoted as

$$N_{00}^i \equiv N_0^i(Q_0^*).$$

We are then going to insert the result for N^i as a function of the ordered conserved quantities into Equation (3.4). Now, multiplying Equation (3.57) with the k -fold outer product of the \mathbf{e}^i vectors and contracting with q_i^μ , we have

$$\begin{aligned}
q_i^\mu \left(\bigotimes^k \mathbf{e}^i \right) N^i(Q^*) &= q_i^\mu \left(\bigotimes^k \mathbf{e}^i \right) N_{00}^i + \sum_{\xi \in H} \mathbf{g}(k)_\xi^\mu (\epsilon Q_1^\xi + \epsilon^2 Q_2^\xi) \\
&\quad + \epsilon^2 \sum_{\xi, \eta \in H} \left[\sum_{\zeta \in H} \mathbf{g}(k)_\zeta^\mu \Gamma_{\xi\eta}^\zeta - \Gamma(k)_{\xi\eta}^\mu \right] Q_1^\xi Q_1^\eta \\
&\quad + \epsilon^2 c \sum_{\nu \in K} \sum_{\xi \in H} \frac{\delta(k)_\nu^\mu \otimes \mathbf{g}(1)_\xi^\nu}{\lambda^\nu} \cdot \nabla Q_1^\xi.
\end{aligned}$$

This result can be inserted into Equation (3.4),

$$\frac{\partial Q^\mu}{\partial t} + \nabla \cdot \mathcal{A}^\mu = \sum_{\xi \in H} \nabla \cdot (\mathcal{D}_\xi^\mu \cdot \nabla Q^\xi) + \mathbf{S}^\mu, \mu \in H. \tag{3.58}$$

The advection coefficients are

$$\mathcal{A}^\mu(Q_0^*) \equiv \frac{c}{\Delta t} \sum_{\xi \in H} \left\{ \mathbf{g}(1)_\xi^\mu \left(\frac{1}{\epsilon} Q_1^\xi + Q_2^\xi \right) + \sum_{\eta \in H} \left[\sum_{\zeta \in H} \mathbf{g}(1)_\zeta^\mu \Gamma_{\xi\eta}^\zeta - \Gamma(1)_{\xi\eta}^\mu \right] Q_1^\xi Q_1^\eta \right\}. \quad (3.59)$$

The diffusion coefficients and source terms are given by Equations (3.53) and (3.54), respectively, and all quantities are evaluated at N_{00}^i . Furthermore, the advection operator has an $O(1/\epsilon)$ term and an $O(1)$ term. The former is the dominant term in the equation, if it does not vanish. In this situation, the hydrodynamic equation reduces to the zero-order conservation equation,

$$\nabla \cdot \left[\frac{c}{\Delta t} \sum_{\xi \in H} \mathbf{g}(1)_\xi^\mu Q_1^\xi \right] = 0. \quad (3.60)$$

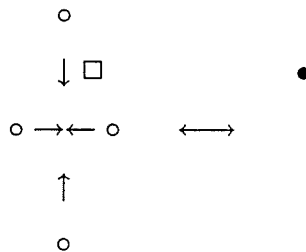
Furthermore, it is interesting to note that the form of the conservation laws (which give us the hydrodynamic modes) is sufficient to predict the form of this equation and compute the advection coefficients. The latter in turn enables a prediction of the speed of sound waves in the lattice gas. The kinetic modes determine the viscosity. In Chapter 4, we use the developed theory to determine the transport coefficients for the 2-D $4m \leftrightarrow 1r$ lattice gas.

Chapter 4

Lattice Gas Fluids

4.1 Analysis of the $4m \leftrightarrow 1r$ ($s = 1$) Lattice Gas

In this chapter we use the theory developed in [16] and summarized in Chapter 3 to derive the propagation speed and viscosity for the $4m \leftrightarrow 1r$ lattice gas in two dimensions. In this model, shown below, four moving particles give rise to a rest particle of mass $4m$ if none existed prior to their coming together. In addition, the reverse event might occur, i.e., the creation of four moving particles if a rest state was occupied and there were no moving particles present.



Once again in the LGA paradigm, we assume that the presence of a bit i at a site represents the presence of a particle of unit mass and momentum $\mathbf{c}^i/\Delta t$. The

ensemble-averaged mass and momentum densities at a site can be determined from the equilibrium densities N^* .

$$Q^\rho = \rho = N^1 + N^2 + N^3 + N^4 + 4N^5. \quad (4.1)$$

$$Q^{\mathbf{u}} = Q^{u_x} + Q^{u_y} = \mathbf{u} = \frac{1}{\Delta t} \sum_{i=1}^5 \mathbf{c}^i N^i, \quad (4.2)$$

where $\mathbf{c}^i = c\mathbf{e}^i$ and

$$\begin{aligned} \mathbf{e}^j &= \hat{\mathbf{x}} \cos \frac{\pi}{2}(j-1) + \hat{\mathbf{y}} \sin \frac{\pi}{2}(j-1), & j = 1, 2, 3, 4 \\ &= \mathbf{0}, & j = 5. \end{aligned} \quad (4.3)$$

There are 3 conserved quantities in the model under consideration. Q^ρ , Q^{u_x} and Q^{u_y} are the ensemble averages of the mass, x momentum and y momentum, respectively, in the lattice gas. In what follows, we shall use natural lattice units ($c = \Delta t = 1$). Since from Equation (3.1),

$$Q^\mu = \sum_{i=1}^5 q_i^\mu N^i(\mathbf{x}, t), \quad \mu = 1, \dots, 3,$$

we have,

$$\begin{aligned} q_i^\rho &= 1, & i = 1, 2, 3, 4 \\ q_i^\rho &= 4, & i = 5. \end{aligned} \quad (4.4)$$

From section 2.5:

$$\begin{aligned}
q_i^1 &= 1, & i &= 1, \dots, 4 \\
&= 4, & i &= 5 \\
q_i^2 &= \hat{x}, & i &= 1 \\
&= -\hat{x}, & i &= 3 \\
&= \mathbf{0}, & i &= 2, 4, 5 \\
q_i^3 &= \hat{y}, & i &= 2 \\
&= -\hat{y}, & i &= 4 \\
&= \mathbf{0}, & i &= 1, 3, 5.
\end{aligned}$$

For an incompressible fluid, the conserved densities are ordered in the expansion parameter [20].

$$\rho = \rho_0 + \epsilon^2 \rho_2. \quad (4.5)$$

$$\mathbf{u} = \epsilon \mathbf{u}_1. \quad (4.6)$$

The ordering of the conserved quantities as explained in section 3.7 for this system is then

$$\begin{aligned}
Q &= Q_0 + \epsilon Q_1 + \epsilon^2 Q_2 \\
&= \begin{pmatrix} \rho \\ \mathbf{u} \end{pmatrix} = \begin{pmatrix} \rho_0 \\ 0 \end{pmatrix} + \epsilon \begin{pmatrix} 0 \\ \mathbf{u}_1 \end{pmatrix} + \epsilon^2 \begin{pmatrix} \rho_2 \\ 0 \end{pmatrix}. \quad (4.7)
\end{aligned}$$

Thus, the zero-order Fermi-Dirac equilibrium is found by considering only q^ρ in Equation (2.30). Hence we get

$$N_0^i = \frac{1}{1 + e^{-\alpha}} \equiv f_m, \quad i = 1, 2, 3, 4 \quad (4.8)$$

$$= \frac{1}{1 + e^{-4\alpha}} \equiv f_r, \quad i = 5. \quad (4.9)$$

Once again, to be consistent with the notation used in [16], we use $n = N_l$ to represent the total number of particles at any site in the lattice. If the lattice vectors are isotropic to fourth rank, then they must satisfy the following equations, as outlined in [23]:

$$\begin{aligned} \sum_{i=1}^n \mathbf{e}^i &= \mathbf{0} \\ \sum_{i=1}^n \mathbf{e}^i \mathbf{e}^i &= \frac{n}{D} \mathbf{1} \\ \sum_{i=1}^n \mathbf{e}^i \mathbf{e}^i \mathbf{e}^i &= \mathbf{0} \\ \sum_{i=1}^n \mathbf{e}^i \mathbf{e}^i \mathbf{e}^i \mathbf{e}^i &= \frac{nD}{D+2} \Omega, \end{aligned} \quad (4.10)$$

where n is the number of particles, D , the number of dimensions in the lattice gas and

$$\Omega_{ijkl} = \delta_{ij}\delta_{kl} + \delta_{ik}\delta_{jl} + \delta_{il}\delta_{jk}. \quad (4.11)$$

We shall make use of these results for evaluating the generalized Fermi metric and connection. In keeping with the notation presented in [16], we shall interchange the indices $j = \rho$ and $j = \mathbf{u}$ with $j = 1$ and $j = 2$ respectively, for the coefficients q_j of the

conservation equations and also for the elements of the Fermi metric. The next step would be to construct the Fermi metric as outlined in section 3.2. For the $4m \leftrightarrow 1r$ model there are 3 conserved quantities and thus 3 hydrodynamic modes. Hence $g^{\mu\nu}$ from Equation (3.9) could be written as a 3 by 3 matrix.

$$g^{\mu\nu} = N_0^j(1 - N_0^j)q_j^\mu q_j^\nu. \quad (4.12)$$

$$\begin{aligned} g^{\rho\rho} &= N_0^j(1 - N_0^j)q_j^\rho q_j^\rho \\ &= 4f_m(1 - f_m) + 16f_r(1 - f_r) \\ &\equiv g^{11}. \end{aligned} \quad (4.13)$$

$$\begin{aligned} g^{\rho u} &\equiv g^{12} \\ &= N_0^j(1 - N_0^j)q_j^\rho q_j^u \\ &= 0 \\ &= g^{u\rho} \equiv g^{21}. \end{aligned} \quad (4.14)$$

$$\begin{aligned} g^{uu} &\equiv g^{22} \\ &= N_0^j(1 - N_0^j)q_j^u q_j^u \\ &= f_m(1 - f_m) \sum_{i=1}^4 \mathbf{e}^i \mathbf{e}^i = f_m(1 - f_m) \frac{4}{D} \mathbf{1}. \end{aligned} \quad (4.15)$$

Note the 2x2 unity matrix, $\mathbf{1}$ in Equation (4.15). Using Equations (4.12)-(4.15), the tensor $g^{\mu\nu}$ can then be written in matrix form as

$$g^{\mu\nu} = \begin{pmatrix} 4f_m(1-f_m) + 16f_r(1-f_r) & 0 \\ 0 & 4f_m(1-f_m)\frac{1}{D} \end{pmatrix}^{\mu\nu}, \quad (4.16)$$

where the indices μ and ν are used to denote the row and column of the metric, respectively. The Fermi metric could also be written out as a 3x3 matrix in the following manner:

$$g^{\mu\nu} = \begin{pmatrix} 4f_m(1-f_m) + 16f_r(1-f_r) & 0 & 0 \\ 0 & 4f_m(1-f_m)\frac{1}{D} & 0 \\ 0 & 0 & 4f_m(1-f_m)\frac{1}{D} \end{pmatrix}^{\mu\nu}. \quad (4.17)$$

Next, we calculate the components of the generalized Fermi metric, described in Equation (3.16),

$$\mathbf{g}(k)^{\mu\nu} \equiv N_0^j(1-N_0^j)q_j^\mu q_j^\nu \left(\bigotimes^k \mathbf{e}^j \right). \quad (4.18)$$

$$\mathbf{g}(k)^{11} = f_m(1-f_m) \sum_{j=1}^4 \bigotimes^k \mathbf{e}^j \quad (4.19)$$

$$\mathbf{g}(k)^{12} = f_m(1-f_m) \sum_{j=1}^4 \bigotimes^{k+1} \mathbf{e}^j = \mathbf{g}(k)^{21} \quad (4.20)$$

$$\mathbf{g}(k)^{22} = f_m(1-f_m) \sum_{j=1}^4 \bigotimes^{k+2} \mathbf{e}^j. \quad (4.21)$$

The Fermi connection is defined as

$$\Gamma_{\mu\nu}^\eta \equiv -\frac{1}{2}g_{\xi\mu}g_{\nu\zeta}N_0^j(1-N_0^j)(1-2N_0^j)q_j^\eta q_j^\xi q_j^\zeta. \quad (4.22)$$

The generalized Fermi connection is

$$\Gamma(k)_{\mu\nu}^{\eta} \equiv -\frac{1}{2}g_{\xi\mu}g_{\nu\zeta}N_0^j(1-N_0^j)(1-2N_0^j)q_j^{\eta}q_j^{\xi}q_j^{\zeta}\left(\bigotimes^k e^j\right). \quad (4.23)$$

The advection coefficients are

$$\mathcal{A}^{\mu}(Q_0^*) \equiv \frac{c}{\Delta t} \sum_{\xi \in H} \left\{ \mathbf{g}(1)_{\xi}^{\mu} \left(\frac{1}{\epsilon} Q_1^{\xi} + Q_2^{\xi} \right) + \sum_{\eta \in H} \left[\sum_{\zeta \in H} \mathbf{g}(1)_{\zeta}^{\mu} \Gamma_{\xi\eta}^{\zeta} - \Gamma(1)_{\xi\eta}^{\mu} \right] Q_1^{\xi} Q_1^{\eta} \right\}. \quad (4.24)$$

We are now going to determine the advection coefficients for the lattice gas. This is done twice. Once for $\mu = 1 \equiv \rho$ and then for $\mu = 2 \equiv \mathbf{u}$. These could then be inserted into Equation (3.55) and collecting terms of the same orders we could deduce certain mathematical properties for the lattice gas. The first property which will be demonstrated in the process is the incompressibility condition. In order to evaluate Equation (4.24) we shall rewrite it as

$$\mathcal{A}^{\mu}(Q_0^*) \equiv [\mathcal{A}^{\mu}(Q_0^*)]^I + [\mathcal{A}^{\mu}(Q_0^*)]^{II}, \quad (4.25)$$

where,

$$\begin{aligned} [\mathcal{A}^{\mathbf{u}}(\rho_0)]^I &= \sum_{\xi \in H} \left\{ \mathbf{g}(1)_{\xi}^{\mathbf{u}} \left(\frac{1}{\epsilon} Q_1^{\xi} + Q_2^{\xi} \right) \right\}, \\ [\mathcal{A}^{\mu}(Q_0^*)]^{II} &= \sum_{\xi \in H} \sum_{\eta \in H} \left[\sum_{\zeta \in H} \mathbf{g}(1)_{\zeta}^{\mu} \Gamma_{\xi\eta}^{\zeta} - \Gamma(1)_{\xi\eta}^{\mu} \right] Q_1^{\xi} Q_1^{\eta}. \end{aligned} \quad (4.26)$$

Again we have chosen natural lattice units $c = \Delta t = 1$.

Also from Equation (4.7), the only value of the index ξ for which Q_1^{ξ} is non-zero is $\xi = 2 \equiv \mathbf{u}$.

$$Q_1^\xi = Q_1^u = \mathbf{u}_1. \quad (4.27)$$

We now evaluate the components of the advection coefficients for $\mu = \rho = 1$.

The components of the Fermi metric,

$$\begin{aligned} \mathbf{g}(1)_1^1 &= \mathbf{g}(1)^{11}g_{11} + \mathbf{g}(1)^{12}g_{21} \\ &= 0, \end{aligned} \quad (4.28)$$

since $N_0^j(1 - N_0^j)q_j^1q_j^1 \left(\bigotimes^{k=1} \mathbf{e}^j \right) = 0$ and $g_{21} = 0$.

$$\begin{aligned} \mathbf{g}(1)_2^1 &= \mathbf{g}(1)^{11}g_{12} + \mathbf{g}(1)^{12}g_{22} \\ &= N_0^j(1 - N_0^j)q_j^1q_j^2 \left(\bigotimes^{k=1} \mathbf{e}^j \right) \frac{1}{N_0^j(1 - N_0^j)q_j^2q_j^2} \\ &= 1. \end{aligned} \quad (4.29)$$

Next, we calculate the components of the Fermi connection defined as

$$\Gamma_{\mu\nu}^\eta = -\frac{1}{2}g_{\xi\mu}g_{\nu\zeta}N_0^j(1 - N_0^j)(1 - 2N_0^j)q_j^\eta q_j^\xi q_j^\zeta. \quad (4.30)$$

$$\begin{aligned} \Gamma_{22}^2 &= -\frac{1}{2}g_{\xi 2}g_{2\zeta}N_0^j(1 - N_0^j)(1 - 2N_0^j)q_j^2q_j^\xi q_j^\zeta \\ &= -\frac{1}{2}(g_{22})^2N_0^j(1 - N_0^j)(1 - 2N_0^j)q_j^2q_j^2q_j^2 \\ &= -\frac{1}{2}(g_{22})^2N_0^j(1 - N_0^j)(1 - 2N_0^j)q_j^1 \left(\bigotimes^{k=3} \mathbf{e}^j \right) \\ &= 0. \end{aligned} \quad (4.31)$$

Now moving on to the generalized Fermi connection,

$$\Gamma(k)_{\mu\nu}^{\eta} \equiv -\frac{1}{2}g_{\xi\mu}g_{\nu\zeta}N_0^j(1-N_0^j)(1-2N_0^j)q_j^{\eta}q_j^{\xi}q_j^{\zeta}\left(\bigotimes^k e^j\right). \quad (4.32)$$

$$\begin{aligned} \Gamma(1)_{22}^1 &= -\frac{1}{2}g_{2\xi}g_{2\zeta}N_0^j(1-N_0^j)(1-2N_0^j)q_j^1q_j^{\xi}q_j^{\zeta}\left(\bigotimes^{k=1} e^j\right) \\ &= -\frac{1}{2}(g_{22})^2N_0^j(1-N_0^j)(1-2N_0^j)q_j^1q_j^2q_j^2\left(\bigotimes^{k=1} e^j\right) \\ &= -\frac{1}{2}(g_{22})^2N_0^j(1-N_0^j)(1-2N_0^j)q_j^1\left(\bigotimes^{k=3} e^j\right) \\ &= 0. \end{aligned} \quad (4.33)$$

Thus,

$$[\mathcal{A}^{\rho}(Q_0^*)]^{II} = 0. \quad (4.34)$$

Then, all we have left is,

$$\mathcal{A}^{\mu}(Q_0^*) \equiv [\mathcal{A}^{\mu}(Q_0^*)]^I. \quad (4.35)$$

Rewriting Equation (3.55), with only the dominant term, $O(1/\epsilon)$,

$$\begin{aligned} 0 &= \nabla \cdot [\mathcal{A}^{\rho}(Q_0^*)]^I \\ &= \nabla \cdot [\mathbf{g}(1)_{\xi}^{\rho}Q_1^{\xi}]. \end{aligned} \quad (4.36)$$

From (4.28) and (4.29), $\mathbf{g}(1)_1^1 = 0$ and $\mathbf{g}(1)_2^1 = 1$.

Also, from Equation (4.27), $Q_1^{\xi} = Q_1^{\mathbf{u}} = \mathbf{u}_1$. Hence, we get

$$\nabla \cdot \mathbf{u}_1 = 0. \quad (4.37)$$

This then verifies our original assumption; that if the conserved quantities are ordered as in Equations (4.5) and (4.6), the fluid is incompressible (since for an incompressible fluid, $\nabla \cdot \mathbf{v} = 0$, where \mathbf{v} is flow velocity).

Next we evaluate the advection coefficients for $\mu = \mathbf{u} = 2$,

$$[\mathcal{A}^{\mathbf{u}}(Q_0^*)]^{II} = \sum_{\xi \in H} \sum_{\eta \in H} \left[\sum_{\zeta \in H} \mathbf{g}(1)_{\zeta}^{\mathbf{u}} \Gamma_{\xi\eta}^{\zeta} - \Gamma(1)_{\xi\eta}^{\mathbf{u}} \right] Q_1^{\xi} Q_1^{\eta}. \quad (4.38)$$

The components of the generalized Fermi metric are

$$\begin{aligned} \mathbf{g}(1)_2^2 &= \mathbf{g}(1)^{21} g_{12} + \mathbf{g}(1)^{22} g_{22} \\ &= 0. \end{aligned} \quad (4.39)$$

Since $\mathbf{g}(1)^{22} = N_0^j (1 - N_0^j) (\otimes^{k=3} \mathbf{e}^j) = 0$ and $g_{12} = 0$,

$$\begin{aligned} \mathbf{g}(1)_1^2 &= \mathbf{g}(1)^{22} g_{21} + \mathbf{g}(1)^{21} g_{11} \\ &= \left[f_m (1 - f_m) \sum_{j=1}^4 \left(\otimes^{k=2} \mathbf{e}^j \right) \right] \frac{1}{g^{11}} \\ &= \left[f_m (1 - f_m) \left(\frac{4}{D} \mathbf{1} \right) \right] \frac{1}{4f_m(1 - f_m) + 16f_r(1 - f_r)} \\ &= \frac{4f_m(1 - f_m)}{D [4f_m(1 - f_m) + 16f_r(1 - f_r)]} \mathbf{1}. \end{aligned} \quad (4.40)$$

$$\Gamma_{22}^1 = -\frac{1}{2} g_{22} g_{22} N_0^j (1 - N_0^j) (1 - 2N_0^j) q_j^1 q_j^2 q_j^2$$

$$\begin{aligned}
&= -\frac{1}{2}(g_{22})^2 N_0^j (1 - N_0^j) (1 - 2N_0^j) q_j^2 q_j^2 q_j^2 \\
&= -\frac{1}{2}(g_{22})^2 N_0^j (1 - N_0^j) (1 - 2N_0^j) q_j^1 \left(\bigotimes^{k=2} \mathbf{e}^j \right) \\
&= -\frac{1}{2}(g_{22})^2 N_0^j (1 - N_0^j) (1 - 2N_0^j) q_j^1 \left(\bigotimes^{k=2} \mathbf{e}^j \right) \\
&= -\frac{1}{2} \frac{1}{\left[4f_m(1 - f_m) \frac{1}{D} \right]^2} f_m(1 - f_m) (1 - 2f_m) \frac{4}{D} \mathbf{1} \\
&= -\frac{1}{2} \frac{(1 - 2f_m)}{[4f_m(1 - f_m)]} D \mathbf{1}.
\end{aligned} \tag{4.41}$$

$$\begin{aligned}
\Gamma(1)_{22}^2 &= -\frac{1}{2} g_{2\xi} g_{2\zeta} N_0^j (1 - N_0^j) (1 - 2N_0^j) q_j^2 q_j^\xi q_j^\zeta \left(\bigotimes^{k=1} \mathbf{e}^j \right) \\
&= -\frac{1}{2} (g_{22})^2 N_0^j (1 - N_0^j) (1 - 2N_0^j) q_j^2 q_j^2 q_j^2 \left(\bigotimes^{k=1} \mathbf{e}^j \right) \\
&= -\frac{1}{2} \frac{1}{(g^{22})^2} N_0^j (1 - N_0^j) (1 - 2N_0^j) q_j^1 \left(\bigotimes^{k=4} \mathbf{e}^j \right) \\
&= -\frac{1}{2} \frac{1}{\left[4f_m(1 - f_m) \frac{1}{D} \right]^2} f_m(1 - f_m) (1 - 2f_m) \left(\frac{4}{D(D+2)} \Omega \right) \\
&= -\frac{1}{2} \frac{(1 - 2f_m)}{[4f_m(1 - f_m)]} \frac{D}{(D+2)} \Omega.
\end{aligned} \tag{4.42}$$

$$\begin{aligned}
[\mathcal{A}^u(\rho_0)]^{II} &= \sum_{\xi, \eta \in H} \left[\mathbf{g}(1)_1^u \Gamma_{\xi\eta}^1 - \Gamma(1)_{\xi\eta}^u \right] Q_1^\xi Q_1^\eta \\
&= \left[\mathbf{g}(1)_1^u \Gamma_{22}^1 - \Gamma(1)_{22}^u \right] Q_1^2 Q_1^2 \\
&= \left\{ -\frac{1}{2} \frac{(1 - 2f_m)}{[4f_m(1 - f_m) + 16f_r(1 - f_r)]} \mathbf{1} \right. \\
&\quad \left. + \frac{1}{2} \frac{(1 - 2f_m)}{[4f_m(1 - f_m)]} \frac{D}{(D+2)} \Omega \right\} : \mathbf{u}_1 \mathbf{u}_1 \\
&= [\mathcal{A}^u(\rho_0)]_a^{II} + [\mathcal{A}^u(\rho_0)]_b^{II}.
\end{aligned} \tag{4.43}$$

$$[\mathcal{A}^u(\rho_0)]_a^{II} = -\frac{1}{2} \frac{(1 - 2f_m) u_1^2}{[4f_m(1 - f_m) + 16f_r(1 - f_r)]} \mathbf{1}. \tag{4.44}$$

$$\begin{aligned}
[\mathcal{A}^u(\rho_0)]_b^{II} &= \frac{1}{2} \frac{(1-2f_m)}{[4f_m(1-f_m)]} \frac{D}{(D+2)} (\delta_{ij}\delta_{kl} + \delta_{ik}\delta_{jl} + \delta_{il}\delta_{jk}) : (\mathbf{u}_1)_i (\mathbf{u}_1)_j \\
&= \frac{1}{2} \frac{(1-2f_m)}{[4f_m(1-f_m)]} \frac{D}{(D+2)} (u_1^2 \mathbf{1} + (\mathbf{u}_1)_k (\mathbf{u}_1)_l + (\mathbf{u}_1)_l (\mathbf{u}_1)_k) \\
&= \frac{1}{2} \frac{(1-2f_m)}{[4f_m(1-f_m)]} \frac{D}{(D+2)} (u_1^2 \mathbf{1} + 2\mathbf{u}_1 \mathbf{u}_1).
\end{aligned} \tag{4.45}$$

$$\begin{aligned}
[\mathcal{A}^u(\rho_0)]^I &= \sum_{\xi \in H} \left\{ \mathbf{g}(1)_\xi^u \left(\frac{1}{\epsilon} Q_1^\xi + Q_2^\xi \right) \right\} \\
&= \mathbf{g}(1)_1^2 Q_2^1 \\
&= \frac{4f_m(1-f_m)}{D [4f_m(1-f_m) + 16f_r(1-f_r)]} \rho_2 \mathbf{1}.
\end{aligned} \tag{4.46}$$

And we have

$$\begin{aligned}
\mathcal{A}^u(\rho_0) &\equiv [\mathcal{A}^u(\rho_0)]^I + [\mathcal{A}^u(\rho_0)]^{II} \\
&= P \mathbf{1} + g(f) \mathbf{u}_1 \mathbf{u}_1.
\end{aligned} \tag{4.47}$$

where,

$$g(f) = \frac{(1-2f_m)}{[4f_m(1-f_m)]} \frac{D}{(D+2)}. \tag{4.48}$$

The pressure,

$$\begin{aligned}
P &= \frac{4f_m(1-f_m)}{D [4f_m(1-f_m) + 16f_r(1-f_r)]} \rho_2 - \frac{1}{2} \frac{(1-2f_m)u_1^2}{[4f_m(1-f_m) + 16f_r(1-f_r)]} \\
&\quad + \frac{1}{2} \frac{(1-2f_m)}{[4f_m(1-f_m)]} \frac{D}{(D+2)} u_1^2.
\end{aligned} \tag{4.49}$$

The propagation speed for the 2-D $4m \leftrightarrow 1r$ incompressible fluid model (derived in Appendix A) is then given by

$$\begin{aligned} c_s &= \sqrt{\frac{\partial P}{\partial \rho_2}} \\ &= \sqrt{\frac{4f_m(1-f_m)}{D[4f_m(1-f_m) + 16f_r(1-f_r)]}}. \end{aligned} \quad (4.50)$$

In general, for k rest particles of mass $4m$ each,

$$c_s = \sqrt{\frac{4f_m(1-f_m)}{D[4f_m(1-f_m) + (16k)f_r(1-f_r)]}}. \quad (4.51)$$

This could be easily deduced by writing the g^{11} component of the symmetric rank-two tensor. Inserting this into Equation (4.46) would then give us the general form.

We now wish to evaluate the diffusion coefficients (which in turn will enable a prediction of the viscosity of the 2-D $4m \leftrightarrow 1r$ model) given by Equation (3.53),

$$\mathbf{D}_\xi^\mu(Q^*) = \left[\frac{c^2}{\Delta t} \left(\sum_{\nu \in K} \frac{\delta(1)_\nu^\mu \otimes \mathbf{g}(1)_\xi^\nu}{-\lambda^\nu} - \frac{1}{2} \mathbf{g}(2)_\xi^\mu \right) \right]. \quad (4.52)$$

In order to evaluate \mathcal{D}_u^u , we consider the following:

$$\delta(1)_\nu^u = q_j^u \mathbf{e}^j q_\nu^j = \sum_{j=1}^n q_\nu^j \mathbf{e}^j \mathbf{e}^j.$$

$$\begin{aligned} \mathbf{g}(1)_u^\nu &= \mathbf{g}(1)^{uv} g_{uu} \\ &= \sum_{j=1}^n f_m(1-f_m) q_j^\nu \mathbf{e}^j \mathbf{e}^j \frac{D}{4f_m(1-f_m)} \\ &= \frac{D}{4} \sum_{j=1}^n q_j^\nu \mathbf{e}^j \mathbf{e}^j. \end{aligned}$$

$$\begin{aligned}
\mathbf{g}(2)_{\mathbf{u}}^{\mathbf{u}} &= \mathbf{g}(2)^{\mathbf{uu}} g_{\mathbf{uu}} \\
&= \sum_{j=1}^n f_m(1-f_m) \mathbf{e}^j \mathbf{e}^j \mathbf{e}^j \mathbf{e}^j \frac{D}{4f_m(1-f_m)} \\
&= \frac{D}{4} \frac{4}{D(D+2)} \Omega \\
&= \frac{\Omega}{D+2}.
\end{aligned}$$

Hence, the diffusivity tensor could be written as

$$\begin{aligned}
(\mathcal{D}_{u_l}^{u_i})^j &= \frac{c^2}{\Delta t} \left\{ \frac{D}{4} \mathbf{e}_i^m \mathbf{e}_j^m \mathbf{e}_k^p \mathbf{e}_l^p \left[\sum_{\nu \in K} \frac{q_\nu^m q_\nu^p}{-\lambda^\nu} \right] - \frac{1}{2} \frac{\Omega}{D+2} \right\} \\
&= \frac{c^2}{(D+2)\Delta t} \left\{ \frac{D(D+2)}{4} \mathbf{e}_i^m \mathbf{e}_j^m \mathbf{e}_k^p \mathbf{e}_l^p \left[\sum_{\nu \in K} \frac{q_\nu^m q_\nu^p}{-\lambda^\nu} \right] - \frac{1}{2} \Omega \right\}. \quad (4.53)
\end{aligned}$$

$\mathcal{D}_{\mathbf{u}}^{\mathbf{u}}$ is a fourth-rank object and there is an implicit sum over m and p . Since we have specified that the fourth-rank tensor constructed from the lattice vectors is isotropic (Equation (4.10)), the diffusivity tensor must be isotropic as well. This implies that it must be of the form:

$$(\mathcal{D}_{u_l}^{u_i})^j = \nu \delta_{il} \delta_{jk} + \alpha \delta_{ij} \delta_{lk} + \beta \delta_{ik} \delta_{lj}. \quad (4.54)$$

Hence to derive the diffusive term on the right-hand side of the hydrodynamic equation,

$$\begin{aligned}
\nabla_j (\mathcal{D}_{u_l}^{u_i})^j \nabla_k u_l &= \nabla_j \nu \delta_{il} \delta_{jk} \nabla_k u_l + \nabla_j \alpha \delta_{ij} \delta_{lk} \nabla_k u_l + \nabla_j \beta \delta_{ik} \delta_{lj} \nabla_k u_l \\
&= \nu \nabla^2 + \nabla_i \alpha \nabla_l u_l + \nabla_l \beta \nabla_i u_l \\
&= \nu \nabla^2 + \nabla_i [(\alpha + \beta) \nabla \cdot \mathbf{u}]. \quad (4.55)
\end{aligned}$$

The second term on the right vanishes thanks to the incompressibility condition ($\nabla \cdot \mathbf{v} = 0$), and we have the following hydrodynamic equation:

$$\frac{\partial \mathbf{u}_1}{\partial t} + g(f) \mathbf{u}_1 \cdot \nabla \mathbf{u}_1 = -\nabla P + \nu \nabla^2 \mathbf{u}_1. \quad (4.56)$$

This is the form of the Navier-Stokes equation except for the factor $g(f)$. ν is the shear viscosity. In order to get a closed expression for ν , we take the following traces of Equation (4.54):

$$\begin{aligned} (\mathcal{D}_{u_i}^{u_i})^j &= \nu \delta_{ii} \delta_{jj} + \alpha \delta_{ij} \delta_{ij} + \beta \delta_{ij} \delta_{ij} \\ &= \nu D^2 + \beta D + \alpha D. \end{aligned}$$

Similarly,

$$\begin{aligned} (\mathcal{D}_{u_j}^{u_i})^j &= \nu D + \beta D^2 + \alpha D \\ (\mathcal{D}_{u_j}^{u_i})^i &= \nu D + \beta D + \alpha D^2. \end{aligned}$$

The above equations may be solved for ν ,

$$\nu = \frac{(D+1) (\mathcal{D}_{u_i}^{u_i})^j - (\mathcal{D}_{u_j}^{u_i})^j - (\mathcal{D}_{u_j}^{u_i})^i}{D(D-1)(D+2)}. \quad (4.57)$$

From Equation (4.53),

$$\begin{aligned} (\mathcal{D}_{u_i}^{u_i})^j &= \frac{c^2}{(D+2)\Delta t} \left\{ \frac{D(D+2)}{4} \mathbf{e}_i^m \mathbf{e}_j^m \mathbf{e}_j^p \mathbf{e}_i^p \left[\sum_{\nu \in K} \frac{q_\nu^m q_\nu^p}{-\lambda^\nu} \right] - \frac{1}{2} \Omega \right\} \\ &= \frac{c^2}{(D+2)\Delta t} \left\{ \frac{D(D+2)}{4} \mathbf{e}_i^m \mathbf{e}_i^p \mathbf{e}_j^m \mathbf{e}_j^p \left[\sum_{\nu \in K} \frac{q_\nu^m q_\nu^p}{-\lambda^\nu} \right] - \frac{1}{2} \Omega \right\} \\ &= \frac{c^2}{(D+2)\Delta t} \left\{ \frac{D(D+2)}{4} \left[\sum_{\nu \in K} \frac{q_\nu^m (\mathbf{e}^m \cdot \mathbf{e}^n)^2 q_\nu^p}{-\lambda^\nu} \right] - \frac{1}{2} \Omega \right\}, \end{aligned}$$

where,

$$\begin{aligned}
 \Omega &= \delta_{ij}\delta_{kl} + \delta_{ik}\delta_{jl} + \delta_{il}\delta_{jk} \\
 &= \delta_{ij}\delta_{ji} + \delta_{ij}\delta_{ji} + \delta_{ii}\delta_{jj} \\
 &= 2\delta_{ij} + \delta_{ii}\delta_{jj} \\
 &= D(D+2).
 \end{aligned}$$

Similarly,

$$\left(\mathcal{D}_{u_j}^{u_i}\right)_i^j = \frac{c^2}{(D+2)\Delta t} \left\{ \frac{D(D+2)}{4} \left[\sum_{\nu \in K} \frac{q_\nu^m (\mathbf{e}^m \cdot \mathbf{e}^n)^2 q_n^\nu}{-\lambda^\nu} \right] - \frac{1}{2}\Omega \right\}$$

and

$$\begin{aligned}
 \left(\mathcal{D}_{u_j}^{u_i}\right)_j^i &= \frac{c^2}{(D+2)\Delta t} \left\{ \frac{D(D+2)}{4} \left[\sum_{\nu \in K} \frac{q_\nu^m (\mathbf{e}^m \cdot \mathbf{e}^m) (\mathbf{e}^n \cdot \mathbf{e}^n) q_n^\nu}{-\lambda^\nu} \right] - \frac{1}{2}\Omega \right\} \\
 &= \frac{c^2}{(D+2)\Delta t} \left\{ \frac{D(D+2)}{4} \left[\sum_{\nu \in K} \frac{q_\nu^m q_n^\nu}{-\lambda^\nu} \right] - \frac{1}{2}\Omega \right\},
 \end{aligned}$$

where,

$$\Omega = D(D+2).$$

Inserting the above into Equation (4.57),

$$\begin{aligned}
 \nu &= \frac{c^2}{(D+2)\Delta t} \left(\frac{D}{4(D-1)} \left[\sum_{\nu \in K} \frac{q_\nu^m (\mathbf{e}^m \cdot \mathbf{e}^n)^2 q_n^\nu}{-\lambda^\nu} \right] - \frac{1}{2} \right) \\
 &\quad - \frac{c^2}{(D+2)\Delta t} \left(\frac{1}{4(D-1)} \left[\sum_{\nu \in K} \frac{q_\nu^m q_n^\nu}{-\lambda^\nu} \right] \right). \tag{4.58}
 \end{aligned}$$

In order to write the Jacobian of the collision operator at equilibrium for the $4m \leftrightarrow 1r$ model we consider the ensemble-averaged collision operator,

$$\begin{aligned} C_E &= \overline{N_E N_N \overline{N_W N_S}} - N_E \overline{N_N N_W \overline{N_S}} - N_E N_N N_W N_S \overline{N_R} + \overline{N_E N_N N_W N_S N_R} \\ &= C_W \end{aligned}$$

$$\begin{aligned} C_N &= N_E \overline{N_N N_W \overline{N_S}} - \overline{N_E N_N \overline{N_W N_S}} - N_E N_N N_W N_S \overline{N_R} + \overline{N_E N_N N_W N_S N_R} \\ &= C_S. \end{aligned}$$

$$C_R = N_E N_N N_W N_S \overline{N_R} - \overline{N_E N_N N_W N_S N_R}.$$

The Jacobian matrix of the lowest-order collision operator at equilibrium is defined as

$$J_j^i \equiv \left. \frac{\partial C_0^i}{\partial N^j} \right|_{N=N_0}.$$

Since our lattice gas obeys semi-detailed balance, the equilibrium particle distributions are given by

$$\begin{aligned} N_0^j &= f_m, & j = N, S, E, W \\ &= f_r, & j = R, \end{aligned}$$

where, f_r can be expressed in terms of f_m .

Hence,

$$J_j^i = \begin{pmatrix} -u-v & u-v & -u-v & u-v & w \\ u-v & -u-v & u-v & -u-v & w \\ -u-v & u-v & -u-v & u-v & w \\ u-v & -u-v & u-v & -u-v & w \\ v & v & v & v & -w \end{pmatrix}^{ij},$$

where,

$$\begin{aligned} u &= f_m^2(1-f_m) + (1-f_m)^2 f_m \\ v &= f_m^3(1-f_r) + (1-f_m)^3 f_r \\ w &= f_m^4 + (1-f_m)^4. \end{aligned}$$

The eigenvalues and eigenvectors were found using MAPLE,

$$\begin{aligned} \lambda^1 &= 0 \\ \lambda^2 &= 0 \\ \lambda^3 &= 0 \\ \lambda^4 &= -4u \\ \lambda^5 &= -4v - w. \end{aligned}$$

We have exactly 3 zero eigenvalues and this means that the rule has exactly 3, and no additional conserved quantities. The left eigenvectors are

$$q_1 = \begin{pmatrix} +1 & +1 & 0 & 0 & +2 \end{pmatrix}$$

$$q_2 = \begin{pmatrix} -1 & 0 & +1 & 0 & 0 \end{pmatrix}$$

$$q_3 = \begin{pmatrix} +1 & 0 & 0 & +1 & +2 \end{pmatrix}$$

$$q_4 = \begin{pmatrix} -1 & +1 & -1 & +1 & 0 \end{pmatrix}$$

$$q_5 = \begin{pmatrix} -\frac{v}{w} & -\frac{v}{w} & -\frac{v}{w} & -\frac{v}{w} & +1 \end{pmatrix}.$$

The right eigenvectors are

$$q^1 = \begin{pmatrix} -1 \\ 0 \\ +1 \\ 0 \\ 0 \end{pmatrix} \quad q^2 = \begin{pmatrix} +1 \\ +1 \\ 0 \\ 0 \\ +\frac{2v}{w} \end{pmatrix} \quad q^3 = \begin{pmatrix} +1 \\ 0 \\ 0 \\ +1 \\ +\frac{2v}{w} \end{pmatrix}$$

$$q^4 = \begin{pmatrix} -1 \\ +1 \\ -1 \\ +1 \\ 0 \end{pmatrix} \quad q^5 = \begin{pmatrix} -1 \\ -1 \\ -1 \\ -1 \\ +1 \end{pmatrix}.$$

In two dimensions ($D = 2$), with four moving particles per site ($n = 4$), the lattice vectors are given by

$$\begin{aligned} \mathbf{e}^j &= \cos\left(\frac{2\pi j}{4}\right) \hat{\mathbf{x}} + \sin\left(\frac{2\pi j}{4}\right) \hat{\mathbf{y}}, & j = 1 \dots 4 \\ &= \mathbf{0}, & j = 5. \end{aligned}$$

In the case of the HPP, the 4th rank tensor in Equation (4.10) constructed from the lattice vectors is anisotropic [23]. Hence the viscosity does not obey Equation (4.57). This equation is valid only in the situation in which the tensor is isotropic up to 4th rank. The tensors in the HPP case are isotropic up to third rank and hence we can use the analysis to determine the Fermi-Dirac equilibrium and the advection coefficients (from which we can determine the propagation speed of sound waves). However, in order that we might demonstrate the application of the above general formulae, the viscosity can be calculated as follows:

$$(\mathbf{e}^j \cdot \mathbf{e}^k)^2 = \cos^2\left(\frac{2\pi(j-k)}{4}\right) = \begin{pmatrix} +1 & 0 & +1 & 0 & 0 \\ 0 & +1 & 0 & +1 & 0 \\ +1 & 0 & +1 & 0 & 0 \\ 0 & +1 & 0 & +1 & 0 \\ 0 & 0 & 0 & 0 & 0 \end{pmatrix}^{jk}.$$

Now plugging the above values into the expression for the viscosity (Equation (4.58)), we obtain

$$\nu = \frac{c^2}{4\Delta t} \left[\frac{1}{4w} + \frac{1}{2(4v+w)} + \frac{1}{u} - \frac{1}{2} \right]. \quad (4.59)$$

4.2 Summary of Results

We shall now summarize some of the results derived using the analysis described in Chapters 3 and 4. In the case of the HPP lattice gas automaton, the propagation

speed of sound waves is a constant value of $\frac{1}{\sqrt{2}}$ and is independent of the background density of moving particles. In the $4m \leftrightarrow 1r$ lattice gas with k rest particles, the equilibrium concentrations of moving (f_m) and rest particles (f_r) are related in the following manner:

$$f_r = \frac{f_m^4}{f_m^4 + (1 - f_m)^4}.$$

The propagation speed, c_s , of sound waves in this lattice gas with k rest particles of mass $4m$ is given by the following relationship:

$$c_s = \sqrt{\frac{4f_m(1 - f_m)}{D [4f_m(1 - f_m) + (16k)f_r(1 - f_r)]}}.$$

In the $2m \leftrightarrow 1r$ lattice gas with k rest particles the Fermi-Dirac equilibrium requires that moving and rest particle concentrations, f_m and f_r , are related in the following manner:

$$f_r = \frac{f_m^2}{f_m^2 + (1 - f_m)^2}.$$

The propagation speed c_s in the situation where we have k rest particles could once again be deduced from the mass conservation equation for this model and the g^{11} component of the symmetric rank-two tensor (Equation (4.13)) and is as follows:

$$c_s = \sqrt{\frac{4f_m(1 - f_m)}{D [4f_m(1 - f_m) + (4k)f_r(1 - f_r)]}}.$$

It can be seen that the value for c_s in both the equations reduces to the HPP case when $f_r = 0$, as expected.

Chapter 5

LGA Experiments for Homogeneous Systems

In this chapter we compare results for experiments conducted on CAM-8 with theoretical results derived in Chapter 4. Results for the Fermi-Dirac equilibria were presented in Chapter 2. We shall now measure the propagation speed of sound waves in homogeneous systems using the HPP, $4m \leftrightarrow 1r$, $2m \leftrightarrow 1r$ and the FHP - $6m \leftrightarrow 1r$ models for different stack lengths. As well, we describe a lattice gas mixture using the $4m \leftrightarrow 1r$ rule which has sites in the lattice with different stack lengths (also known as a lattice gas mixture).

5.1 Measurements for Propagation Speed

The lattice is two dimensional as shown in Figure 5.1, and has dimensions $N_x \Delta x * N_y \Delta y$, where $\Delta x = \Delta y = \Delta$ is one lattice unit. N_x and N_y are the number of cells in the x and y directions, respectively. The lattice is initialized with a certain background density, ρ_0 . If the density of moving particles per direction in the lattice

is f_m , then the density of rest particles per site in the lattice is given by Equations (2.37) and (2.41) for rest particles of mass $4m$ and $2m$, respectively. A gaussian-pulsed, x-directed, plane wave is propagated through the lattice. This is done by superimposing particles in the lattice according to the following equation:

$$\rho_p = \rho_m \exp\left(\frac{(x - x_0)^2}{\tau^2}\right).$$

The gaussian is thus centred, i.e., has its maximum value ρ_m at x_0 . A square sampling window counts the number of particles within it at each time step and hence we can monitor the perturbation as it propagates across the lattice. Please see Appendix B for details on the calculation of propagation speed.

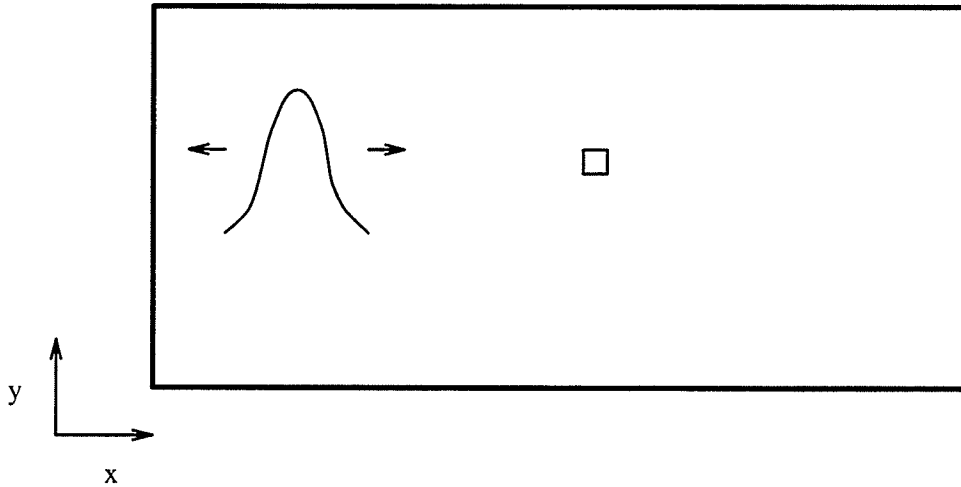


Figure 5.1: The two dimensional lattice.

5.1.1 The HPP Model

In this section we use the HPP lattice gas rule with no rest particles. The rectangular lattice was initialized with a uniform density of particles. A plane wave was excited

background density	propagation speed
0.25	0.71986
0.35	0.70963
0.55	0.69306

Table 5.1: Propagation speeds in the HPP model

by superimposing a gaussian distribution (centred at $x_0 = 100\Delta$) of particles on top of the existing background. The lattice size in this series of experiments was 2048 x 256. The maximum size of the initial perturbation, ρ_m (peak of the gaussian), was at 20% above the background. The pulse width of the gaussian was $\tau = 50\Delta x$. The square sampling window (size 49 x 49) centred at $x = 575$, $y = 150$, was used to determine the macroscopic quantity $\rho = \rho_0 + \rho_p$. Using Equation (4.50) with $f_r = 0$, $D = 2$, we expect the wave to propagate with a speed of $c_s = \frac{1}{\sqrt{2}}$, irrespective of the background density of particles. The lattice had *wrap-around* boundaries (please see Appendix B). That is, all particles that exit from the left end of the lattice re-enter from the right and vice-versa.

Numerical experiments with varying background densities (0.15, 0.35, 0.55), yield time-domain waveforms shown in Figure 5.2(a) and experimental results obtained using the method outlined in Appendix B to calculate propagation speed, are summarized in Table 5.1.

Form the above table it could be seen that c_s decreases with an increase in background density. This could be because of viscosity (a function of particle density) which causes dispersion due to the higher frequency components in the wave being attenuated more than the lower frequency components.

5.1.2 The $4m \leftrightarrow 1r$ Model

In this experiment, the moving and rest particles in the lattice were initialized using Equation (2.37). The lattice size in this series of experiments was 2048 x 256. The square sampling window (size 49 x 49) was centred at $x = 575$, $y = 150$. The maximum size of the initial perturbation, ρ_m (peak of the gaussian), was at 20% above the background. Varying the background density, the propagation speed was measured. The theoretical speed is

$$c_s = \sqrt{\frac{4f_m(1-f_m)}{2[4f_m(1-f_m) + 16f_r(1-f_r)]}}. \quad (5.1)$$

The time domain waveforms are shown in Figure 5.2(b), and the propagation speed versus density per cell of moving particles is plotted in Figure 5.3(a).

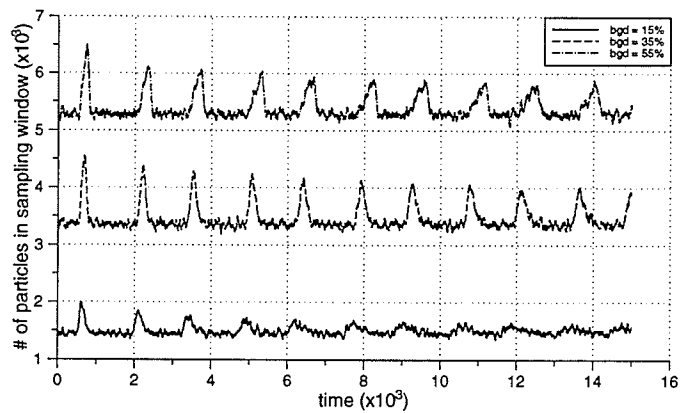
For the stack of length two, explained in section 2.11 (Figure 2.17), Figure 5.3(b) shows the experimental and theoretical values of propagation speed versus density per cell of moving particles. The theoretical values of propagation speed are given by the formula ($k = 2$ in Equation (4.51)),

$$c_s = \sqrt{\frac{4f_m(1-f_m)}{2[4f_m(1-f_m) + 32f_r(1-f_r)]}}. \quad (5.2)$$

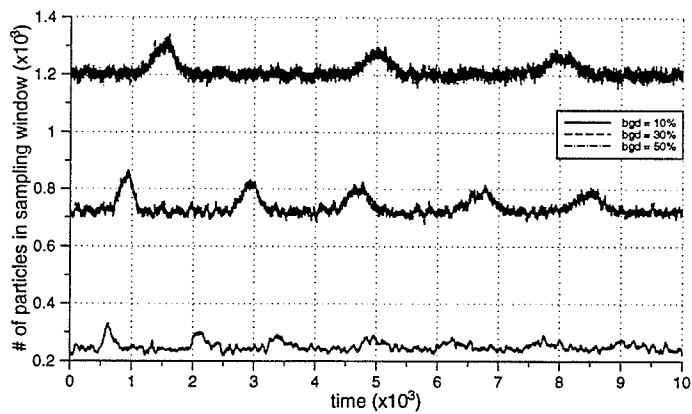
f_m and f_r are related as in Equation (2.37).

5.1.3 The $2m \leftrightarrow 1r$ Model

This model which was described in sections 2.8.2 (stack length = 1) and 2.11 (stack length = 2 and 3). The rules are given in Figures (2.5), (2.16) and (2.20)(a) for stack

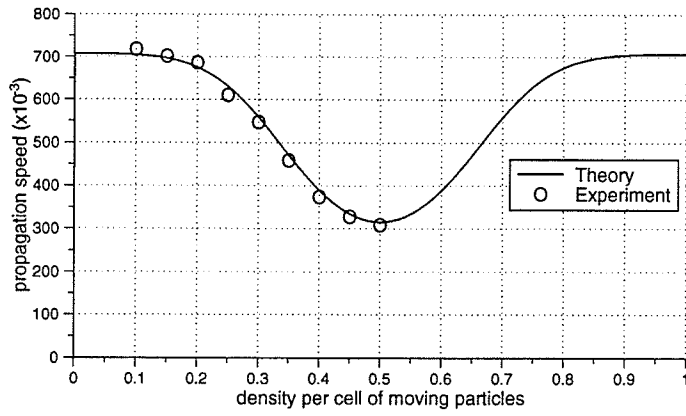


(a)HPP

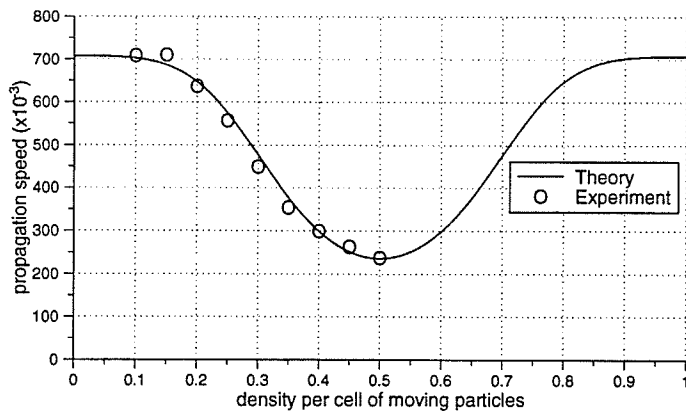


(b)4m ↔ 1r

Figure 5.2: Time domain waveforms



(a)stack = 1



(b)stack = 2

Figure 5.3: Propagation speeds for the $4m \leftrightarrow 1r$ model

lengths of one, two and three, respectively. A rectangular lattice of dimensions 4096 x 256 was used in the following experiments. The pulsewidth of the gaussian was $\tau = 100$ lattice units and it was centred at $x_0 = 200 \Delta$. The maximum size of the initial perturbation, ρ_m , was at 20% above the background. The square sampling window (99 x 99) was centred at $x = 1150, y = 150$. The propagation speed is given by the following equation:

$$c_s = \sqrt{\frac{4f_m(1-f_m)}{2[4f_m(1-f_m) + 4kf_r(1-f_r)]}} \quad (5.3)$$

k is the maximum stack length. Results for $k = 1, 2$ and 3 are shown in Figure 5.4 (a), (b) and (c), respectively.

5.1.4 The FHP $6m \leftrightarrow 1r$ Model

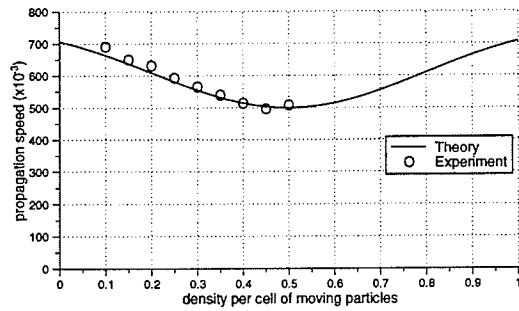
This automaton uses a triangular lattice with hexagonal symmetry as explained earlier in section 1.2.2. A maximum of seven particles can exist at a site (6 moving + 1 rest) with velocities:

$$\begin{aligned} \mathbf{e}^j &= \hat{x} \cos \frac{2\pi}{6}(j-1) + \hat{y} \sin \frac{2\pi}{6}(j-1), & j = 1, 2, 3, 4, 5, 6. \\ \mathbf{e}^j &= \mathbf{0}, & j = 7. \end{aligned} \quad (5.4)$$

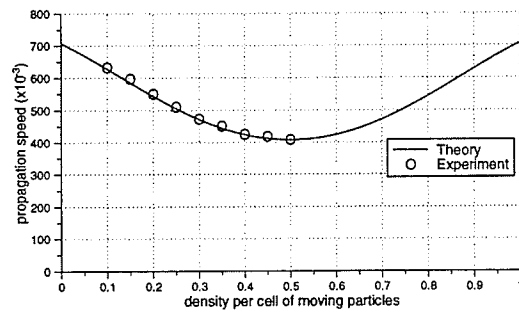
Collision details for this model are shown in Figure 5.6(a).

From Figure 5.5 it could be seen that the inter-cell spacing in the y and x directions, Δy and Δx respectively, differ and

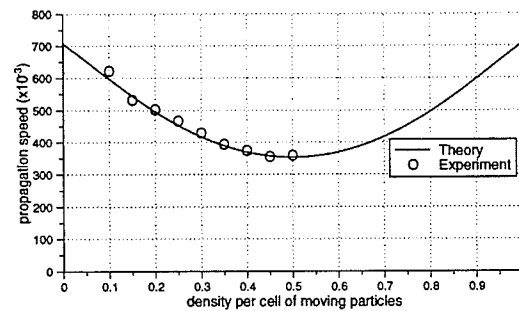
$$\frac{\Delta y}{\Delta x} = \frac{\sqrt{3}}{2}.$$



(a) $k = 1$



(b) $k = 2$



(c) $k = 3$

Figure 5.4: Propagation speeds for the $2m \leftrightarrow 1r$ model

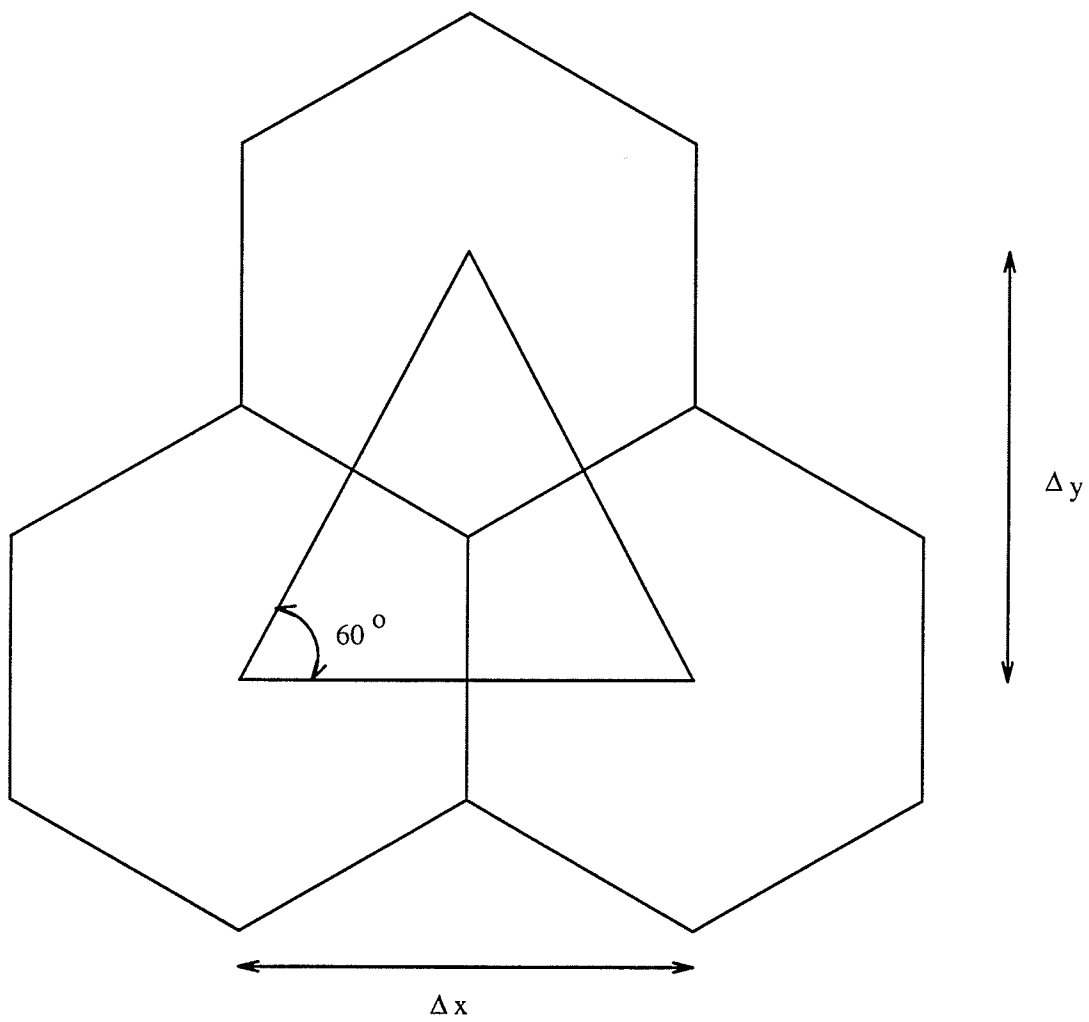
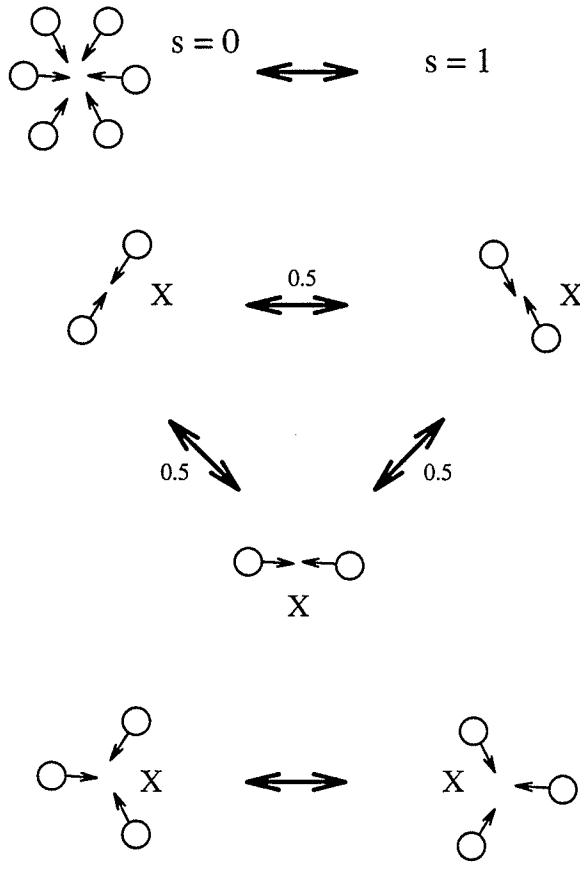
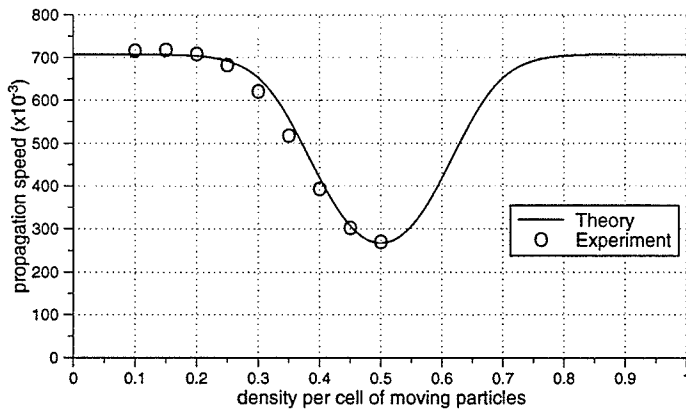


Figure 5.5: The hexagonal lattice.



(a) Rules



(b) Propagation Speeds

Figure 5.6: The FHP $6m \leftrightarrow 1r$ model.

The speed of sound for this model is

$$c_s = \sqrt{\frac{6f_m(1-f_m)}{2[6f_m(1-f_m) + 36f_r(1-f_r)]}}. \quad (5.5)$$

f_r and f_m are the densities of the rest and moving particles respectively and are related to each other in the following manner:

$$f_r = \frac{f_m^6}{f_m^6 + (1-f_m)^6}. \quad (5.6)$$

The above formulae could be deduced from the mass conservation equation for the $6m \leftrightarrow 1r$ model and the g^{11} component of the symmetric rank-two tensor, Equation (4.13). A rectangular lattice of dimensions 4096 x 256 was used in the following experiments. The pulsewidth of the gaussian was $\tau = 100$ lattice units and it was centred at $x_0 = 200 \Delta$. The maximum size of the initial perturbation, ρ_m , was at 20% above the background. The square sampling window (99 x 99) was centred at $x = 1150$, $y = 150$. The solid curve in Figure 5.6(b) shows the theoretical propagation speed, c_s , as a function of the density per cell of moving particles. The experimental values are plotted as well.

5.2 Lattice Gas Mixtures

In the previous experiments, lattice rules were considered where the entire lattice consisted of sites which allowed for stack lengths of zero, one, two or three. We shall define a lattice gas mixture as one in which sites with non-uniform stack lengths of rest particles are uniformly distributed at random within the lattice. For instance a lattice might have sites at which no rest particles are created as well as those at which

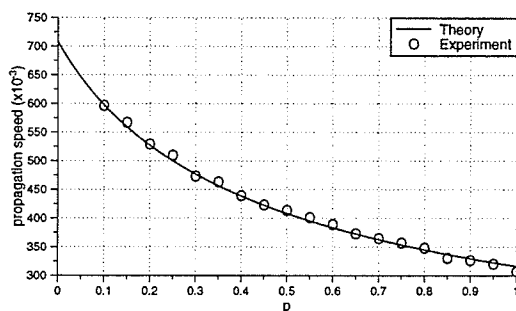
a maximum of one rest particle is allowed. The properties of such a mixture would depend on the relative proportions of these two different types of sites in the lattice. In a $4m \leftrightarrow 1r$ ($s=1$) and HPP lattice gas ($4m \leftrightarrow 1r$ ($s=0$)) mixture one might expect a propagation speed governed by the following equation:

$$c_s = \sqrt{\frac{4f_m(1-f_m)}{2[4f_m(1-f_m) + 16pf_r(1-f_r)]}}. \quad (5.7)$$

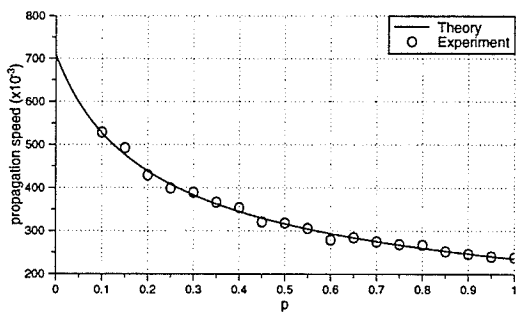
p is the ratio of sites in the lattice at which a rest particle may be created. In the situation where all sites within the lattice are allowed to hold one rest particle, $p = 1$. Although a rigorous theoretical proof is not developed for this formula, this could be deduced from the g^{11} component of the isotropic rank-two tensor (Equation (4.13)). Using mixtures then, it would be possible to achieve any propagation speed between 0.707 (HPP, $p = 0$) and 0.316 (minimum in $4m \leftrightarrow 1r$, with $p = 1$ and $f_m = 0.50$). The lattice size in this series of experiments was 2048 x 256. The square sampling window (size 49 x 49) was centred at $x = 575$, $y = 150$. The maximum size of the initial perturbation, ρ_m (peak of the gaussian), was at 20% above the background. The pulse width of the gaussian was $\tau = 50\Delta x$. The square sampling window (size 49 x 49) was centred at $x = 575$, $y = 150$. With the moving particle density, f_m , fixed at 0.50, the results for c_s in the $4m \leftrightarrow 1r$ ($s=1$) and HPP lattice gas mixture are shown in Figure 5.7(a).

The propagation speed for a $4m \leftrightarrow 1r$ ($s=2$) and HPP lattice gas mixture could be deduced in a similar manner and would be

$$c_s = \sqrt{\frac{4f_m(1-f_m)}{2[4f_m(1-f_m) + 32pf_r(1-f_r)]}}. \quad (5.8)$$



(a) $stack = 1$



(b) $stack = 2$

Figure 5.7: Propagation speeds for the $4m \leftrightarrow 1r$ lattice gas mixture as a function of the density of sites in the lattice which can hold rest particles

Results from such a simulation (using the same lattice dimensions, pulse width and window size as in the previous experiment) with the moving particle density, f_m , fixed at 0.50, are shown in Figure 5.7(b).

If we were now to create a lattice gas mixture with sites having stack lengths of zero, one and two, we might expect the propagation speed within this mixture to be

$$c_s = \sqrt{\frac{4f_m(1-f_m)}{2[4f_m(1-f_m) + 16p_1f_r(1-f_r) + 32p_2f_r(1-f_r)]}} \quad (5.9)$$

p_1 and p_2 are the ratios of sites having stack lengths of one and two, respectively. Furthermore, $p_1 + p_2 \leq 1$. If $p_1 = 0.35$ and $p_2 = 0.25$, the theoretical value of c_s is 0.3371. The experimentally determined value is found to be 0.3336.

5.3 Viscosity

The viscosity of the $4m \leftrightarrow 1r$ ($s=1$) lattice gas model derived in Chapter 4 was found to be

$$\nu = \frac{c^2}{4\Delta t} \left[\frac{1}{4w} + \frac{1}{2(4v+w)} + \frac{1}{u} - \frac{1}{2} \right],$$

where,

$$u = f_m^2(1-f_m) + (1-f_m)^2 f_m$$

$$v = f_m^3(1-f_r) + (1-f_m)^3 f_r$$

$$w = f_m^4 + (1-f_m)^4.$$

f_m and f_r are the densities of the moving and rest particles, respectively. It should be noted that this result was derived under the assumption that for this model the tensors constructed from the lattice vectors are isotropic upto 4th rank. This is an incorrect assumption for any HPP based model. However, we shall plot the viscosity as a function of the density per cell of moving particles in Figure 5.8.

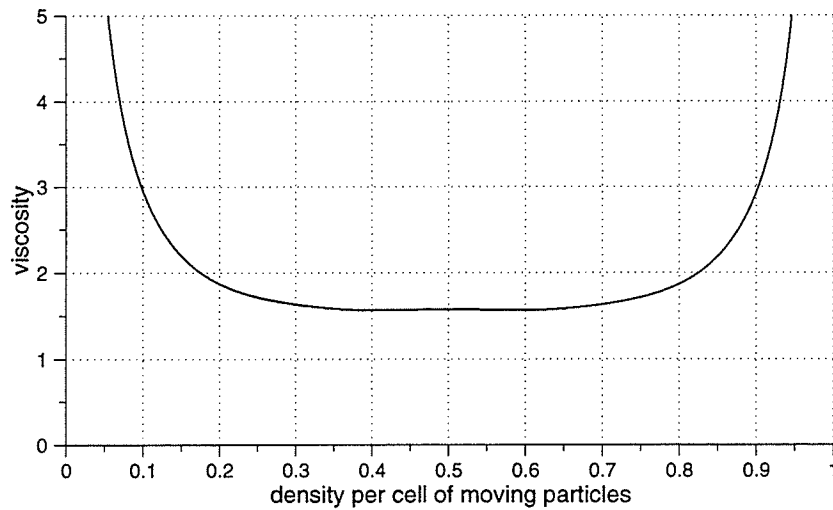


Figure 5.8: Viscosity as a function of moving particle density.

Chapter 6

LGA Experiments for Heterogeneous Systems

In this chapter we conduct lattice gas experiments with lattices which are divided into regions. These regions differ in the maximum number of rest particles which the sites within them can hold. The first step would be to determine whether such regions can exist in some sort of particle equilibrium which prevents the initial conditions (particle concentrations) from changing with time.

6.1 Boundaries Between Different Media

A two dimensional lattice could be divided into two regions as shown in Figure 6.1. One region (Region II) contains sites which allow for upto one rest particle and the other (Region I) has sites which allow no rest particles at any site.

The lattice is initialized with moving and rest particles such that the moving particle density, f_m , is the same in both parts. This is done so that the two regions are in (moving particle) equilibrium. Then Region II is initialized with a rest particle

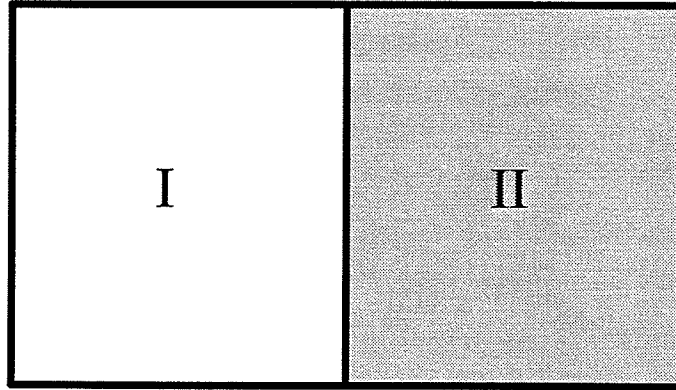


Figure 6.1: The two dimensional lattice with two regions.

density, f_r , according to Equation (6.1). This is done in order that there be an equilibrium between moving and rest particles in Region II. Thus, the entire lattice will be in equilibrium and moving and rest particle densities should not change with time.

$$f_r = \frac{f_m^4}{f_m^4 + (1 - f_m)^4}. \quad (6.1)$$

We are interested in determining whether there would be any kind of deviation from the initial equilibrium conditions (caused by particle flow across the boundary). The following experiment was carried out: The two dimensional lattice had dimensions $N_x \Delta x * N_y \Delta y$, where $\Delta x = \Delta y = \Delta$ is one lattice unit. $N_x = 2048$ and $N_y = 512$ were the number of cells in the x and y directions, respectively. The number of moving and rest particles within both regions is shown in Figure 6.2. In this case, $f_m = 0.35$ within both regions and $f_r = 0.07755$ in Region II. As expected, Region I has no rest particles and the total number of rest and moving particles within the two regions doesn't fluctuate significantly with time.

The test was repeated with Region I sites which could hold a maximum of one rest particle and Region II sites which allowed for upto two rest particles at a site.

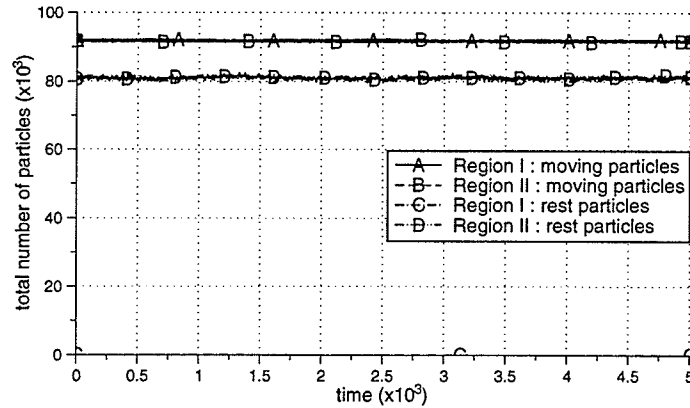


Figure 6.2: Equilibria between Region I ($s=0$) and Region II ($s=1$).

$f_m = 0.25$ and $f_r = 0.01220$ are the moving and rest particle densities in both regions. Figure 6.3 shows unchanging moving and rest particle populations as expected.

6.2 Numerical Experiments

In the last section we determined the necessary criteria for two regions to exist in equilibrium and the propagation speed within each of these two media. The next step would be to test the propagation of a small perturbation in a lattice, across a boundary. The magnitudes of the reflected and transmitted wave are then functions of the propagation speed within the two media. The modelling of two dimensional TM or TE electromagnetic phenomena [24] could be described by the linear scalar wave equation,

$$\nabla^2 \phi = \frac{1}{c^2} \frac{\partial^2 \phi}{\partial t^2},$$

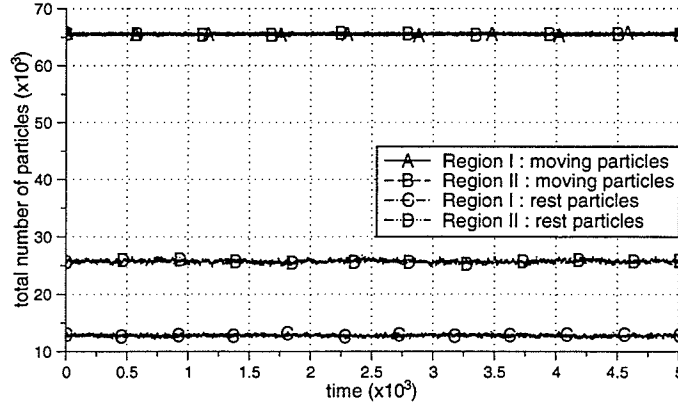


Figure 6.3: Equilibria between Region I ($s=1$) and Region II ($s=2$).

with the application of appropriate boundary conditions and sources. For problems independent of the z -direction, $\phi = E_z$ or H_z for the TM or TE cases, respectively. Using the analogy between acoustics and electromagnetic fields [25], for TM problems, the macroscopic excess pressure, p , (please see Appendix A) can be equated to the electric field E_z , and the x and y components of the flow velocity, $\mathbf{u} = (u_x, u_y)$, can be equated to the magnetic field components, H_y and H_x , respectively.

6.2.1 Wave Propagation Across an Interface Using the $4m \leftrightarrow 1r$ ($s = 1$) Lattice Gas

In this section we shall investigate wave propagation through a lattice which has two regions of different permittivities. These regions are modelled by allowing for $4m \leftrightarrow 1r$ ($s=1$) collisions in one and HPP (no rest) collisions in the other.

The simulation space was a two dimensional lattice as shown in Figure 6.4 with

x and y dimensions of 4096 and 2048 lattice units, respectively. A gaussian-pulsed plane wave of width 100Δ was centred at $1200 \Delta x$. The lattice was equally divided into two regions. As mentioned earlier, Region I did not allow for the creation of rest particles (HPP, no rest) at any site while each site within Region II could hold up to a maximum of one rest particle ($4m \leftrightarrow 1r$ ($s=1$)). The lattice used in this experiment had reflecting boundaries as shown in Figure 6.5. For example, an East moving particle incident at the right boundary turned into a West moving particle and was thus reflected back.

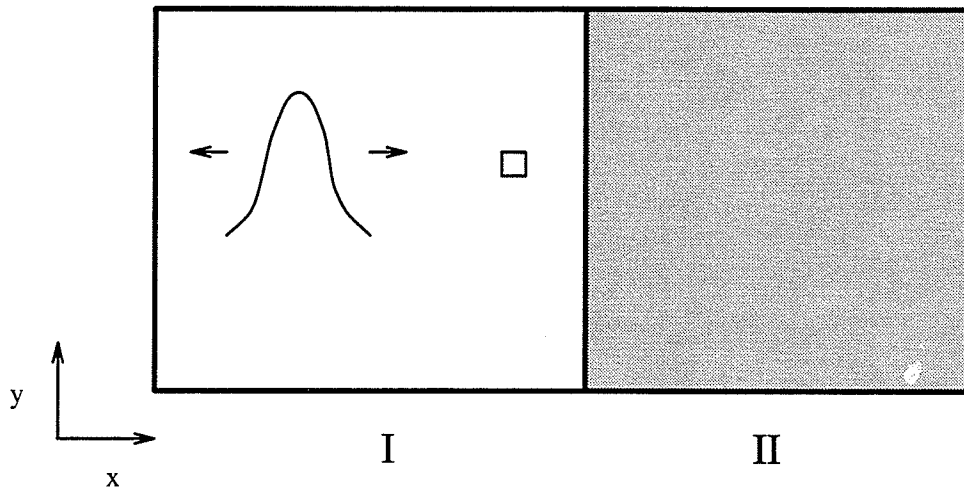


Figure 6.4: The two dimensional lattice with two regions.

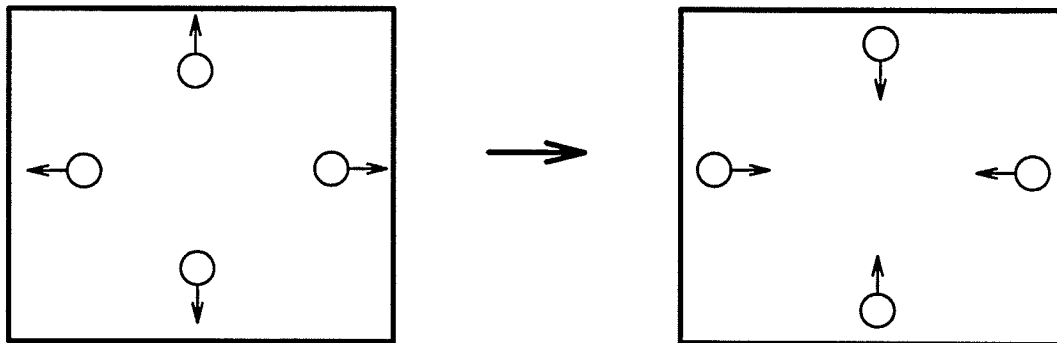


Figure 6.5: Reflecting lattice boundaries.

A square sampling window of dimensions $99 \Delta \times 99 \Delta$, was centred at $1700 \Delta x$, $1024 \Delta y$. Moving particles within both regions were initialized with a probability of 0.40 ($= f_m$). In accordance with Equation (2.37), rest particles within Region II were then initialized with a probability of 0.1649 ($= f_r$). The propagation speed c_s could be calculated using Equation (4.50).

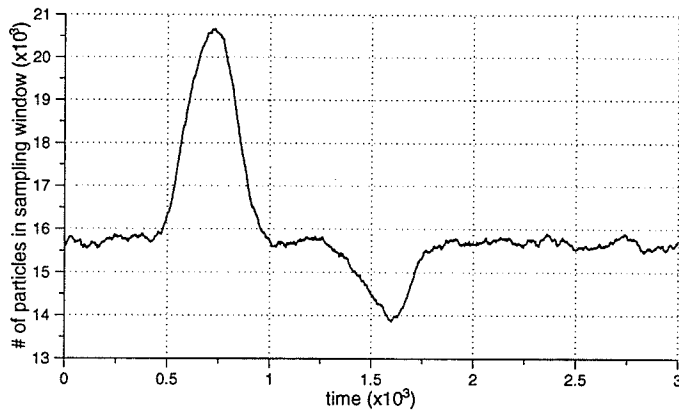
$$c_s = \sqrt{\frac{4f_m(1-f_m)}{2[4f_m(1-f_m) + 16f_r(1-f_r)]}}. \quad (6.2)$$

In this experiment, $c_s = 0.3895$. The propagation speed in Region I is $\frac{1}{\sqrt{2}}$. Assuming a relative dielectric constant $\epsilon_I = 1$ for Region I, the dielectric constant ϵ_{II} for Region II is

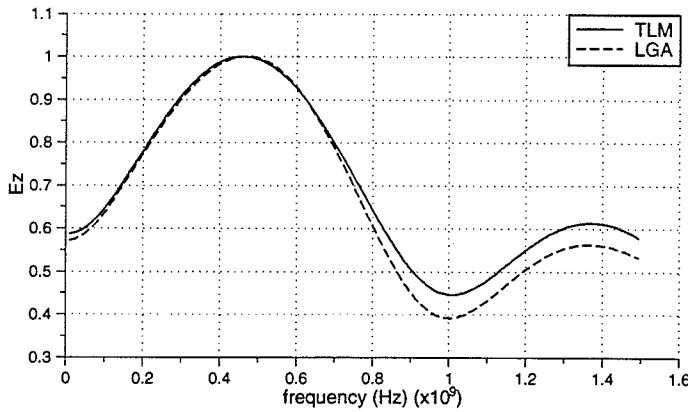
$$\begin{aligned} \epsilon_{II} &= \frac{1}{2c_s^2} \\ &= 3.2957. \end{aligned}$$

Particles were counted within the sampling window for 3000 time steps and the results are shown in Figure 6.6(a).

A Fourier transform was applied to the time domain waveform of Figure 6.6(a) to obtain the frequency response shown in Figure 6.6(b). The results are compared with those obtained using the Transmission Line Matrix method [26]. The TLM method is a general numerical technique that can be applied to obtain an approximate solution to the time-dependent form of Maxwell's equations. The method belongs to the same class of numerical techniques that include the various Time-Domain Finite-Difference [27], Finite-Volume [28], and Finite-Element [29] methods. An overview of the TLM method can be found in [30], and the application of the method to a variety of electromagnetic radiation and scattering problems is provided in [31]. The



(a) Time Domain



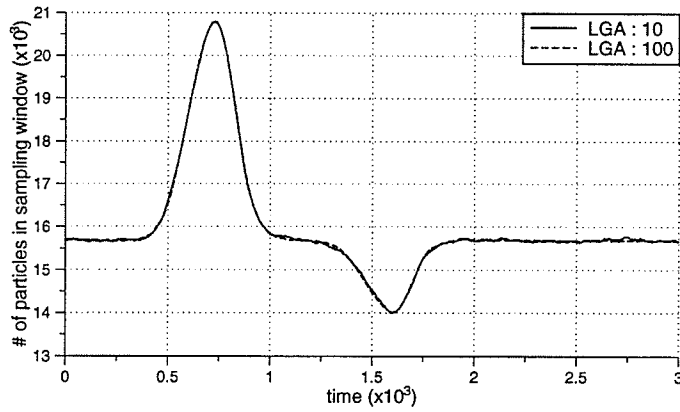
(b) Frequency Response

Figure 6.6: The two region interface: HPP and $4m \leftrightarrow 1r$ ($s=1$), $f_m = 0.40$.

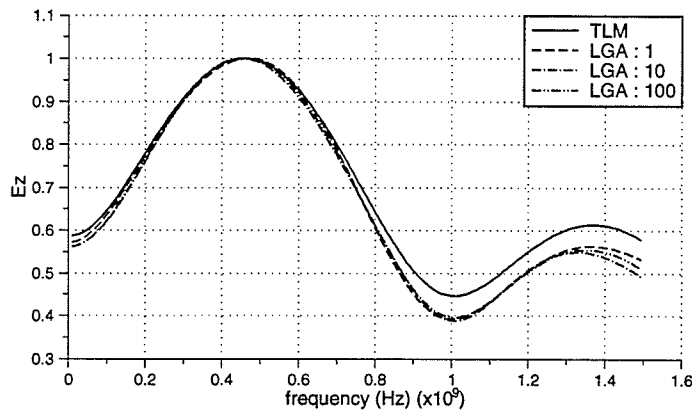
standard interpretation of the algorithm is that it follows the interaction of idealized voltage pulses propagating on a transmission line grid. Although this representation is quite different from the standard finite-difference or finite-element methods, the TLM method still requires all the same quantities to analyze a given problem. Appropriate boundary conditions and initial conditions are required to compute a solution.

In order to compare the TLM and LGA methods, results are normalized to their maximum values. In the TLM program, the two dimensional lattice had dimensions 400×200 while in our LGA experiments, the lattice had dimensions 4096×2048 . In order to make a comparison, the LGA inter-nodal spacing ($\Delta x = \Delta y = \Delta$) was taken to be 0.0005m , while the in TLM lattice Δ was 0.005m . Hence the LGA lattice was about 100 times bigger in area than the TLM lattice. The propagation speed, c_s , in the LGA experiments for the HPP (no rest) model was normalized to the speed of light in vacuum, $3 * 10^8 \text{ m/s}$.

In the previous experiment, during the lattice initialization process, a random number generator was used to initialize the lattice sites with particles. For example, in Region I, if the random number generated was less than 0.40, the North direction of a site was initialized to 1. In a similar manner, the East, West and South directions of each site in the lattice were initialized. It could be then said that the density of moving particles in the lattice was $f_m = 0.40$. The simulation program utilized an initial *seed* and each successive random number was the seed for the next. In an attempt to create a more random experiment, the simulation was executed a number of times using different seeds. One would then expect that an ensemble of simulations would give a better representation of the time-domain waveform. As shown in Figure 6.7(a), the time domain waveform becomes less noisy as the number of simulations in the ensemble increases from 10 to 100. The frequency response as shown in Figure 6.7(b), however, does not change by very much.



(a) Time Domain



(b) Frequency Response

Figure 6.7: Ensemble averaging for the two region interface: HPP and $4m \leftrightarrow 1r$ ($s=1$), $f_m = 0.40$.

From transmission line theory, we would expect the magnitude of the reflection coefficient, Γ , to be

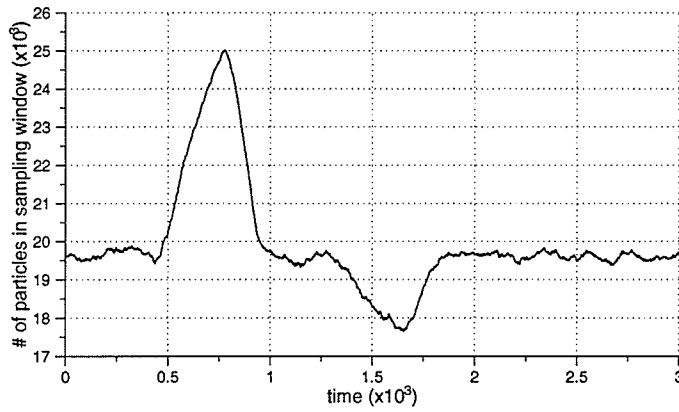
$$\begin{aligned}\Gamma &= \frac{Z_{II} - Z_I}{Z_{II} + Z_I} \\ &= \frac{\frac{1}{\sqrt{\epsilon_{II}}} - \frac{1}{\sqrt{\epsilon_I}}}{\frac{1}{\sqrt{\epsilon_{II}}} + \frac{1}{\sqrt{\epsilon_I}}} \\ &= \frac{\frac{1}{\sqrt{3.2957}} - 1}{\frac{1}{\sqrt{3.2957}} + 1} \\ &= -0.2896.\end{aligned}$$

Using the peak values of the incident and reflected wave, E_z^{inc} and E_z^{ref} , respectively, the experimental value of the reflection coefficient is $\Gamma = E_z^{ref} / E_z^{inc} = -0.3258$.

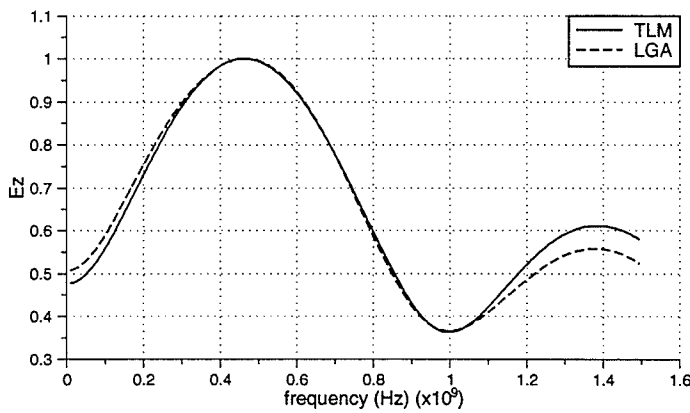
The moving particles were then initialized with a density of $f_m = 0.50$ in both regions. The propagation speed, c_s , in Region II is 0.316228 and the resulting relative permittivity is 5.00. The time domain waveform, which results from counting the particles within a sampling window of dimensions 99 x 99, centred at $1700\Delta x$, $1024\Delta y$, is shown in Figure 6.8(a). From transmission line theory, we would expect the reflection coefficient, $\Gamma = -0.3820$. The experimental results yield a value of $\Gamma = -0.3628$.

For the same problem with $f_m = 0.50$, the square sampling window was then centred at $2060\Delta x$, $1024\Delta y$ and particles counted for 4000 time steps in order to measure the transmitted wave. The resulting time-domain waveform is shown in Figure 6.9. According to theory, the transmission coefficient (T) is given by

$$\begin{aligned}T &= 1 + \Gamma \\ &= 0.61803.\end{aligned}$$



(a) Time Domain



(b) Frequency Response

Figure 6.8: The two region interface: HPP and $4m \leftrightarrow 1r$ ($s=1$), $f_m = 0.50$.

Using the peak incident value from Figure 6.8(a) and the peak transmitted value from Figure 6.9, the value calculated from experiment is $\Gamma = 0.5081$.

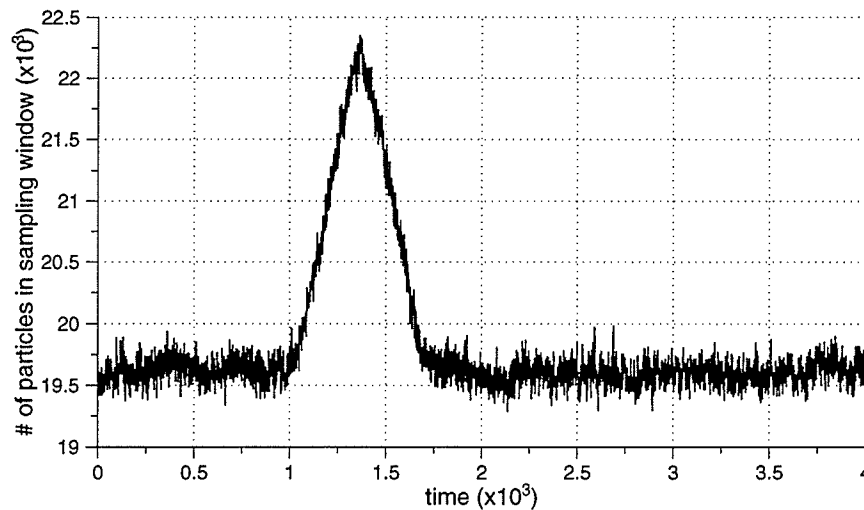


Figure 6.9: Time domain waveform (in the dielectric region) for $4m \leftrightarrow 1r$ ($s=1$), $f_m = 0.50$.

The frequency response of the reflected wave was also compared with results obtained using the TLM method and is shown in Figure 6.8(b).

6.2.2 Wave Propagation Across an Interface Using the $4m \leftrightarrow 1r$ ($s = 2$) Lattice Gas

In this section, we perform experiments similar to those in the previous section with the exception that Region II contains sites, all of which can hold upto a maximum of

two rest particles. Sites within Region I do not hold rest particles. The simulation space was a two dimensional lattice with x and y dimensions of 4096 and 2048 lattice units, respectively. A gaussian-pulsed plane wave of width 100Δ was centred at $1200 \Delta x$. The maximum size of the perturbation was 20% above the background density. The lattice was equally divided into two regions. Region I did not allow for the creation of rest particles at any site while each site within Region II held up to a maximum of two rest particles (of mass $4m$ each). In other words, the maximum stack length in Region II was two. The lattice again had reflecting boundaries. The square sampling window was centred at $1700 \Delta x$, $1024 \Delta y$ and was of dimensions $99 \Delta \times 99 \Delta$. Moving particles within both regions were initialized with a probability of $f_m = 0.35$. Rest particles within Region II were initialized with a probability of $f_r = 0.0775$, in accordance with Equation (2.37). The propagation speed c_s could be calculated using Equation (4.51) with $k = 2$,

$$c_s = \sqrt{\frac{4f_m(1-f_m)}{2[4f_m(1-f_m) + 32f_r(1-f_r)]}}$$

In this experiment, $c_s = 0.3771$. Assuming the propagation speed in Region I is $\frac{1}{\sqrt{2}}$, the dielectric constant ϵ_{II} for Region II could be then calculated as,

$$\begin{aligned} \epsilon_{II} &= \frac{1}{2c_s^2} \\ &= 3.5155. \end{aligned}$$

The resulting time domain waveform for 3000 time steps is shown in Figure 6.10.

Comparing the theoretical and experimental reflection coefficients, $\Gamma_{theory} = -0.30434$ and $\Gamma_{exp} = -0.36701$.

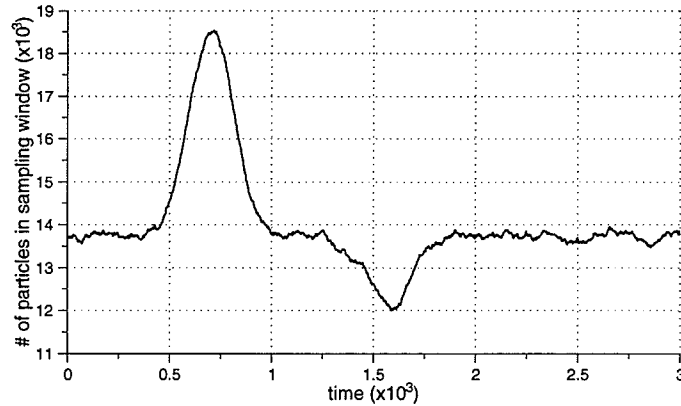


Figure 6.10: Time domain waveform for the two region test; $4m \leftrightarrow 1r$ ($s=2$), $f_m = 0.35$.

We applied the Fourier transform to the time domain waveform to obtain the frequency response shown in Figure 6.11. The results are again compared with those obtained using the Transmission Line Matrix method.

In another experiment with two regions, the background moving particle density in each was chosen to be $f_m = 0.50$. The corresponding rest particle density in Region II is $f_r = 0.50$. The propagation speed is $c_s = 0.2357$ and relative permittivity is $\epsilon_{II} = 9.00$ in Region II. The dimensions of the lattice, window position, window size, location of the source and pulse width of the gaussian are the same as in the previous experiment.

Comparing the theoretical and experimental reflection coefficients, $\Gamma_{theory} = -0.50$ and $\Gamma_{exp} = -0.45556$.

The Fourier transformed results are shown in Figure 6.12 and compared with those obtained using the TLM method.

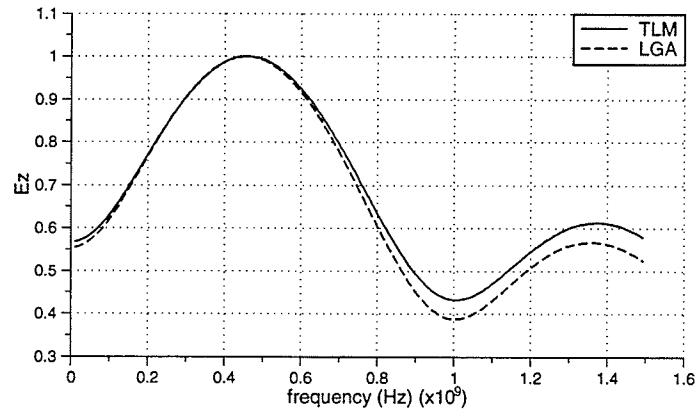


Figure 6.11: Frequency response for the reflected wave in Region I; $4m \leftrightarrow 1r$ ($s=2$), $f_m = 0.35$.

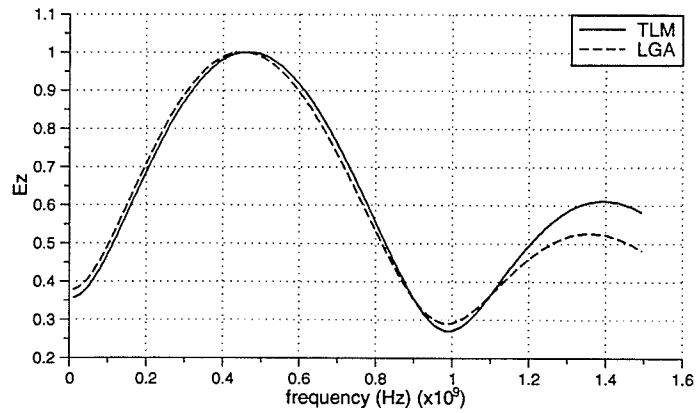


Figure 6.12: Frequency response for the reflected wave in Region I; $4m \leftrightarrow 1r$ ($s=2$), $f_m = 0.50$.

6.2.3 Wave Propagation Across an Interface Using the $4m \leftrightarrow 1r$ Lattice Gas Mixture

In the previous experiments, Region II consisted of sites, all of which allowed for 1 rest particle. In this experiment, Region II has a mixture of sites which allow for either 0 or 1 rest particle. In other words, Region II is a lattice gas mixture. The propagation speed in this region was previously given by Equation (5.7) as

$$c_s = \sqrt{\frac{4f_m(1-f_m)}{2[4f_m(1-f_m) + 16pf_r(1-f_r)]}} \quad (6.3)$$

For $p = 0.40$, $f_m = 0.50$ and $f_r = 0.50$, $c_s = 0.4385$. The relative permittivity of Region II was 2.60. Region I had a relative permittivity of 1. The lattice had dimensions 4096 x 2048 and the source and observation point locations were the same as in the previous experiments. The problem was modelled using the TLM method with a simulation space of dimensions 400 x 200. The Fourier transform was applied to the time domain waveforms from each experiment and results are shown in Figure 6.13.

Comparing the theoretical and experimental reflection coefficients from time domain results, $\Gamma_{theory} = -0.2344$ and $\Gamma_{exp} = -0.1778$.

In another experiment, the Region II mixture consisted of a mixture of zero and two rest particle sites. This time we used $p = 0.35$ with $f_m = 0.50$ and $f_r = 0.50$ in Region II. Using these values to calculate c_s from Equation (5.8),

$$c_s = \sqrt{\frac{4f_m(1-f_m)}{2[4f_m(1-f_m) + 32pf_r(1-f_r)]}} \quad (6.4)$$

we get $c_s = 0.3627$. The relative permittivity of Region II is subsequently 3.80. The dimensions of the lattice, window position, window size, location of the source and

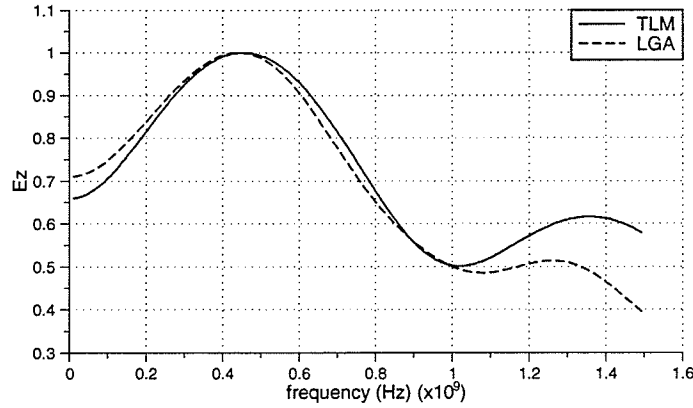


Figure 6.13: Frequency response for the two region experiment; $4m \leftrightarrow 1r$ ($s=1$) and HPP (no rest) rest mixture.

pulse width of the gaussian were the same as in the previous experiment. The problem was also modelled using the TLM method with a simulation space of dimensions 400×200 . The Fourier transform was applied to the time domain waveforms from both simulations and the results are shown in Figure 6.14.

Comparing the theoretical and experimental reflection coefficients, $\Gamma_{theory} = -0.3219$ and $\Gamma_{exp} = -0.2830$.

6.2.4 Modelling a Dielectric Strip Using the $4m \leftrightarrow 1r$ Model.

In this section we model a dielectric strip using the $4m \leftrightarrow 1r$ ($s=1$) lattice gas. The region surrounding the strip was modelled using the HPP (no rest) model. In this experiment, the lattice as shown in Figure 6.15, had dimensions 4096×2048 . The dielectric strip of 100Δ thickness ($\epsilon_{strip} = 3.2957$) was placed at $2000 < x < 2100$. This was accomplished by using the one rest particle model in the strip region with

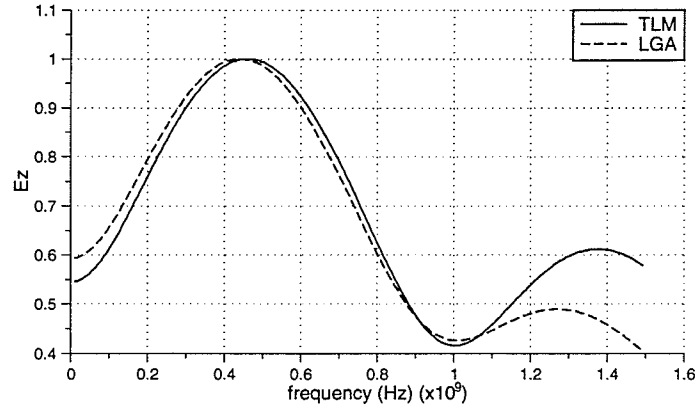


Figure 6.14: Frequency response for the two region experiment; $4m \leftrightarrow 1r$ ($s=2$) and HPP (no rest) rest mixture.

$f_m = 0.40$ and $f_r = 0.1649$. The moving particle density in the surrounding region was $f_m = 0.40$. A gaussian-pulsed plane wave source was located at $1200 \Delta x$. Its maximum amplitude was 20% above the background density and the pulsewidth $\tau = 100\Delta$. A square sampling window was located at $1700 \Delta x$, $1024 \Delta y$.

The resulting time domain waveform is shown in Figure 6.16. This waveform is the result of an ensemble average of 100 simulation results using different initial conditions everytime.

The theoretical value of the reflection coefficient is $\Gamma_{theory} = -0.2896$. From the experiment however, $\Gamma_{exp} = -0.3169$. In Figure 6.17, results from a TLM simulation using a lattice of size 400×200 (all other variables such as pulse width, source location, etc. are scaled accordingly) are compared with the lattice gas results obtained by ensemble-averaging 1, 10 and 100 simulations.

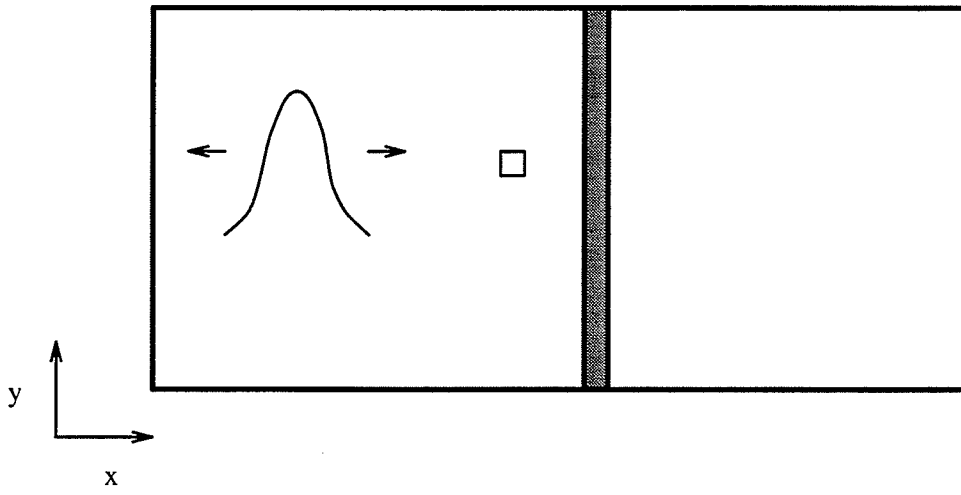


Figure 6.15: The two dimensional lattice with dielectric strip; $\epsilon_{strip} = 3.2957$.

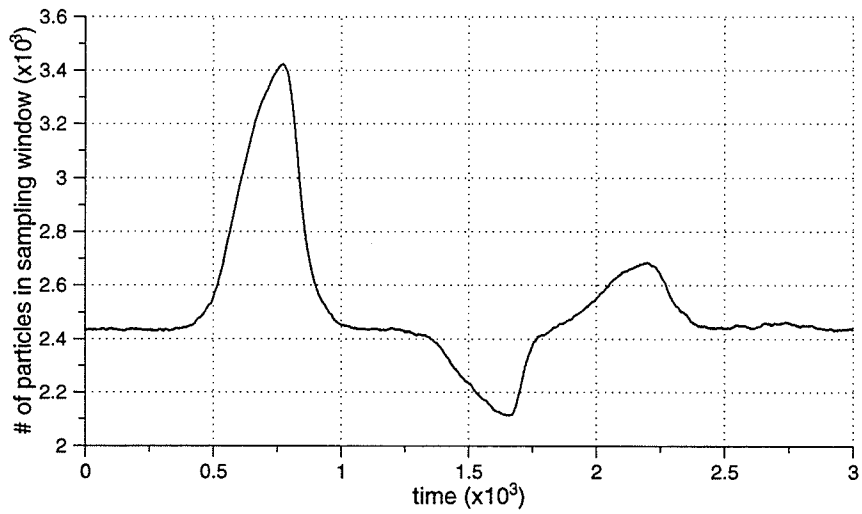


Figure 6.16: Time domain waveform for dielectric strip.

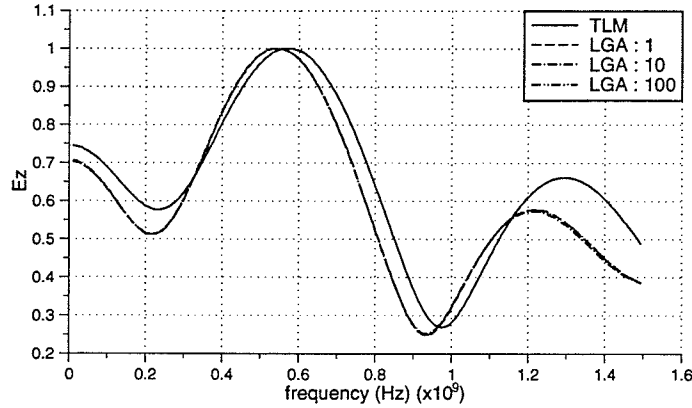


Figure 6.17: Frequency response for dielectric strip.

6.2.5 The Two-Layered Dielectric Cylinder

In this section we create an inhomogeneous dielectric cylinder, made up of two concentric layers as shown in Figure 6.19. The size of the lattice was 4096×2048 . The gaussian plane wave was generated as before by superimposing additional particles on the lattice with a 20% fill at the maximum of the distribution. The cylinder was centred at $x = 2000\Delta$, $y = 1024\Delta$. The inner radius was 80Δ with a relative permittivity of 3.31, the outer radius being 100Δ with a relative permittivity of 1.96. This was implemented by allowing a maximum of 1 rest particle in the outer region and up to 3 rest particles in the inner region. The rules for this lattice gas are shown in Figure 6.18. The inter-nodal spacing in the lattice was defined to be 0.001m . The system was evolved for 3000 iterations and observations were made at a $40\Delta \times 40\Delta$ square window, centred at $x = 1700\Delta$, $y = 1024\Delta$. The Fourier transform was applied to the time domain waveform and compared with results from a TLM simulation of the same problem with lattice dimensions 400×200 . The results are

shown in Figure 6.20.

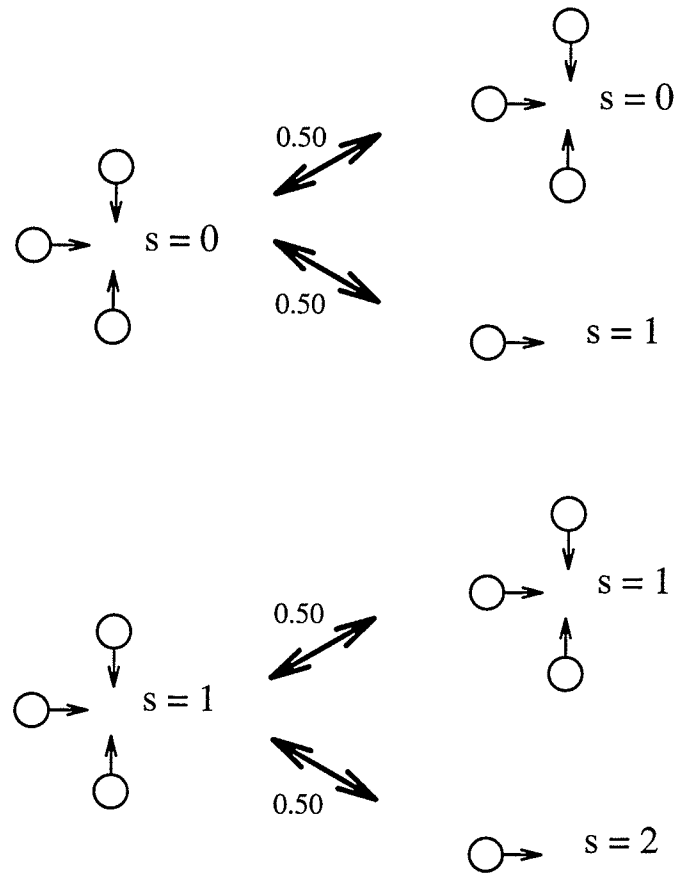


Figure 6.18: Collision rules for the creation of rest particles.

It should be noted that the rule in this experiment violates semi-detailed balance following the arguments presented in section 2.11. Hence, the analysis presented in Chapter 4 does not apply to this model. The relative permittivities for the two regions were calculated using a rectangular lattice, propagating a plane wave across it and then calculating the propagation speed, c_s , using the method described in Appendix B (observing the peaks of the gaussian plane wave).

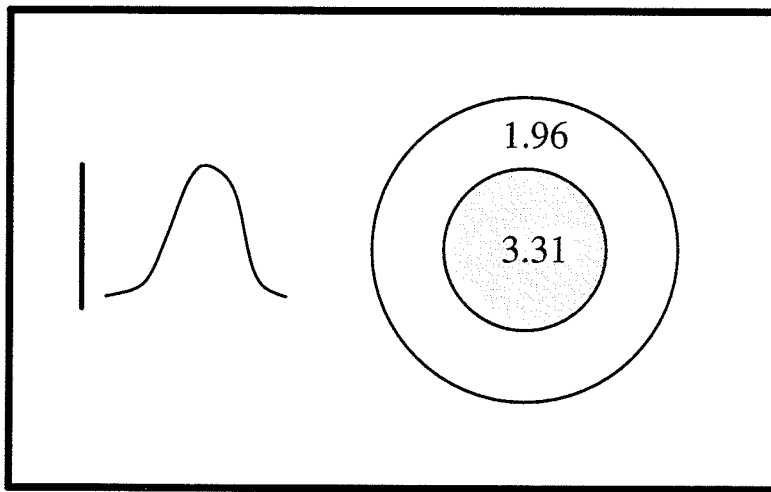


Figure 6.19: Two dimensional lattice with dielectric cylinder.

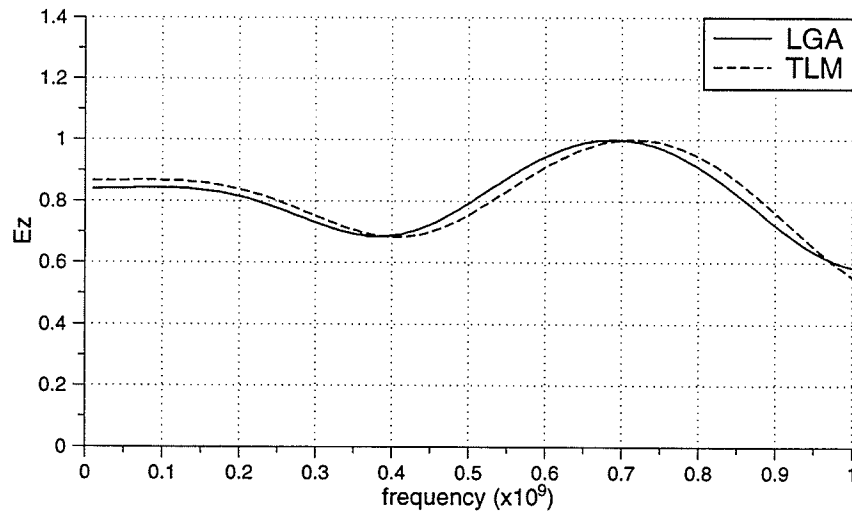


Figure 6.20: Two dimensional lattice with dielectric cylinder: results.

Chapter 7

Conclusions

In this thesis, we have demonstrated the validity of the lattice gas automata approach for simulating the scalar wave equation in two dimensions in the presence of inhomogeneous media. Experiments to investigate electromagnetic plane wave interaction with dielectric media have been performed and yield reasonable results. For the HPP and FHP lattice gas models (with and without rest particles), theoretical as well as experimental Boltzmann equilibria are in good agreement with each other. The Fermi-Dirac distribution enables a prediction of the ratio of moving to rest particles in a lattice gas simulation, provided the semi-detailed balance condition is obeyed.

7.1 CA Versus Conventional Numerical Techniques

The differences between cellular automata methods and conventional numerical techniques are numerous and at times quite difficult to quantify. The cellular automata approach to modelling physical systems is a departure from the traditional differential equation based methods which are widely used. It is important to note the difference between cellular automata and partial differential equations and their finite-difference

counterparts [18]. In partial differential equations, the spatial and temporal coordinates and the dependent variables are continuous quantities. In the corresponding finite-difference approximations, space and time are discretized, while the dependent variables are continuous. In the cellular automata environment however, space, time and the dependent variable are all discrete.

Due to its discrete nature, an invertible CA simulation preserves all the information and can be reversed at any time to yield the initial condition. This, however, is not possible in finite-difference based methods owing to floating-point, round-off errors. Furthermore, since lattice gas operations are bit oriented, they execute more naturally on a computer [32].

While differential equation based algorithms may become unstable, lattice gas methods are obviously quite stable since the process only involves averaging.

7.2 Simulation Time

A comparison of simulation times using different methods was not attempted in this thesis. The reason for this being a lack of a suitable measure of performance. As mentioned in [18] it would indeed be unfair to compare parallel implementations of CA with serial implementations of floating-point methods. Furthermore, it remains to be determined as to what size of simulation space (how many cells, size of sampling window, etc.) is required to produce accurate numerical results. It should be noted that the computational complexity involved in the binary operations of one lattice gas cell is considerably less than the complexity of a finite-difference floating-point operation. However, in our experiments, 10 lattice gas cells represent one finite-difference cell. In addition, the size of the sampling window used to determine the magnitude of the macroscopic variable at one finite-difference node was 40×40 . Again, these

are only preliminary estimates and much work remains to be done in order that we might predict the optimal mesh dimensions to model a particular structure.

7.3 Advantages of the CA Approach

An interesting and oft cited property of CA is the complexity that emerges from a system which might be very simple at the microscopic level. The CA's rules must therefore capture the essence of the phenomenon under investigation and then the appropriate macroscopic behaviour would hopefully emerge. In addition CA may be used to model systems which are very difficult to describe using differential equations.

7.4 Modelling Inhomogenieties

With an increase in the number of rest particles (stack length), it is possible to model materials having higher permittivities. The graph in Figure 7.1 illustrates the manner in which relative permittivity varies with the maximum number of rest particles in the $4m \leftrightarrow 1r$ model.

7.5 Special-Purpose Architectures

CA simulations, when run on general-purpose, floating-point processor based serial machines take very long. As explained earlier, CA operations are bit oriented, simple logical operations and a floating point processor would indeed be unnecessary. Thanks to the development of special-purpose architectures like CAM-8 by the Information Mechanics Group at MIT, large scale CA simulations are now quite feasible. Furthermore, the machine has the ability to display generated data (bits at sites in

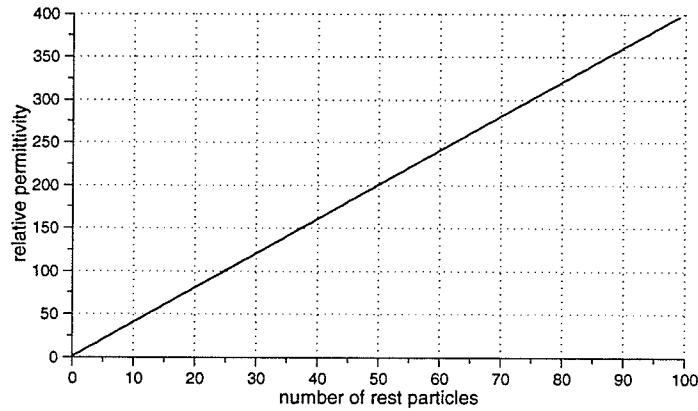


Figure 7.1: ϵ_r as a function of k

the lattice) in real time, on a monitor. This immediate visualization in turn enables a better understanding of the problem under investigation. Only a small degree of parallelism (a factor of 8) is utilized by CAM-8. This means that the simulation space is divided into 8 equal parts and processed simultaneously. Each part on its own is processed serially. For models with 16 bits per site, the 8-module prototype performs 200 million site updates per second on spaces of up to 32 million sites [13]. Furthermore, the architecture consists primarily of SRAM (look-up tables) and DRAM (cells) and is indefinitely scalable in three spatial dimensions. CAM-8 contains effectively the same quality and quantity of digital hardware as a typical workstation (and therefore costs about the same).

7.6 Future Work

The models used in this thesis are used for the scalar wave equation in two dimensions and the extension to three dimensions would require modifications to the rule. Furthermore, we would have to create new rules to model the vector wave equation.

Lattice gas automata could be used as an environment in which we could model electromagnetic interactions with biological systems. This would require arbitrarily shaped regions in the lattice with sites which can hold different numbers of rest particles.

In order that an assessment of the feasibility of the lattice gas approach be made, a detailed analysis of the accuracy of numerical results must be made. As explained in Chapter 4, the HPP model yields an anisotropic viscous term. The viscosity is used to predict damping in the perturbation as it propagates through the lattice. Hence in order that we might accurately predict this quantity, it would be necessary to switch to hexagonal lattice based models such as the FHP.

Appendix A

Acoustic Waves in Fluids

This appendix gives details of the derivation of the wave equation which is derived in [25] from the conservation equations. During the course of this derivation we shall restrict the discussion to one dimension.

A.1 Conservation of Mass

We begin by considering a *control volume* in space between the planes at x and $x + dx$ as shown in Figure A.1 which has the form of a parallelepiped with the surface normal to the x-axis having unit area.

The mass of fluid per unit time entering the volume through the surface at x at time t is

$$M(x, t) = \rho(x, t)U(x, t). \quad (\text{A.1})$$

This is called the *mass flux*. The rate of mass which leaves the volume through the surface at $x + dx$ at the same time t is $M(x + dx, t)$. The net mass influx to the

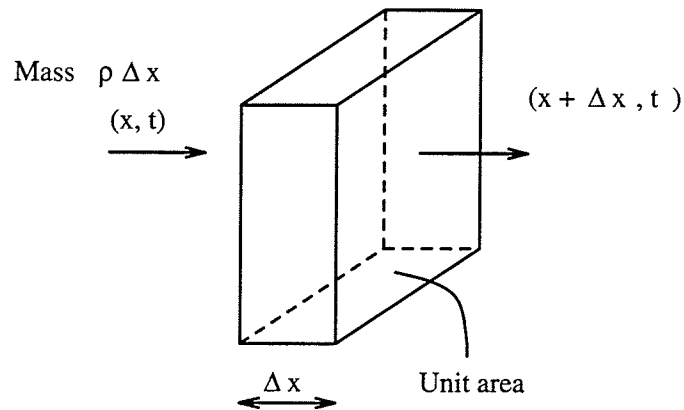


Figure A.1: Control volume

control volume is then

$$M(x, t) - M(x + dx, t) = - \left(\frac{\partial M}{\partial x} \right) dx \quad (\text{A.2})$$

for small dx .

$\rho(x, t)dx$ is the total mass inside the control volume at time t . The time rate of change of the mass inside the volume is equal to the influx, or

$$\frac{\partial \rho}{\partial t} + \frac{\partial M}{\partial x} = 0. \quad (\text{A.3})$$

This is often referred to as the continuity equation.

A.2 Conservation of Momentum

Similarly, the conservation of momentum equation can be expressed in terms of a momentum density and a momentum flux. While the thermal motion does not contribute to the mass flux, it does contribute to the momentum flux, which, by definition is the pressure P in the fluid.

As discussed in the previous section, the rate of mass transported through the surface at x is $M = \rho U$. The momentum of this mass, transferred to the control volume from the left, is MU . As well, the momentum transfer due to the thermal motion is expressed by the pressure $P(x, t)$, which results from the collisions between the particles on the left with those inside the volume. Hence, the total rate of momentum transferred to the particles in the control volume through the surface at x is

$$G = P + \rho U^2 = \frac{\partial M}{\partial t}. \quad (\text{A.4})$$

A.3 Acoustic Field Equations

We shall now discuss the equations for acoustic waves in a fluid. The following discussion is presented in [25].

The unperturbed field variables are assumed to be time independent (denoted by the subscript 0). Perturbations of density, velocity, mass flux and pressure are denoted by $\hat{\rho}$, u , m and p . The density perturbation is assumed to be small, so that $\hat{\rho} \ll \rho_0$. We obtain the corresponding pressure perturbation by expanding $P(\rho + \hat{\rho})$ in a Taylor series

$$P(\rho + \hat{\rho}) \approx P_0 + \left(\frac{dP}{d\rho}\right) \hat{\rho} + \left(\frac{1}{2}\right) \left(\frac{d^2P}{d\rho^2}\right) \hat{\rho}^2 + \dots \quad (\text{A.5})$$

$$\simeq P_0 + \left(\frac{dP}{d\rho}\right) \hat{\rho}. \quad (\text{A.6})$$

$$P_0 = P(\rho_0). \quad (\text{A.7})$$

$$p = \left(\frac{dP}{d\rho} \right) \hat{\rho}. \quad (\text{A.8})$$

The compressibility is defined as

$$k = \frac{1}{\rho_0} \frac{d\rho}{dP}. \quad (\text{A.9})$$

Using this in Equation (A.8),

$$p = \left(\frac{1}{k\rho_0} \right) \hat{\rho}. \quad (\text{A.10})$$

The perturbation in the mass flux is $m_1 = (\rho_0 + \hat{\rho})(U_0 + u) - \rho_0 U_0$. The unperturbed fluid is assumed to be at rest ($U_0 = 0$). Thus, $m_1 \simeq \rho_0 u$, where we have assumed that $\hat{\rho} \ll \rho_0$. The perturbation in the total momentum flux $G = \rho U^2 + P$ is $G_1 \simeq p$, since, $\rho_0 u^2$ is negligible compared to p if U is much smaller than wave speed. The conservation equations then reduce to

$$\rho_0 \frac{\partial U}{\partial t} = -\frac{\partial p}{\partial x}, \quad (\text{A.11})$$

$$k \frac{\partial p}{\partial t} = -\frac{\partial U}{\partial x}. \quad (\text{A.12})$$

By taking the spatial derivative of the first of these equations and time derivative of the second, we can eliminate U to obtain the wave equation,

$$\frac{\partial^2 p}{\partial t^2} = v^2 \frac{\partial^2 p}{\partial x^2}, \quad (\text{A.13})$$

where $v = 1/\sqrt{(\rho_0 k)}$ is the sound speed.

Appendix B

Propagation Speed Measurements

In order to measure the propagation speed (relative permittivity) of a lattice gas having a certain background density of moving and rest particles, we have employed the following method:

Let us consider the $2m \leftrightarrow 1r$ ($s=1$) model with $f_m = 0.4500$, $f_r = 0.4010$. The lattice dimensions are 4096×256 .

A gaussian perturbation is created in the lattice and a square sampling window is used to monitor the wave as it propagates. The number of particles within the window are counted at every time step. The lattice has *periodic* or *wrap-around* boundaries. This simply means that when the wave reaches one end of the two-dimensional lattice, it wraps around and re-enters at the opposite end. When the gaussian pulse starts out, it splits equally into 2 pulses, one moving to the left and the other to the right (labelled L and R, respectively in Figure B.1).

Figure B.2 shows four pulses. The first pulse is R when it propagates to the sampling window. In the meantime L travels to the West boundary of the lattice and re-enters at the East end. Pulse 2 is this perturbation when it propagates to the sampling window. Pulse 3 is R after it travels to the East boundary wraps around

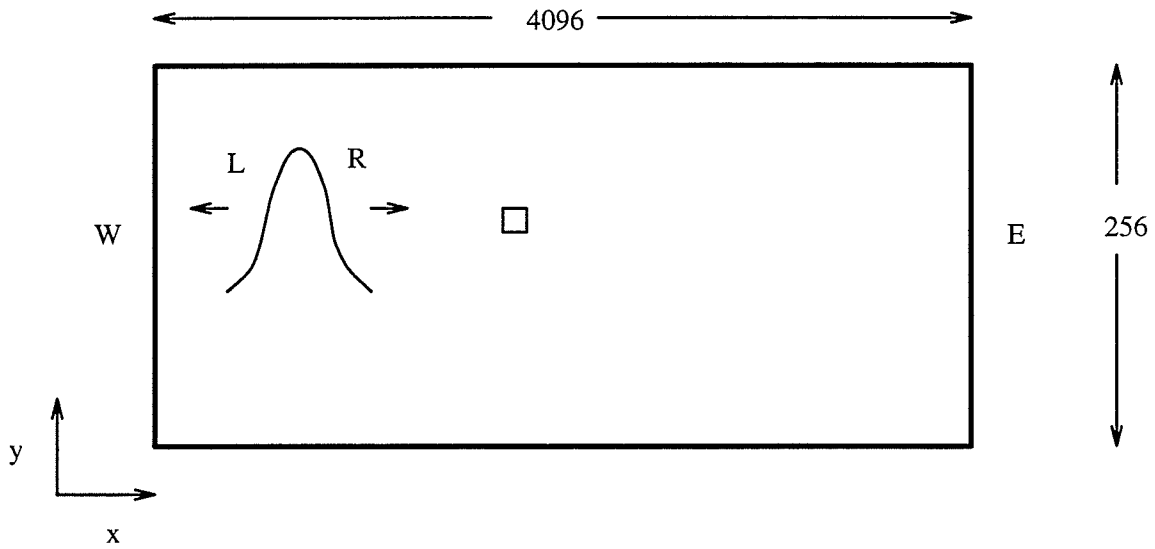


Figure B.1: Two dimensional lattice.

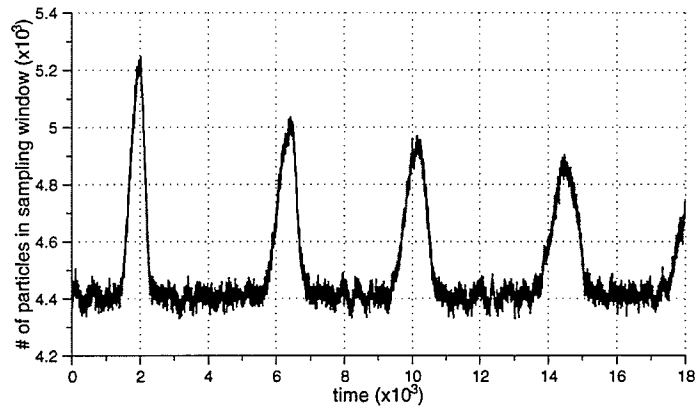


Figure B.2: Time domain waveforms.

to the West boundary and propagates to the window. Similarly pulse 4 is L. The number of time steps between pulse 1 and 3 or 2 and 4 is the time the wave takes to propagate across the lattice. The speed c_s then is simply

$$\begin{aligned} c_s &= \frac{4096}{14480 - 6424} \\ &= 0.5084. \end{aligned}$$

The theoretical speed is given by the formula

$$\begin{aligned} c_s &= \sqrt{\frac{4f_m(1-f_m)}{2[4f_m(1-f_m) + 4f_r(1-f_r)]}} \\ &= 0.5037. \end{aligned}$$

The propagation speed could also be determined by calculating the phase difference between pulses 2 and 4. At a frequency of 1.745×10^7 Hz this difference is found to be 1.054. This corresponds to a lattice size of $4096 * 0.0005$ in the x direction (lattice spacing, $\Delta = 0.0005$ m). The propagation speed in the HPP model is $\frac{1}{\sqrt{2}}$ which corresponds to the speed of light (used when performing the discrete Fourier transform). The propagation speed could then be calculated,

$$\begin{aligned} c_s &= \frac{1.745 * 10^7 * 2\pi * 4096 * 0.0005}{1.054 * 3.0 * 10^8} \frac{1}{\sqrt{2}} \\ &= 0.50221. \end{aligned}$$

Since the experimental result using the phase difference method is very close to that obtained using the peak observation method, we have used the latter in the thesis.

Bibliography

- [1] Toffoli, Tommaso, and Norman Margolus, *Cellular Automata Machines - A New Environment for Modeling*, Cambridge: MIT Press, (1987).
- [2] Toffoli, Tommaso, "What are nature's 'natural' ways of computing?" *Workshop on Physics of Computation - PhysComp '92*, IEEE Computer Society Press (1993), 5-9.
- [3] Von Neumann, John, *Theory of Self-Reproducing Automata* (edited and completed by Arthur Burks), Univ. of Illinois Press, (1966).
- [4] Wolfram S., *Cellular Automata and Complexity - Collected Papers*, Addison-Wesley, Reading, MA, (1994).
- [5] Weimar, J., J. Tyson and L. Watson. "Diffusion and wave propagation in cellular automaton modes of excitable media," *Physica D*, 55:309-327, 1992.
- [6] Ancona, M. G., "Lattice-Gas Approach to Semiconductor Device Simulation," *Solid-State Electronics*, Vol. 33, No. 12, pp. 1633-1642, (1990).
- [7] Chowdhury, D., P. Subbarao and P. Chaudhuri. Built-in self-test. *Journal of Electronic Testing*, 5(1):67, Feb. 1994. "A class of two-dimensional cellular automata and their applications in random pattern testing."

- [8] Creutz, Michael, "Deterministic Ising Dynamics," *Annals of Physics* **167** (1986), 62-76.
- [9] Boghosian, Bruce M., and C. David Levermore. "A Cellular Automaton for Burgers' Equation." *Complex Systems* **1** (1987):17-30.
- [10] Hardy, J., O. De Pazzis and Yves Pomeau, "Molecular dynamics of a classical lattice gas: Transport properties and time correlation functions," *Phys. Rev.* **A13** (1976), 1949-1960.
- [11] Frisch, Uriel, Brosl Hasslacher, and Yves Pomeau, "Lattice-Gas Automata for the Navier-Stokes Equation," *Phys. Rev. Lett.* **56** (1986), 1505-1508.
- [12] Diemer, K., K. Hunt, S. Chen, T. Shimomura and G. Doolen, "Density and Velocity Dependence of Reynolds Numbers for Several Lattice Gas Models." *Lattice Gas Methods for Partial Differential Equations*. Santa Fe Institute, (1990).
- [13] Margolus, Norman, "CAM-8: a computer architecture based on cellular automata," *Pattern Formation and Lattice Gas Automata*, American Mathematics Society (Fields Institute Series), Providence, RI, (1995).
- [14] Shah, M., "An optimized CAM-8 simulator for the SPARC architecture," M. S. Thesis in EECS, MIT (May 1992).
- [15] Press, W.H., Flannery, B.P., Teukolsky, S.A., and Vetterling, W.T., *Numerical Recipes: The Art of Scientific Computing*, Cambridge University Press, Cambridge, (1986).
- [16] Boghosian, B. and W. Taylor, "Correlations and renormalization in lattice gases," MIT Report MIT-CTP-2265, March 11, (1994).

- [17] D'Humieres, D. and P. Lallemand, " Numerical Simulations of hydrodynamics with lattice gas automata in two dimensions," *Complex Systems*, **1**, 599-632 (1987).
- [18] Boghosian, B. M., "Lattice Gases," 1989 Lectures in Complex Systems, SFI Studies in the Sciences of Complexity, Lect. Vol II, Erica Jen, Ed., Addison-Wesley, (1990).
- [19] Smith, M., "Cellular Automata Methods in Mathematical Physics," PhD thesis, MIT (1994).
- [20] Landau, L., and E. Lifschitz, *Fluid Dynamics*, Pergamon, New York (1959).
- [21] Toffoli, Tommaso, and Norman Margolus, "Invertible Cellular Automata: A Review," *Physica D* **45** (1990), 1-3.
- [22] Feynman, R. P. R. Leighton, M. Sands, it The Feynman Lectures on Physics, 6-6, (1965).
- [23] Wolfram, S., *J. Stat. Phys.*, **45** (1986) 471.
- [24] Simons, N. R. S., G. E. Bridges, B. W. Podaima and A. Sebak, "Cellular Automata as an environment for simulating electromagnetic phenomena," *IEEE Microwave and Guided Wave Letters*, **4**, 247-249 (1994).
- [25] Ingard K. U., *Fundamentals of Waves and Oscillations*, Cambridge University Press, Cambridge, (1970).
- [26] Simons, N. R. S., "Development and Application of Differential-Equation Based Numerical Techniques to Electromagnetic Scattering and Radiation Problems," PhD thesis, University of Manitoba, (1994).

- [27] Taflove, A. and K. R. Umashanka, "Review of FD-TD Numerical Modelling of Electromagnetic Wave Scattering and Radar Cross Section," *Proceedings of the IEEE*, 1989, **77**, pp. 682-699.
- [28] Shankar, V., W. F. Hall and A. H. Mohammadian, "A Time-Domain Differential Solver for Electromagnetic Scattering Problems," *Proceedings of the IEEE*, 1989, **77**, pp. 709-721.
- [29] Lynch, D. R. and K. D. Paulsen, "Time-Domain Integration of the Maxwell Equations on Finite Elements," *IEEE Trans. Antennas and Propagation*, 1990, **AP-38**, pp. 1933-1942.
- [30] Hoefler, W. J. R., "The Transmission-Line Matrix (TLM) Method," in, Itoh, T. (ed), *Numerical Techniques for Microwave and Millimeter Wave Passive Structures*, New York: Wiley, 1989.
- [31] Simons, N. R. S., A. Sebak and A. Ittipiboon, "Analysis of Aperture-Coupled Microstrip Antenna and Circuit Structures Using the Transmission Line Matrix Method," *IEEE Antennas and Propagation Magazine*, vol. 37, no. 4, pp. 27-37, August 1995.
- [32] Hasslacher, Brosl, "discrete fluids," *Los Alamos Science*. Special Issue (1987), pp. 175-217.
- [33] Doolen, G., Uriel Frisch, Brosl Hasslacher, S. Orszag and S. Wolfram, Ed., *Lattice Gas Methods for Partial Differential Equations*. Santa Fe Institute, (1990).